Structural-Functional Analysis of Unique Features of *Escherichia coli* Citrate Synthase using In Vitro Mutagenesis

By

David John Stokell

A Thesis Submitted to the Faculty of Graduate Studies in Partial Fulfillment of the Requirements for the Degree of Masters of Science

Department of Chemistry
University of Manitoba
Winnipeg, Manitoba

THE UNIVERSITY OF MANITOBA

FACULTY OF GRADUATE STUDIES

*****

COPYRIGHT PERMISSION PAGE

STRUCTURAL-FUNCTIONAL ANALYSIS OF UNIQUE FEATURES OF *ESCHERICHIA COLI* CITRATE SYNTHASE USING IN VITRO MUTAGENESIS

BY

David John Stokell

A Thesis/Practicum submitted to the Faculty of Graduate Studies of The University of Manitoba in partial fulfillment of the requirements of the degree of

Master of Science

To my wife, Suzi,
you are my inspiration.
Thank you for all your love,
support, and patience these
past three years.

Acknowledgements

I would like to thank Dr. H. W. Duckworth for providing me with the opportunity to work in his lab for the past three years. His encouragment, support, and wisdom have taught me to strive for excellence and understanding in all life's tasks.

Thanks to the members of my committee, Dr. J. O'Neil and Dr. P. Loewen for taking the time to read and provide constructive criticism of my thesis.

Thank you to Dr. L. Donald for her friendship, encouragement and advice on many aspects of work presented in this thesis. Her work in the area of mass spectrometry, which provided crucial information for many of the variants, was particularly appreciated.

Thanks to Dr. D. Brayer, Nham Nguyen and Robert Maurus of the University of British Columbia, for providing the crystallographic information on the *E. coli* enzyme.

Thanks to the students of the Duckworth and Jamieson labs for their friendship and advice along the way. In particular, to Brian Sithoo, your friendship and great personality made every day in the lab an enjoyable experience.

Finally, I would like to thank my family and friends for their love and support. Thanks to my dad who taught me that hard work and persistence is the key to success and to my mother for her constant encouragment to better myself. To my brother James and sister-in-law Dana for their love and support (thanks for reading the thesis Dana).

Abstract

Gram negative bacteria may be distinguished from other prokaryotes and eukaryotes by the fact that they contain a citrate synthase (CS), designated Type II, that has a hexameric subunit structure, and is allosterically inhibited by NADH and activated by KCl. Citrate synthases from gram positive bacteria, archeaeobacteria and eucaryotes are classified as Type I and are non-allosteric dimers. Recently, a crystal structure has been obtained for CS from *Escherichia coli*, the first structure for a Type II enzyme. A crystal structure for NADH bound to an *E. coli* CS variant protein, F383A, has also been obtained. These structures show a number of features that are absent from Type I enzymes: an NADH binding site; a central cationic pore lined with 18 arginine residues (three from each of the six subunits); and a novel N-terminal domain. In this Thesis, site-directed mutagenesis has been used to investigate the functions of these structural features.

To investigate the NADH binding site, nine residues, whose side chains appeared to be positioned so as to form hydrogen bonds to the bound NADH, were chosen for mutagenesis. Kinetic studies, along with NADH binding and inhibition studies, were conducted in order to test the significance of each residue for NADH binding, and the effects each had on the allosteric equilibrium of the enzyme. Nanospray ionization time-of-flight mass spectrometry was also used to assess the effect of each mutation on the multimeric structure of the enzyme.

Site directed mutagenesis was also used to remove each of the three classes of arginines that contribute to the cationic central pore. In all three mutants, the

dimer/hexamer equilibrium was shifted towards hexamer, which suggests that the cationic pore is responsible for destabilizing the hexamer through electrostatic repulsion. This phenomenon would explain why KCl, which also shifts the dimer/hexamer equilibrium towards hexamer, has its activity – presumably high levels of salt would attenuate the effects of charge repulsion. Kinetic measurements on these mutants, however, shows that they are still dependent on KCl activation, so that KCl must be interacting with the enzyme in more than one location.

Finally, the role of the novel N-terminal domain was explored by preparing a truncated mutant which lacked the first 39 amino acids of the polypeptide. This protein folds up normally, has a dimer/hexamer equilibrium similar to that of the wild type enzyme, and binds NADH, but it appears to be completely inactive. A crystal structure is not yet available for this mutant, but it seems that removal of the N-terminal domain induces structural changes that are transmitted to the active site.

Table of Contents

List of Abbreviations

AcCoA:	Acetyl coenzyme A
AMP, ADP, ATP:	Adenosine mono, di, or triphosphate
bp:	Base pairs
$CaCl_2$:	Calcium chloride
CIAP:	Calf Intestinal Alkaline Phosphatase
CoA:	Coenzyme A
CS:	Citrate synthase
Da:	Daltons
DE:	Diethyl amino ethyl
DMSO:	Dimethylsulfoxide
DNA:	Deoxyribonucleic acid
DTNB:	5, 5'-dithio-2-nitrobenzoic acid
EDTA:	Ethylenediaminetetraacetic acid
ESI:	Electrospray ionization
$FADH_2$:	Flavin adenine dinucleotide (reduced form)
H-Bond	Hydrogen bond
IPTG:	Isopropyl-β-D-thiogalactosidase
K_{AcCoA}:	Michaelis constant for acetyl coenzyme A
KCl:	Potassium chloride
K_D:	Dissociation constant for NADH (absence of substrates)
α-KG:	α-ketoglutarate
K_i:	Inhibition constant for NADH (presence of substrates)
K_m, KCl:	Michaelis constant for KCl
K_{OAA}:	Michaelis constant for oxaloacetate
LB:	Luria-Burrous bacterial media
MW:	Molecular weight
MWC:	Monod-Wyman-Changeux
MWCO:	Molecular weight cut off
m/z:	mass-to-charge ratio
NADH:	Nicotinamide adenine dinucleotide
OAA:	Oxaloacetate
PCR:	Polymerase chain reaction
PEP:	Phosphoenolpyruvate
RNA:	Ribonucleic acid
SDS PAGE:	Sodium dodecyl sulphate polyacrylamide gel electrophoresis
SF_6:	Sulfur hexafluoride
TCA:	Tricarboxylic acid cycle
TOF:	Time-of-flight
Tris:	Tris-(hydroxymethyl)aminomethane
WT:	Wild type

List Of Figures

List Of Tables

Introduction

Role of Citrate Synthase in Cellular Metabolism

Citrate Synthase (CS), found in almost all organisms, is the key enzyme responsible for the introduction of carbon into the tricarboxylic acid cycle (TCA). CS catalyzes the first step in the cycle which involves the condensation of oxaloacetate (OAA) and acetyl coenzyme A (AcCoA), to form citrate and free coenzyme A (CoA-SH). The condensation reaction involves the transfer of the two-carbon acetyl fragment of acetyl-CoA onto oxaloacetate, generating a six-carbon citrate molecule. Citrate synthase is the only enzyme in the TCA cycle that creates a C-C bond, and its catalytic mechanism is classified as a condensation reaction because it does not use a nucleoside triphosphate energy source.

The TCA cycle is the central pathway in aerobic respiration, and is responsible for the generation of reducing power in the forms of nicotinamide adenine dinucleotide (NADH) and Flavin adenine dinucleotide ($FADH_2$) (Figure 1). The TCA cycle follows the linear enzymatic pathway of glycolysis, which is the breakdown of glucose into pyruvate, and precedes oxidative phosphorylation, which is the reduction of O_2, and the generation of energy in the form of ATP. The introduction of carbon into the cycle is through acetyl-CoA, which is produced via catabolism of amino acids, β oxidation of fatty acids, or oxidation of pyruvate via the pyruvate dehydrogenase complex. When viewing the TCA cycle, there are several key points to note: 1) one acetyl-CoA molecule is required for one turn of the cycle; 2) oxaloacetate is regenerated at the end of each cycle (theoretically 1 OAA could carry out the oxidation of an infinite number of AcCoA molecules entering the cycle); 3) there are four key oxidation steps per cycle which

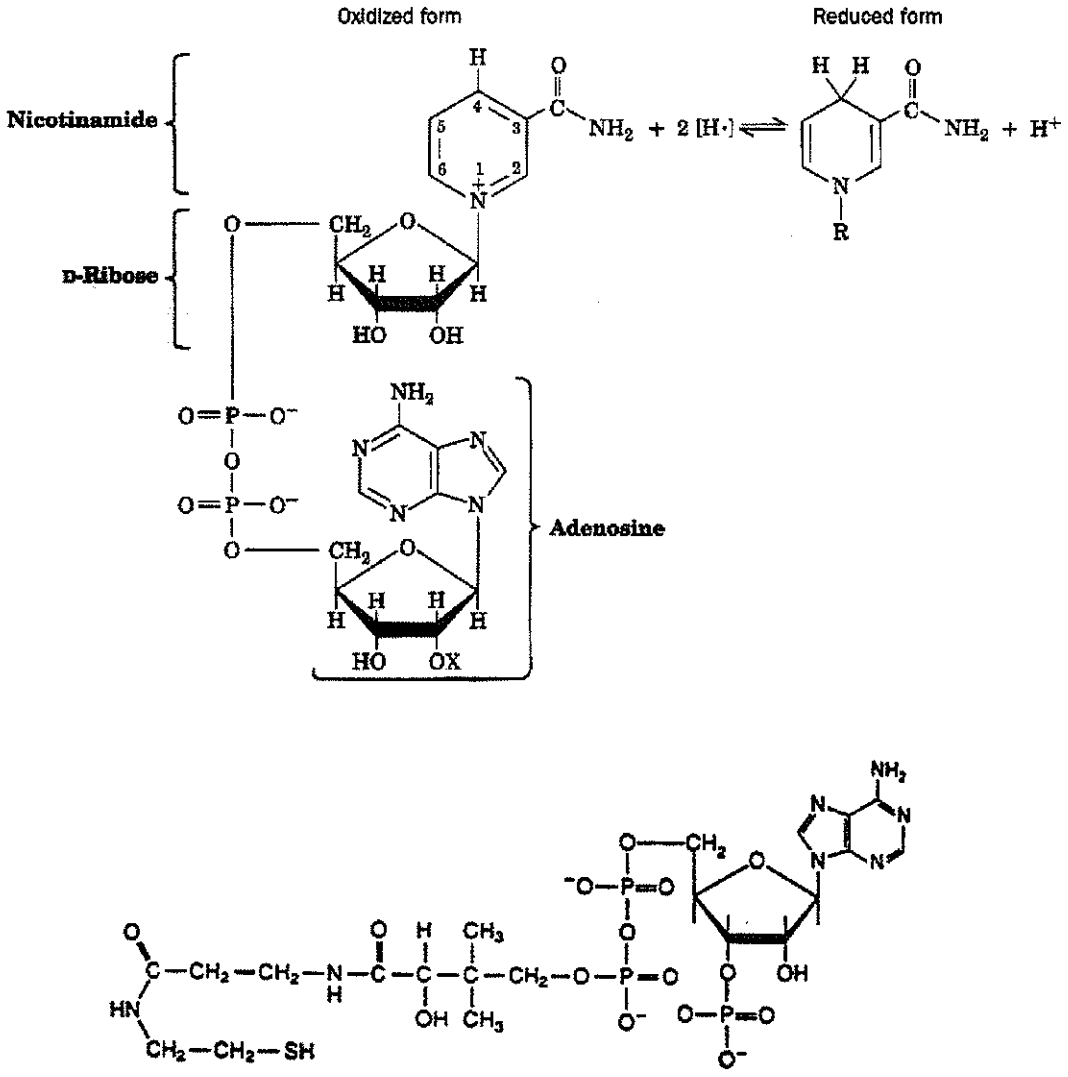

Figure 1: Structures of the two key adenylates, which associate with *E. coli* citrate synthase. A. NAD/NADH (NADH being the allosteric inhibitor); B. Acetyl-CoA, one if the substrates.

are responsible for the generation of $2CO_2$, 3NADH, and $1FADH_2$. The TCA cycle plays a key role in energy metabolism, but is also responsible for providing precursors for a variety of different cellular products such as aspartate (derived from OAA and a precursor of pyrimidines), and glutamate (derived from α-ketoglutarate and amino acids), making it an amphibolic pathway.

A second modified form of the TCA cycle, known as the non-cyclic TCA cycle is found in bacteria that can grow anaerobically such as *E. coli*. The non-cyclic TCA cycle is not responsible for the production of energy, but rather solely for the production of biosynthetic precursors. Figure 3 depicts the non-cyclic TCA cycle, which lacks α-ketoglutarate dehydrogenase, responsible for the conversion of α-ketoglutarate to succinyl-CoA. The first three steps in the non cyclic TCA cycle are the same as in the cyclic TCA cycle leading to the formations of citrate, isocitrate, and α-ketoglutarate, while a set of four different enzymes is responsible for the reversible conversion of oxaloacetate to succinyl-CoA. Under anaerobic conditions, fermentation may provide the cellular energy needed, but it is the non-cyclic TCA cycle that provides required anabolic precursors that are obtained from the TCA cycle under aerobic conditions.

A final pathway involving CS is the glyoxylate cycle, a modified form of the TCA cycle, which skips several of the intermediate steps (Figure 4). The glyoxylate cycle is utilized in plants, invertebrates, and some microorganisms such as *E. coli* for the net conversion of acetate into oxaloacetate, not for direct energy, but rather to provide greater levels of OAA, which in turn may be converted to phosphoenolpyruvate (PEP). PEP is then converted to glucose, which is needed for energy and the synthesis of cellular molecules. Hence, the glyoxylate cycle is responsible for replenishing the carbohydrate

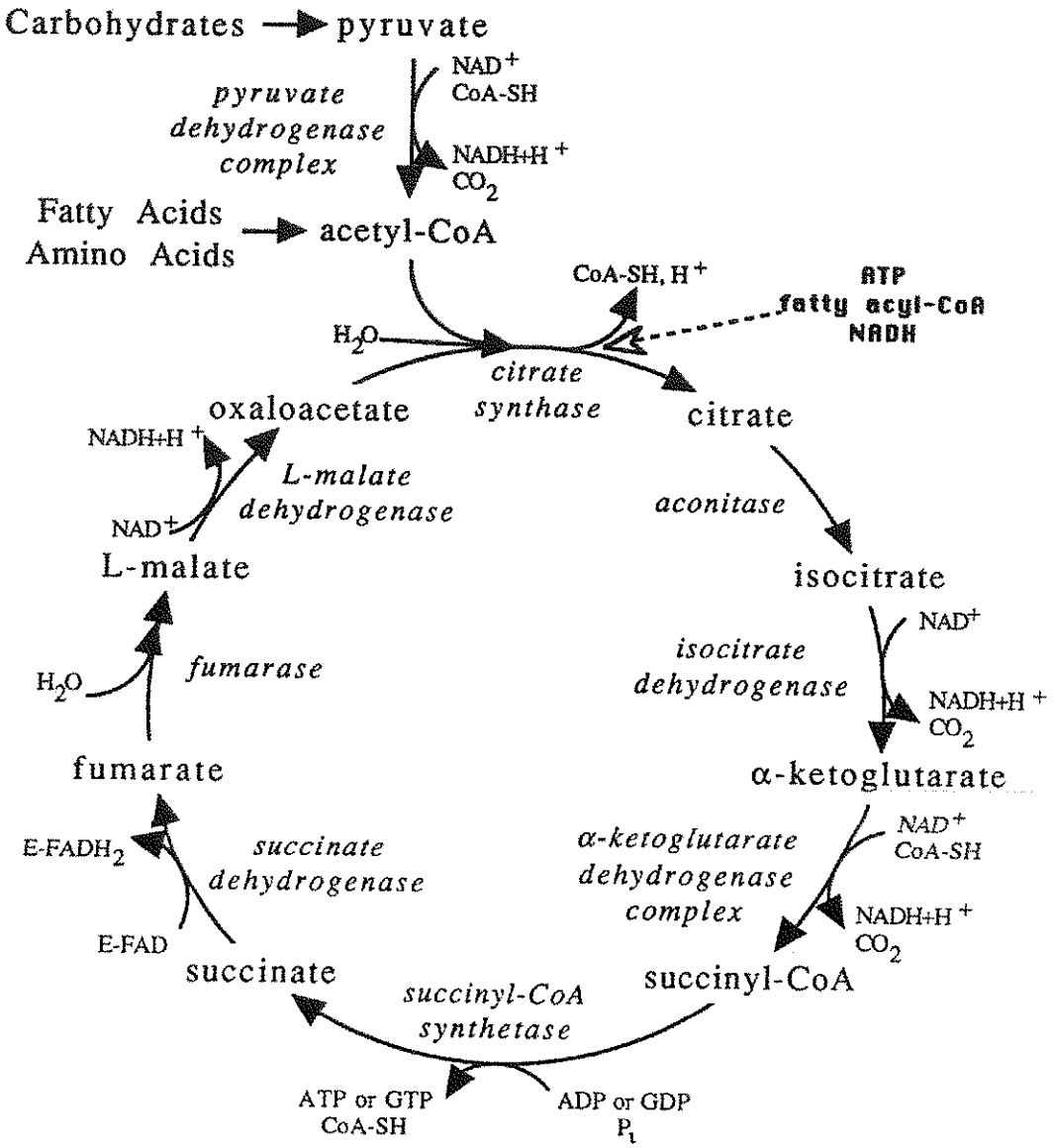

Figure 2: The Tricarboxylic Acid Cycle (Adapted from Molgat, 1990)

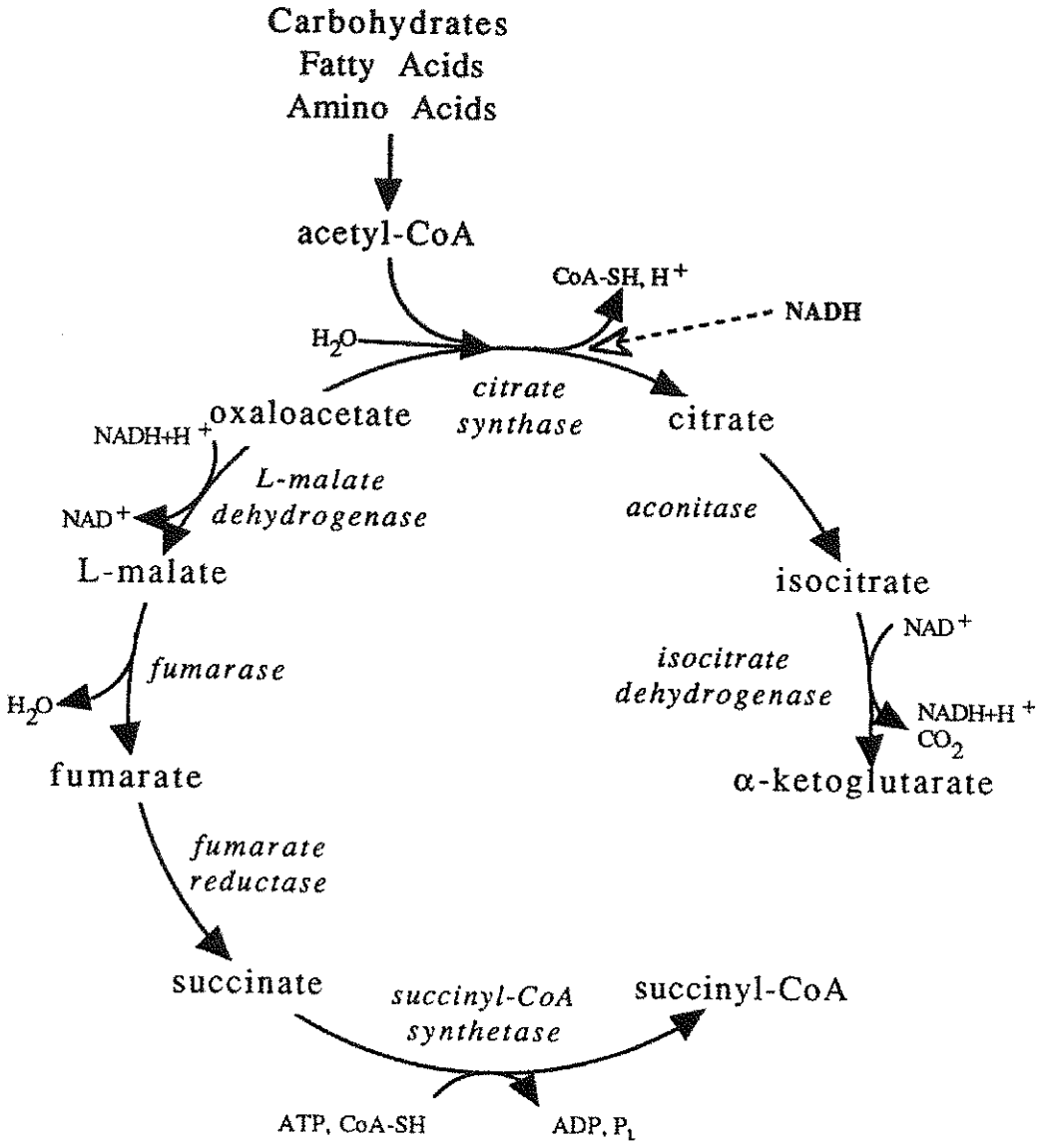

Figure 3: The Non-Cyclic Tricarboxylic Acid Cycle (Adapted from Molgat, 1990)

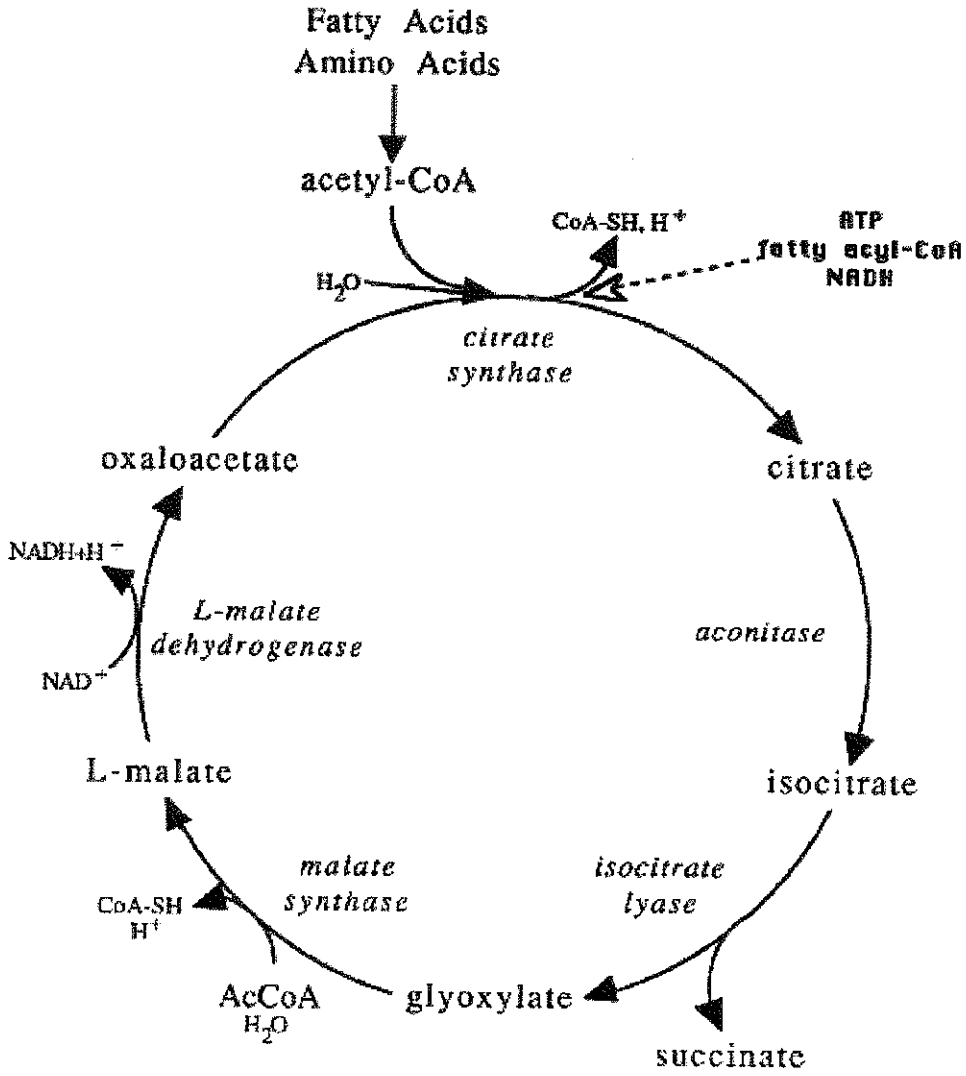

Figure 4: The Glyoxylate Cycle (Adapted from Molgat 1990)

levels within the cell.

In view of the importance of citrate synthase in catalyzing the initial step in the previously mentioned pathways, it is not surprising that CS is under some form of feedback regulation. In the case of the eucaryotic CS (e.g. pig citrate synthase), ATP, in high concentrations (signal of high energy levels), acts as a negative feedback mechanism for the TCA cycle via isosteric inhibition (Weitzman & Jones 1968; Srere, 1972). Gram negative bacteria, such as *E. coli*, also contain a negative feedback mechanism in the form of NADH (product of TCA cycle), which allosterically inhibits citrate synthase activity (Weitzman, 1966a, 1966b; Weitzman & Jones, 1968; Tong & Duckworth, 1975; Weitzman & Danson, 1976). A second negative feedback mechanism for *E. coli* CS, is via α–ketoglutarate, a central intermediate in the TCA cycle, which acts as an isosteric inhibitor of the enzyme (Wright et al., 1967; Pereira et al., 1994). Utilizing the pig CS crystal structure as a model, a good understanding of the *E. coli* CS catalytic mechanism has been obtained, however there has been little insight regarding the allosteric mechanism or the NADH binding site. Now, using the recently-determined crystal structure for *E. coli* CS (Nguyen et al., 2001), one focus of this thesis will be to obtain insights into the NADH binding site and draw inferences about the allosteric mechanism.

Classes of Citrate Synthase

Citrate synthase proteins from different organisms have been grouped into two distinct classes based on subunit number, and regulatory properties including isosteric and allosteric inhibition (Weitzman & Jones, 1968). One feature, which is shared

between the two classes, is the common subunit of ~48000Da. A second feature similar in both classes is the active site which is composed of residues from two adjacent monomers, and therefore is only complete within a dimeric conformation (Else et al., 1988).

Type I CS proteins are found in eucaryotic organisms, gram positive eubacteria, and archaeaobacteria and are designated as "small" citrate synthases. One difference, which has been discovered within the Type I citrate synthases is that the N-terminal domain, which is found in eucaryotic citrate synthase, is not found in gram positives or archaea bacteria. The gram positive and archaea bacteria both show subunits composed of 370-390 amino acids, which lack the N-terminal sequence found in eucaryotic, as well as gram negative citrate synthases, which are composed of ~430 amino acids. On the other hand, all type I CS are composed of two identical subunits arranged in an antiparallel fashion creating a dimer of molecular weight ~100 000 Da (Srere, 1972; Weitzman & Danson, 1976). Type I CS proteins are isosterically inhibited by ATP, which appears to compete for the AcCoA binding site, yet are not inhibited by NADH as Type II enzymes are (Weitzman & Jones 1968; Srere, 1972). Members of the "small" CS family were the first to be crystallized, and therefore provided the first information about the structural aspects of this protein.

Type II CS proteins are found in gram-negative procaryotes and are also designated as "large" citrate synthases. Type II proteins are distinguished from Type I proteins in two ways: 1) they form hexameric complexes of molecular weight ~280 000 Da (hence the large designation); 2) they are specifically and allosterically inhibited by NADH, but are not regulated by ATP (Weitzman, 1966a, 1966b; Weitzman & Jones,

1968; Tong & Duckworth, 1975; Weitzman & Danson, 1976). All Type II citrate synthases share a common subunit composed of 420-440 amino acids, and contain a novel N-terminal domain, which is lacking in archaea and gram positive CS, and which is structurally different from the N-terminal domain of eucaryotic CS (Nguyen et al., 2001). Type II citrate synthases can be further subdivided into two broad groups based on the physiology of their host. This division in the Type II citrate synthases is associated with the effect of AMP on NADH inhibition, which is found when comparing CS from strict aerobes with CS from facultative anaerobes. In the case of strict aerobes such as *Acinetobacter anitratum*, introduction of AMP alleviates NADH inhibition, while in facultative anaerobes, such as *Escherichia coli*, AMP has no effect on NADH inhibition (Weitzman & Jones, 1968). To explain this difference, one must think of high AMP concentrations as signaling low cellular energy levels. With this in mind, it would seem obvious that aerobic organisms which rely specifically on the TCA cycle for energy would require strict regulation of this pathway in the form of both positive and negative controls. Alternatively, facultative anaerobic organisms, such as *E. coli* are capable of recycling their electron carrier (NAD^+) through fermentation, which allows them to obtain a limited but steady energy supply through glycolysis alone.

Citrate Synthase Gene Variation and Isoenzymes

The initial area of study with regards to citrate synthase, as with many proteins, is that of the DNA sequence, which in turn gives the amino acid sequence. To date there have been a wide variety of citrate synthase genes sequenced. Within the eucaryotic and

gram positive type I citrate synthases, 46-92% homology is seen, while members of the type II family show 56-75% homology (Patton et al., 1993). However, there is, on average, 20-26% homology between type I and type II sequences, which indicates a major evolutionary divergence in the past. Although there is little sequence similarity between the two types, as expected, the active site residues are well conserved throughout all the CS genes sequenced thus far.

The complete sequence of the *E. coli* citrate synthase (*gltA*) gene, which is shown in appendix 1, was determined by Ner et al. (1983) and further confirmed via the amino acid sequencing carried out by Bhayana & Duckworth (1984). The sequence codes for 427 amino acid residues, which upon post-translational modification, involving removal of the N-terminal methionine, leaves a 426 amino acid subunit of a molecular weight of 47 887 g/mole. Visual alignment based on maintaining functionally important residues, determined from the pig heart CS structure (Wiegand & Remington, 1986), shows that there are 98 identically conserved residues between the two, which corresponds to ~23% sequence similarity (Donald & Duckworth, 1989). As expected, all active site residues are conserved, with the exception of Arg46, which in the pig model interacts with the 5'-diphosphate of CoA (Wiegand & Remington, 1986). Appendix 2 gives an amino acid sequence alignment for citrate synthase proteins from several different organisms from both classes.

Several organisms to date have been found to contain not one, but two citrate synthase genes. *Bacillus subtilis* is a classic example of an organism with two CS genes, namely, *citZ* and *citA*. Both the *citZ* and the *citA* genes encode a citrate synthase enzyme characteristic of the type I enzyme. The predominant enzyme present is that coded by the

citZ gene. Mutations carried out on both genes individually have demonstrated that loss of the *citA* gene has little to no effect on the overall CS activity or growth, while the *citZ* gene, when mutated causes a 90% loss of overall CS activity and creates a partially glutamate auxotroph (Jin & Sonenshein, 1996). A second organism which has given some insight into the multiple CS gene story is *Saccharomyces cervisiae*. With this organism there are again two CS genes present, namely *CIT1* and *CIT2*, both of which code for type I enzymes (Rosenkrantz et al., 1986). Rosenkrantz's group discovered that there was a distinct amino terminal sequence (coding for 39 amino acids) found in the *CIT1* gene, not present in the *CIT2* gene. Under further investigation, it was determined that this sequence contains a mitochondrial-targeting motif, which allows for the transport of the *CIT1* gene product into the mitochondrion (site of the TCA cycle), leaving the *CIT2* gene product to remain in the cytoplasm. It would appear that these two gene copies represent the early form (CIT2, found in prokaryotes lacking organelles), and the later form (CIT1, eukaryotic organisms containing organelles) of the citrate synthase gene, or the point where the two diverged in evolution.

In the case of *E. coli*, there are also two distinct CS genes present, with the second showing similarity to the shortened enzymes found in gram positive bacteria and archaea. Using the complete sequences of the *E. coli* genome (Kroeger & Wahl, 1997), it was found that along with the active site residues, the two genes share ~30% homology. It has recently been determined that the second CS gene codes for a methyl citrate synthase, which allows for cells to grow in minimal media on propionate as a sole carbon source using a methylcitrate cycle (Textor et al., 1997; Gerike et al., 1998). As the *CIT1* and *CIT2* genes of *Saccharomyces cervisiae* may represent a later divergence point in the

evolution of CS as organisms became more advanced, the two CS genes of *E. coli* may represent an early evolutionary divergence triggered by the onset of the availability of new carbon sources.

Active Site Structure

Much of the work pertaining to the active site of citrate synthase was initially carried out on the pig heart protein (Wu & Yang, 1970; Weitzman et al., 1974; Mahlen, 1975; Bayer et al., 1981; Hammond et al., 1986; Evans et al., 1989). The pig enzyme was also one of the first CS proteins for which a crystal structure was available. The crystal structure showed 2 key structural features: 1) subunits composed of a small domain and a large domain; 2) 2 subunits creating dimers aligned in an antiparallel fashion, with the face of each large domain lying across the other. Crystallization in the presence of substrates and analogues showed the position of the active site within a cleft between the large domain and the small domain of a single subunit (Remington et al., 1982; Wiegand et al., 1984). This group later determined that the active site was composed of residues not only from both domains of a single subunit, but also from several residues from the large domain of the adjacent subunit (Wiegand & Remington, 1986). Therefore the active site is only complete in a dimer conformation.

Sequence alignments have shown the presence of all but one of the active site residues originally identified in the pig protein within the *E. coli* protein (Ner et al., 1982). Confirmation of the importance of individual residues in catalysis for the *E. coli* protein was carried out using site directed mutagenesis (Anderson & Duckworth, 1989;

Pereira et al., 1994). The binding site for OAA is composed of 5 residues including Arg387, Arg314, His305, His229, and R407, while the AcCoA site is made up of His264, Asp362, and Phe383 (number based on the *E. coli* sequence). Note that residue Arg407 is from the large domain of the adjacent subunit. Figure 5 shows the orientation of the substrates with respect to one another and the residues with which each interacts.

With respect to the catalytic mechanism of citrate synthase, most of the structural information has been obtained from the pig model for which the crystal structure has been obtained with substrates and analogues present. The general model consists of three structural conformations, including the open conformation when no substrates are present, partially closed when OAA is bound, and closed which occurs following the production, and prior to the release, of citrate and CoA (Wiegand & Remington, 1986). Apart from the free enzyme, Wiegand and Remington were able to crystallize pig citrate synthase in the presence of OAA, CoA (structural analogue of AcCoA), and citrate. In the crystals containing both OAA and CoA, a partially closed form of the enzyme was seen, while crystals containing citrate and CoA showed a closed conformation. Figure 6 shows the obvious structural differences, which occur during the reaction and the conversion from the open conformation to the closed conformation. Weigand and Remington have determined that there is an 18.5° rotation between the small and large domains and a movement for some atoms of as much as 15Å. With the *E. coli* enzyme being a hexameric structure rather than a dimer, one might expect some structural hindrance could be involved with the shifts associated with the reaction. However, from the crystal structure, it does not appear as though the contact regions would interfere with the movements required, as they lie far from the active sites within the hexamer.

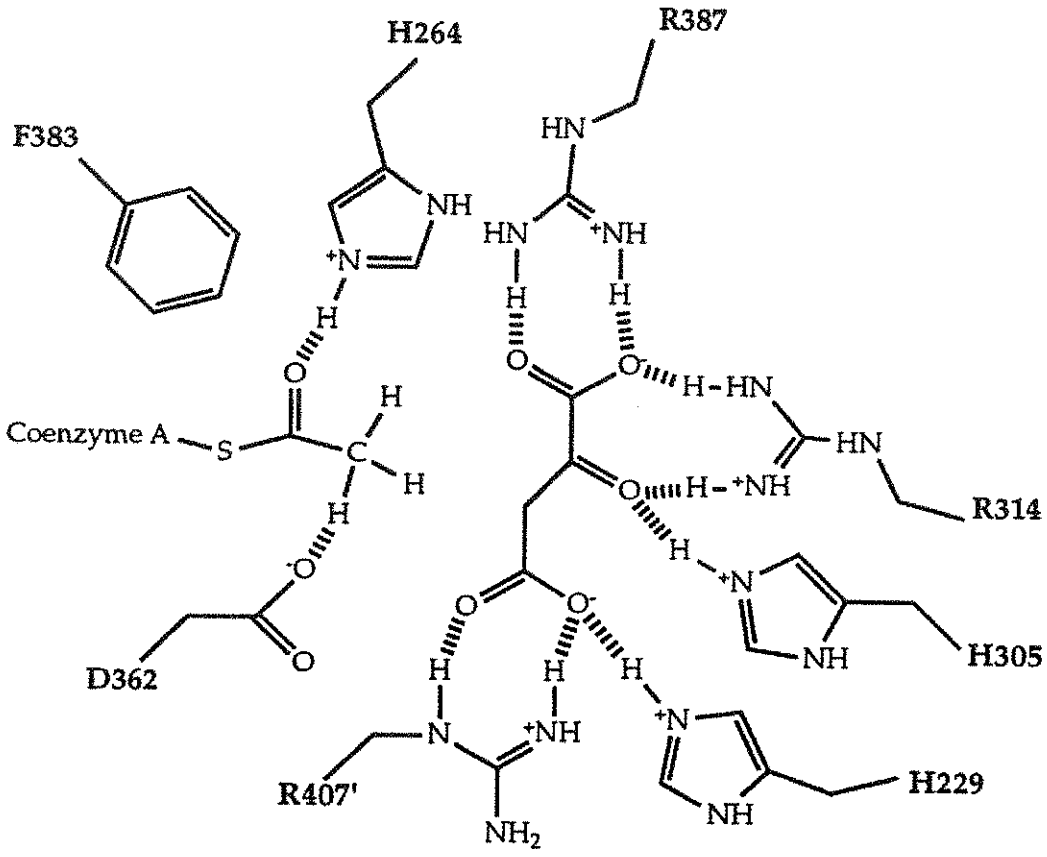

Figure 5: Active site residues involved in hydrogen bonding interactions with bound oxaloacetate and acetyl coenzyme-A (adapted from Ayed, 1998)

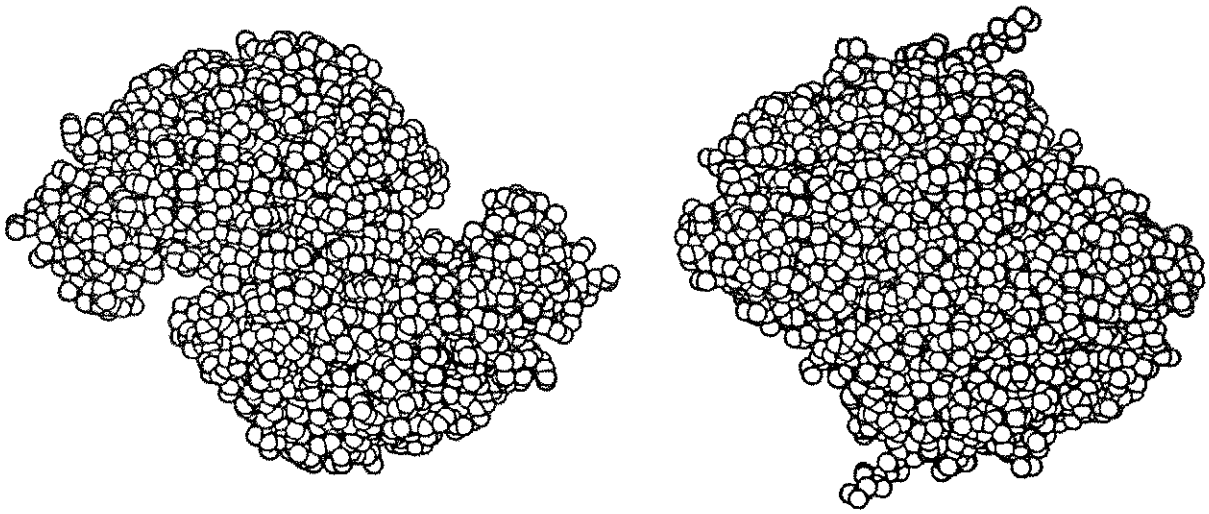

A. B.

Figure 6: Structural variations, which occur in pig citrate synthase upon substrate binding. A. shows the open structure in the absence of substrates. B. depicts the closed structure in the presence of substrates. (adapted from Sadler, 2000)

Catalytic Mechanism

Kinetic studies on both pig CS (Johansson & Petterson, 1974) and *E. coli* CS (Wright & Sanwal, 1971; Tong and Duckworth, 1979) have demonstrated that the catalytic mechanism follows the ordered bisubstrate model proposed by Cleland (1963). Cleland's model, associated with multiple substrates and products, describes a mechanism for which the binding of substrates is ordered, as is the release of the products. Using the pig CS structure, it has been proposed that OAA binds the open conformation, and induces the conformational changes required to reach the closed form, where the small domains of each subunit contact the large domain of the opposite subunit creating the CoA binding site (Johansson & Pettersson, 1974; Remington et al., 1982; Wiegand et al., 1984; Lesk & Chothia., 1984). Initial studies by Johansson and Pettersson (1974) showed that affinity of pig CS for acetyl-CoA, and the analogue propionyl-CoA, increases 20-fold following the binding of OAA. Remington's group demonstrated that the partially closed form is induced upon addition of OAA to crystals, which suggests that the change is induced by OAA. To further strengthen this idea, it was shown that crystals of the closed form fracture upon addition of OAA, which indicates that the open conformation is required for OAA binding (Remington et al., 1982). All of the above facts are consistent with the idea that the binding of substrates to CS is ordered. As for the products of the reaction, the general belief is that citrate is released first, followed by CoA.

The catalytic mechanism for citrate synthase is broken down into three general steps: 1) deprotonation; 2) condensation; and 3) hydrolysis (Evans et al., 1996). (Note:

residue numbering for the following descriptions is based on the *E. coli* enzyme)

The deprotonation reaction involves Asp362, which abstracts a proton from the methyl carbon of AcCoA, in turn generating an enol. The negative charge on the enol oxygen is stabilized through protonation via His264, leaving an enol form of acetyl-CoA.

The condensation reaction is controlled for the most part by Arg314 and His305. The carbonyl carbon of OAA is polarized by Arg314 and His305, making the carbonyl carbon bond very polar, which in turn increases the susceptibility of the carbon to nucleophilic attack (Kurz et al., 1985; Wiegand & Remington, 1986; Kurz & Drysdale, 1987; Anderson & Duckworth, 1989). In rapid sequence, the enol group of AcCoA then attacks the carbonyl group along the *Si* face of OAA, followed by protonation of the carbonyl oxygen, creating the enzyme bound thioester, citryl-CoA.

Following condensation, Asp362 deprotonates the carbonyl carbon of citryl-CoA, followed by protonation of the carbonyl oxygen via His264, creating a mixed anhydride intermediate, primed for hydrolysis. The actual hydrolysis reaction requires the presence of a nearby water molecule, for which evidence has been seen in the pig X-ray structure (Remington et al., 1982; Wiegand & Remington, 1986). The result of the hydrolysis reaction is the formation and release of citrate and free CoA. Figure 7 depicts the three steps just described.

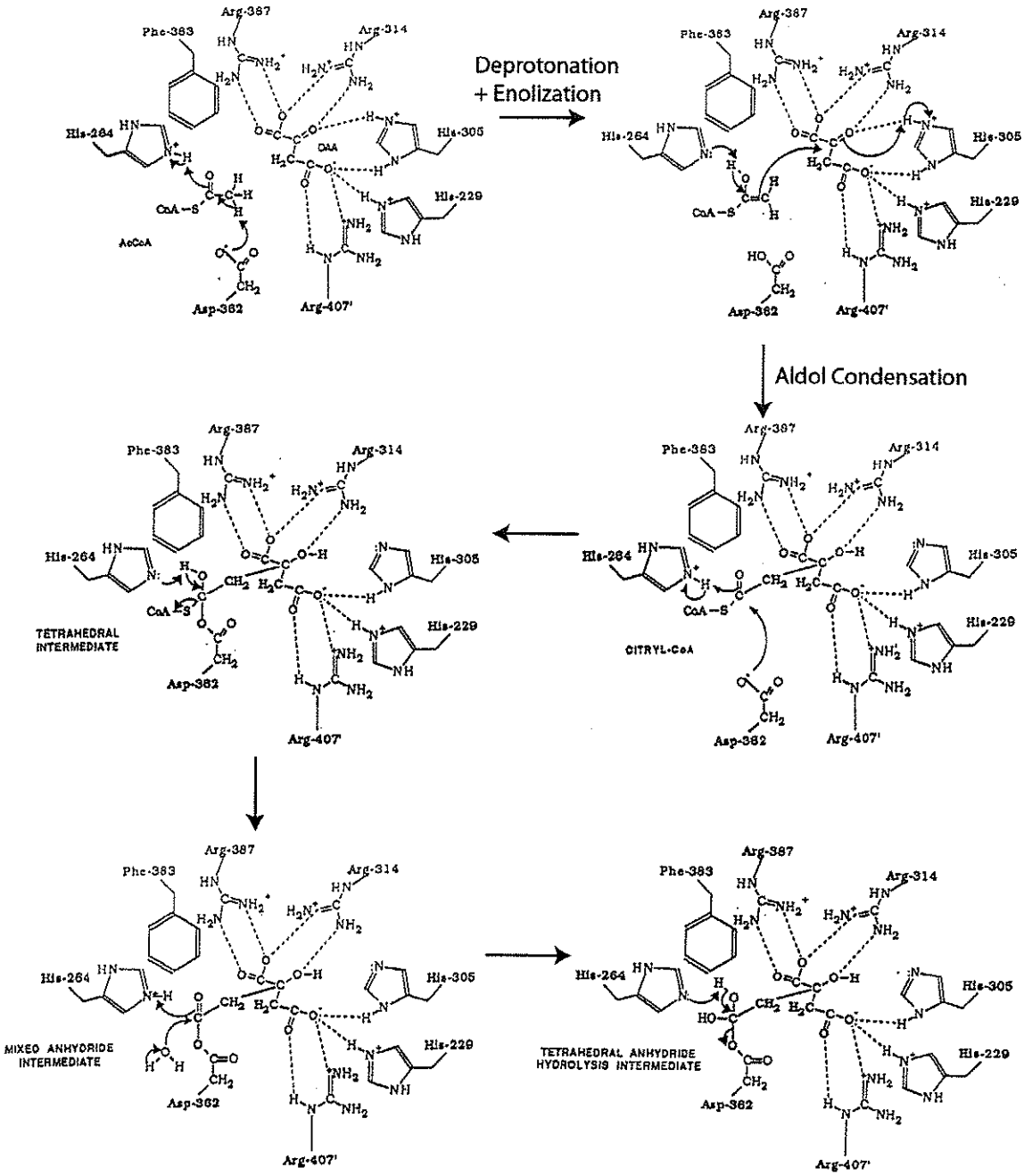

Continued on the following page...

Figure 7: Citrate Synthase Catalytic Mechanism (adapted from Pereira, 1991)

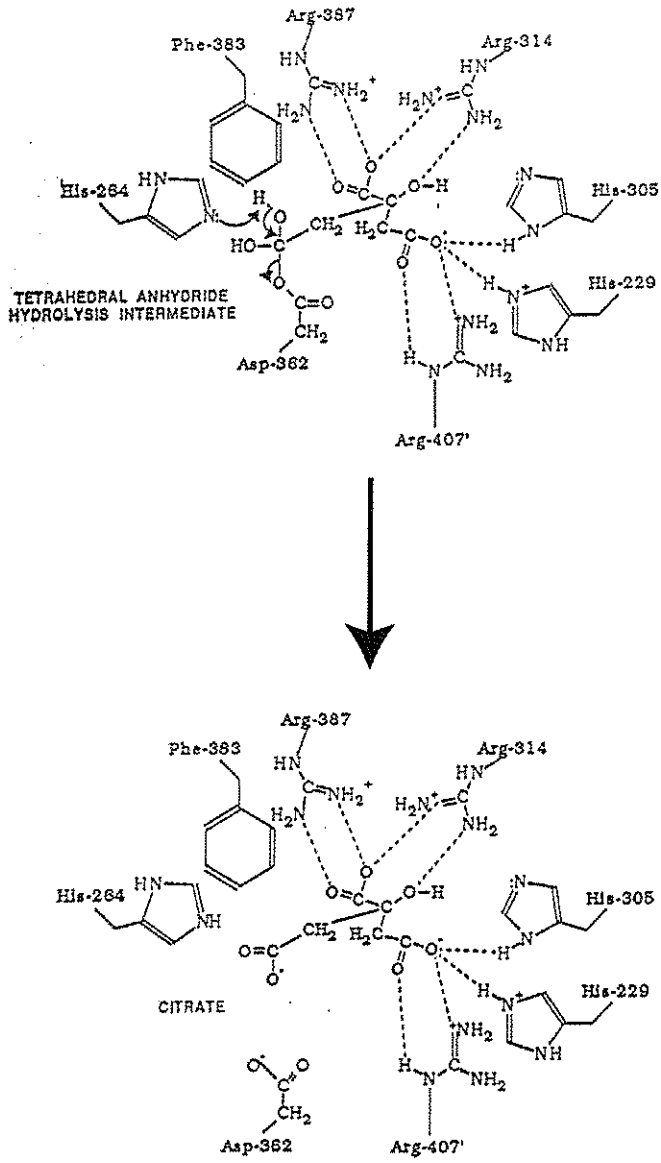
Arg-387
Phe-383
Arg-314
His-264
His-305
His-229
TETRAHEDRAL ANHYDRIDE
HYDROLYSIS INTERMEDIATE
Asp-362
Arg-407'
Arg-387
Phe-383
Arg-314
His-264
His-305
His-229
CITRATE
Asp-362
Arg-407'

Allostery

Allosteric proteins typically catalyze the initial rate-limiting step in biochemical pathways. Regulating the initial reaction of a pathway as opposed to later steps insures that no energy is wasted in the production of unwanted precursor molecules. Allosteric regulation involves the up-regulation (positive) or down-regulation (negative) of protein activity through a modulator, which binds at a distinct (allosteric) site on the protein from that of the active or catalytic site. Modulator associations within the allosteric site include non-covalent interactions (typically hydrogen bonds), which induce structural rearrangements within the protein. The result of modulator binding is either an increase or decrease in the protein's ligand-binding affinity. There are typically two classifications for allosteric regulation: 1) homotropic allostery in which the substrate(s) act as the modulator; 2) heterotropic allostery, which involves a modulator that is distinct from the substrate(s) and is typically an end-product of the pathway.

Allosteric proteins are multimeric complexes composed of several subunits. Some allosteric proteins possess different subunits, one containing the active site for substrate binding, and one containing the allosteric site for modulator binding. The active site may be derived from amino acid residues from several subunits. This subunit-shared active site creates cooperativity between subunits within the complex. In other words, binding of substrate to one subunit may induce conformational changes, which will increase the binding affinity for the same substrate in adjacent subunits. This cooperativity effect causes allosteric proteins to have a characteristic sigmoid substrate-saturation curve rather then the classical Michaelis-Menten. Negative modulators on the

other hand can induce conformational shifts in the same manner, decreasing substrate binding affinity in adjacent subunits, upon binding to one allosteric site in the multimeric complex.

Explaining the kinetics of allosterically regulated proteins has been a difficult endeavor. The most recognized model for allosteric proteins is the symmetry model (Monod et al., 1965). The symmetry model (Figure 8) otherwise known as the Monod-Wyman-Changeux model (MWC) uses the R/T state terminology with respect to the conformation of the subunits within the multimers. The R-state or relaxed state represents a subunit in a conformation which favors substrate binding as well as positive modulators while the T-state favors the binding of negative modulators. The MWC model assumes that allosteric proteins are multimeric and composed of subunits that are symmetrically equivalent with respect to one and other. All subunits can exist in either R or T state, with an equilibrium present whether in the presence or absence of ligands. Ligands may bind to either T or R state, but with decreased or increased efficiency with respect to substrate and modulators as mentioned above. The final assumption of the MWC model is that the subunits within the multimer are unable to exist in mixed conformations, but rather revert from one state to another in a concerted manner. It is the concerted shifting of subunits from T-state to R-state that generates the observed sigmoid curves with respect to substrate saturation experiments.

The MWC model only represents one of many models devised to explain allostery in oligomeric proteins. A second model which is widely used for the analysis of allosteric proteins, is the Sequential model of Koshland, Nemethy and Filmer, (1966),

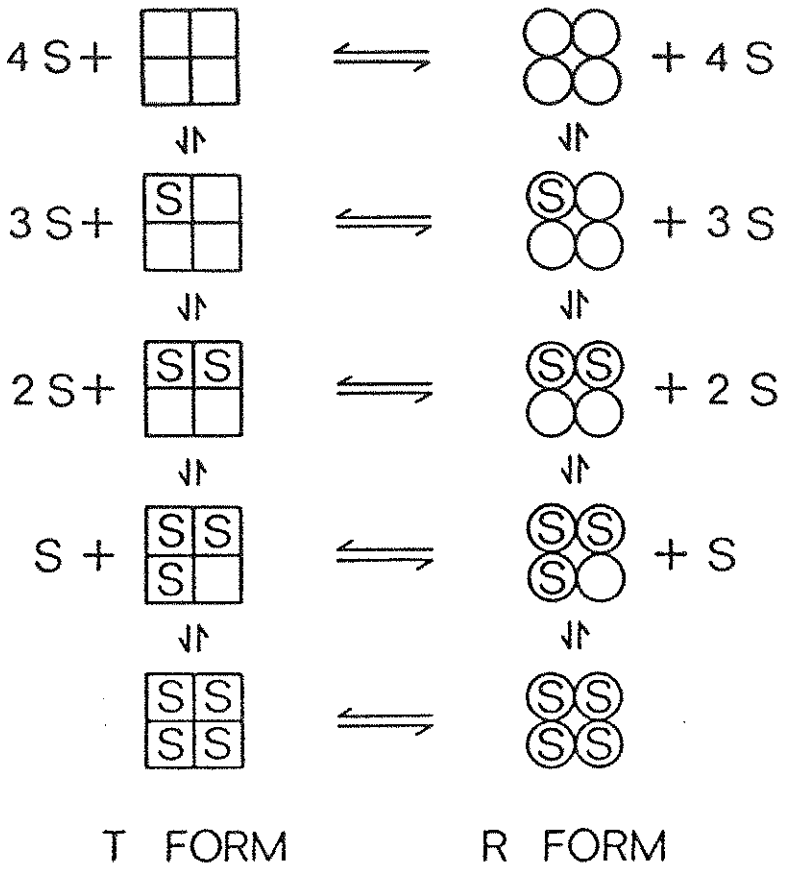

Figure 8: Monod-Wyman-Changeux model, depicting the conversion of subunits in a multimeric complex from an active substrate binding R-state to an inactive inhibitor binding T-state and vice versa. (Fersht, 1985)

which includes the possibility of "hybrid pairs" (subunits in both R and T state, within the same multimer) in its theory. However, both the MWC model and the sequential model are viewed as limiting cases of a more general model involving all possible conformational and ligand bound states of an allosteric protein. One thing that is common to all models is that there are two defined conformational states for the individual subunits, including an active R-state and an inactive T-state. The disadvantage to looking at allosteric proteins from the point of view of a general model as opposed to the MWC model or the symmetry model, is that even though the ideas are basically the same, the general model results in highly complex equations. Therefore, for simplicity, the MWC model is the most widely used for the analysis of allosteric proteins, as it looks at the kinetics in a semi-quantitative way, while using the key ideas found in the general, yet more complex models.

Regulatory Properties of *E. coli* Citrate Synthase

As already mentioned *E. coli* citrate synthase is grouped in the Type II class of enzymes, which are strongly inhibited by NADH in an allosteric fashion. Early studies showed that 100μM NADH is sufficient to eliminate almost all CS activity (Weitzman, 1966a). At pH 7.5 NADH inhibition of *E. coli* CS is almost complete, while at pH 9.2, activity is decreased to ~50% with no apparent NADH inhibition (Weitzman, 1966b). Weitzman's group carried out a titration of NADH at pH 9.2 and found that there were no apparent dissociating groups. Therefore it was concluded that the enzyme undergoes structural modifications at pH 9.2 which affects a separate NADH binding site from that

of the active site (Weitzman, 1966b). To further strengthen this conclusion, reacting the enzyme with DTNB results in the loss of NADH inhibition with a minimal decrease in activity (Danson & Weitzman, 1973; Talgoy et al., 1979). This result implied that the modified sulfhydryl group affects NADH binding but not substrate binding, which indicates unique sites for both ligands. Weitzman's group also showed that several similar pyridine nucleotides, namely the NAD^+, $NADP^+$, and NADPH, show no inhibitory effects (Weiztman, 1966b). Why such structurally similar molecules show no inhibition is not yet understood, however, one possibility (discussed in the structural section) has arisen upon completion of the crystal structure.

Faloona and Srere (1969) determined that *E. coli* CS is strongly activated in the presence of KCl and to a lesser extent by other monovalent cations (e.g. $NH_4^+ > Na^+ > Li^+$). Along with activating *E. coli* CS, KCl also alleviates NADH inhibition, while decreasing the AcCoA binding constant. Typically, *E. coli* CS displays a hyperbolic curve with respect to OAA saturation, while AcCoA saturation follows a sigmoid curve (Anderson et al., 1991). However, in the presence of KCl, the sigmoid AcCoA curve is converted to a classical Michaelis-Menten plot (Faloona & Srere, 1969), which indicates the loss of cooperativity between active sites as a result of the enzyme subunits shifting into a highly active R-state. Under heat denaturing conditions, high KCl concentrations prevent CS precipitation, indicating increased protein stability (Faloona & Srere, 1969). Faloona and Srere also found that upon addition of KCl a shift in the ultraviolet absorption spectrum is observed. It was these findings by Faloona and Srere, which gave initial evidence for structural alterations occurring in the presence of high salt, or in other words a shift in the multimeric-state of the protein as a result of R/T state conversion.

Tong and Duckworth (1975), using equilibrium centrifugation found that in the absence of KCl a mixture of aggregates and dimers are present, while the addition of 50mM KCl results in a dimer hexamer equilibrium. Furthermore, when the concentration of KCl is increased to 100mM, only hexamer is observed. The results of Tong and Duckworth, along with those of Faloona and Srere, imply that the active conformation of *E. coli* citrate synthase is that of a highly stable hexamer, induced in the presence of KCl. However, the possibility of an active dimer, such as occurs in the mammalian and gram (+) protein models should not be ruled out. A CS variant at proline 205 (a residue conserved among the gram negative citrate synthases), showed a strictly dimeric structure, with some activity still intact (Lin Ye and Jennifer Hacking of the Duckworth lab, unpublished). Although the activity was low, this result implies that the possibility of an active dimeric R-state is still feasible. However, this dimeric variant may represent an intermediate, which in the wild type is briefly formed via dissociation of a T-state hexamer followed by conversion to a fully active R-state hexamer upon addition of substrates or KCl.

In general, the allosteric properties of *E. coli* citrate synthase are reflected in the relative binding efficiency of AcCoA. In wild type protein, OAA saturation curves are found to be hyperbolic in the presence of NADH (absence of KCl), as well as under standard assay conditions in the presence or absence of KCl (Anderson et al., 1991). This indicates that OAA is capable of binding both the R and T states with about the same efficiency. However, as already mentioned, in the absence of salt, the saturation curve for AcCoA shows a sigmoid relationship between enzyme activity and AcCoA concentration (Weitzman, 1966a; 1966b). The sigmoid AcCoA saturation curve is the

result of the characteristic cooperativity between subunits as they shift concertedly from T-state to R-state. With the apparent opposing effects of AcCoA and NADH on the R/T equilibrium, one might expect that the concentration of AcCoA would affect NADH inhibition. Early studies showed that NADH inhibition could be overcome by increasing levels of AcCoA (Weitzman, 1966a; Wright & Sanwal, 1971). Duckworth and Tong (1976) confirmed these findings by showing that while NADH binding is slightly weakened in the presence of 0.2M KCl, NADH binding is absent in the presence of 0.1M KCl and 2mM AcCoA. Further, Anderson and Duckworth (1988) showed, through a variant lacking active site residues required for AcCoA binding that NADH binding was still prevented under high AcCoA concentrations. This result implies that AcCoA prevents NADH binding in a two fold manner: 1) via competitive inhibition at the allosteric site; 2) through conversion of the enzyme from an inactive T state, favoring NADH binding, to an active R-state which favors substrate binding.

Along with AcCoA, a variety of adenylic acids have been found to prevent or interfere with NADH binding. This is not surprising, as NADH is composed of adenosine and a nicotinamide group linked via a diphosphate bond (see Figure 1a). Weitzman (1976) discovered that adenosine monophosphate (AMP) and adenosine diphosphate (ADP) at concentrations of 2mM can reactivate NADH inhibited CS. Further studies by Talgoy and Duckworth (1979) involving DTNB protection assays, verified that the adenylates associate in the allosteric site. The protection assays were based on the findings of Danson and Weitzman (1973), who showed that DTNB-reacted CS prevents NADH binding. This result implies the presence of a reactive cysteine near or within the allosteric site. Cysteine 206 was determined to provide the reactive

sulfhydryl group (Donald et al., 1991), and in the presence of NADH is blocked from reacting with DTNB. The protection assays of Talgoy and Duckworth (1979) were carried out using a variety of adenylates (e.g. 3'-AMP, 5'-AMP, ADP-ribose, ATP, NAD^+, $NADP^+$), many of which block the sulfhydryl group of C206. However, even though most adenylic acids are able to bind the allosteric site, all appear to increase enzyme activity, with the exceptions of NADH and 3'-AMP (Talgoy and Duckworth, 1979). Duckworth and Tong (1976) determined that 3'-AMP inhibits CS by associating into the active site and acting as a competitive inhibitor of AcCoA rather then mimicking the inhibitory effect of NADH at the allosteric site.

One final area of study regarding possible inhibitors of *E. coli* citrate synthase is that of the precursor molecules of the TCA cycle. Several studies have focused on α–ketoglutarate (α-KG), which was found early on to be the only TCA intermediate to affect CS activity (Wright et al., 1967). Several groups have broken the tricarboxylic acid cycle down into three major units, with the first unit ending at α-KG (Gray et al., 1966; Amarasingham and Davis, 1965; Hanson and Cox, 1967). α-KG is the first unit break because it represents the first intermediate that not only gives rise to energy, but also branches off from the TCA cycle into the biosynthesis of the glutamate family of molecules (Kornberg, 1963). With α-KG representing the first major branching intermediate of the pathway, it would not be surprising if it had some regulation of the overall rate of the TCA cycle. Sanwal's group showed that α-KG acts as a negative feedback inhibitor of citrate synthase. As with the case of NADH inhibition, they demonstrated that when shifting the pH from 8.0 to 10, α-KG inhibition was lost while 50% of the activity still remained. Furthermore, in the presence of 0.1M KCl, α-KG has

no apparent effect on CS activity. It was these findings which mimic those seen for NADH that led to the initial conclusion that α-ketoglutarate represented a second allosteric inhibitor of *E. coli* citrate synthase (Wright et al., 1967). However, more recent studies by Anderson and Duckworth (1988) have contradicted this conclusion. Anderson and Duckworth demonstrated using active site variants H226Q and H229Q, both involved in oxaloacetate binding, that the decrease in OAA binding as a result of these mutations is mimicked by α-KG. Further, the inhibition via α-KG is lost as a result of these mutations. Therefore it would appear the inhibition of *E. coli* CS via α-ketoglutarate is the result of isosteric inhibition at the OAA binding site.

In light of all the evidence thus far, it would appear that *E. coli* citrate synthase, in its pure form (absence of salt), is in an inactive T-state. This conclusion is based on three simple facts: 1) the pure enzyme shows a sigmoid AcCoA saturation curve, which is converted to hyperbolic upon KCl addition; 2) the pure enzyme favors NADH binding, which is blocked upon KCl addition; and 3) the AcCoA binding constant decreases with the addition of salt. A question that has yet to be answered is, whether there are two forms of the hexamer, namely a T-state hexamer and an R-state hexamer? Evidence to support this two-state hexamer theory has been found in a variety of studies thus far. As already mentioned, Tong and Duckworth (1975) showed through equilibrium centrifugation that KCl induces hexamer formation. This result, coupled with the fact that *E. coli* CS activity increases upon addition of salt, implies the presence of an active R-state hexamer. Conversely, Ayed et al. (1998) showed through mass spectrometry that titration of CS with NADH also induces hexamers. Ayed (1998) further strengthened the two-state hexamer theory by showing that addition of AcCoA and OAA results in a shift

in the dimer/hexamer equilibrium in favor of hexamer. Although direct proof has not been found to validate the existence of both R and T state hexamers, evidence thus far clearly favors the two-state model.

Structural analysis of *E. coli* Citrate Synthase

Early structural information for *E. coli* CS was obtained by building the *E. coli* sequence into the available pig heart coordinates (Duckworth et al., 1987). The initial modeling studies by Duckworth et al. (1987), depicted a 47 887 Da subunit composed of 426 amino acids. Each subunit in this model was composed of 20 α-helices, labeled A to T (following the pig CS nomenclature), and a unique three-strand section of anti-parallel β-sheet. As already mentioned the subunits are subdivided into two separate domains, with the large composed of helices A-M and S-T, and the small made up of helices N-R (see appendix 2 for amino acid sequence alignment). Using the pig structure to derive a working model for the *E. coli* enzyme allowed for decisions to be made with regards to targeting of residues for mutagenic experiments thought to be involved in the catalytic mechanism of the protein. However, with respect to the allosteric properties, the pig-derived model gave no indication as to the allosteric site or the mechanism involved. As well, the type I dimeric pig model gave no information regarding the hexameric arrangement of the subunits found in the type II, *E. coli* enzyme.

Recently, the crystal structure for the *E. coli* enzyme has been solved (Nguyen et al., 2001), leading to a flood of new information and subsequent questions regarding the functional importance of differences seen in the active *E. coli* CS structure compared

with that of the early model based on the pig CS. The *E. coli* structure consists of a hexameric complex composed of a trimer of dimers arranged about a central 3-fold axis (Figure 9). The contact region between dimers is relatively small and includes helical turns FG and IJ, the C-terminal end of helix F and a 7-residue loop between helices J and K, which is unique to type II citrate synthases (Nguyen et al., 2001). One striking feature of the hexameric structure is the presence of a central pore, which is lined with 18 cationic residues and an associated hydrogen-bonding network composed of three arginine residues, namely R119, R125, and R126 (see Figure 10)(Nguyen et al., 2001). The function of the central cationic pore is one focus of this thesis and will be discussed in more detail in the second section of this thesis.

A second interesting aspect of the *E. coli* structure is the presence of the novel N-terminal domain, composed of three anti-parallel β-sheets. Interactions between the first 52 residues from the two subunits of each dimer make up this novel N-terminal domain (see Figure 11). Two general questions to ask regarding this unique Type II domain are: 1) Is this domain involved in the allosteric activity, as it is unique to Type II enzymes; and 2) Could this domain allow Type II enzymes to associate with other proteins in a multienzyme complex of some sort? The function of this novel N-terminal domain was studied by removing the first 39 amino acids.

One surprising and important observation found in the *E. coli* structure is the relative arrangement of a portion of the AcCoA binding site, which differs considerably from that found in type I structures (see Figure 12). H264 and the adenine binding loop (residues 299-303), noted in the pig structure, are as much as 10Å from where they must be for AcCoA binding to occur (Nguyen et al., 2001). This group also observed that the

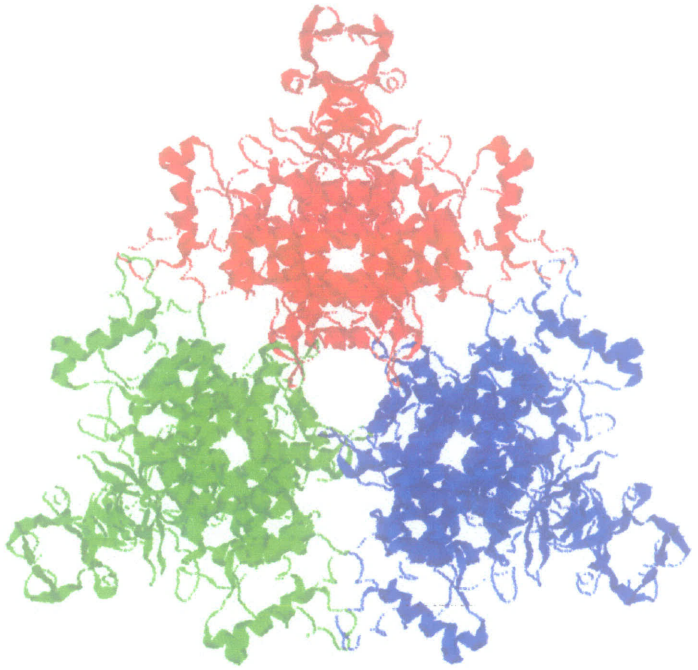

A.

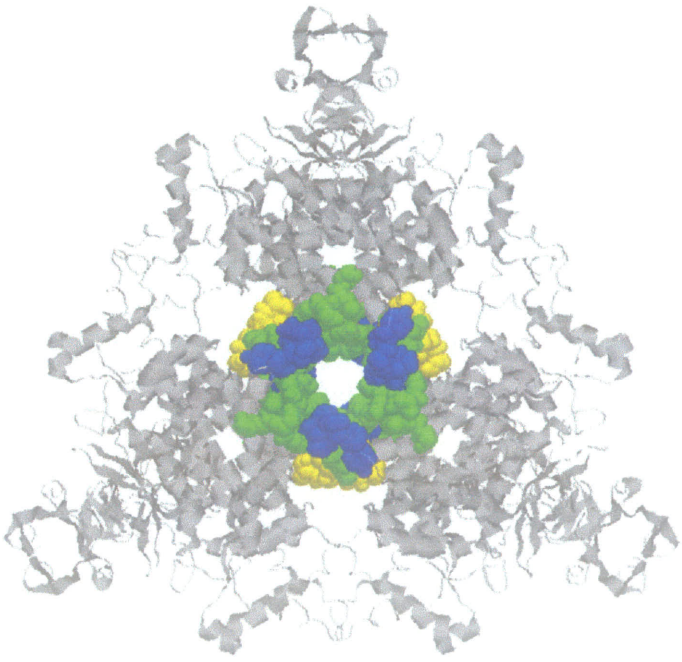

B.

Figure 9: A. depicts the *E. coli* CS hexamer in a ribbon diagram representation, composed of a trimer of dimers (e.g. red, blue, and green). B. highlights the three major contact regions between dimers: 1) FG turn shown in green; 2) IJ turn colored in yellow; and 3) the unique 7 residue loop shown in blue. Figure based on the crystal structure of Nguyen et al., 2001.

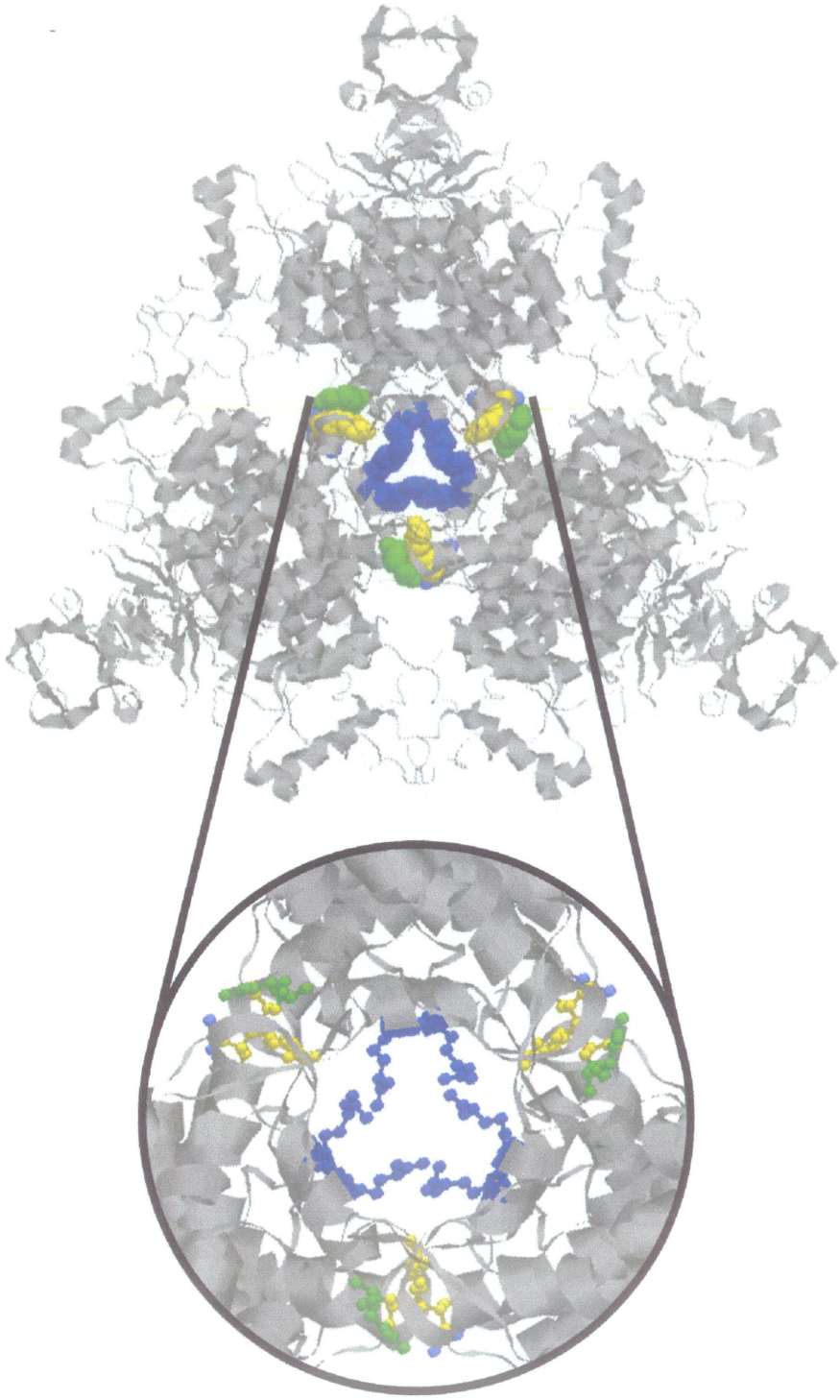

Figure 10: Central hydrogen bonding network, composed of arginine residues 119 (yellow), 125 (green), and 126 (yellow). Figure based on the crystal structure of Nguyen et al., 2001.

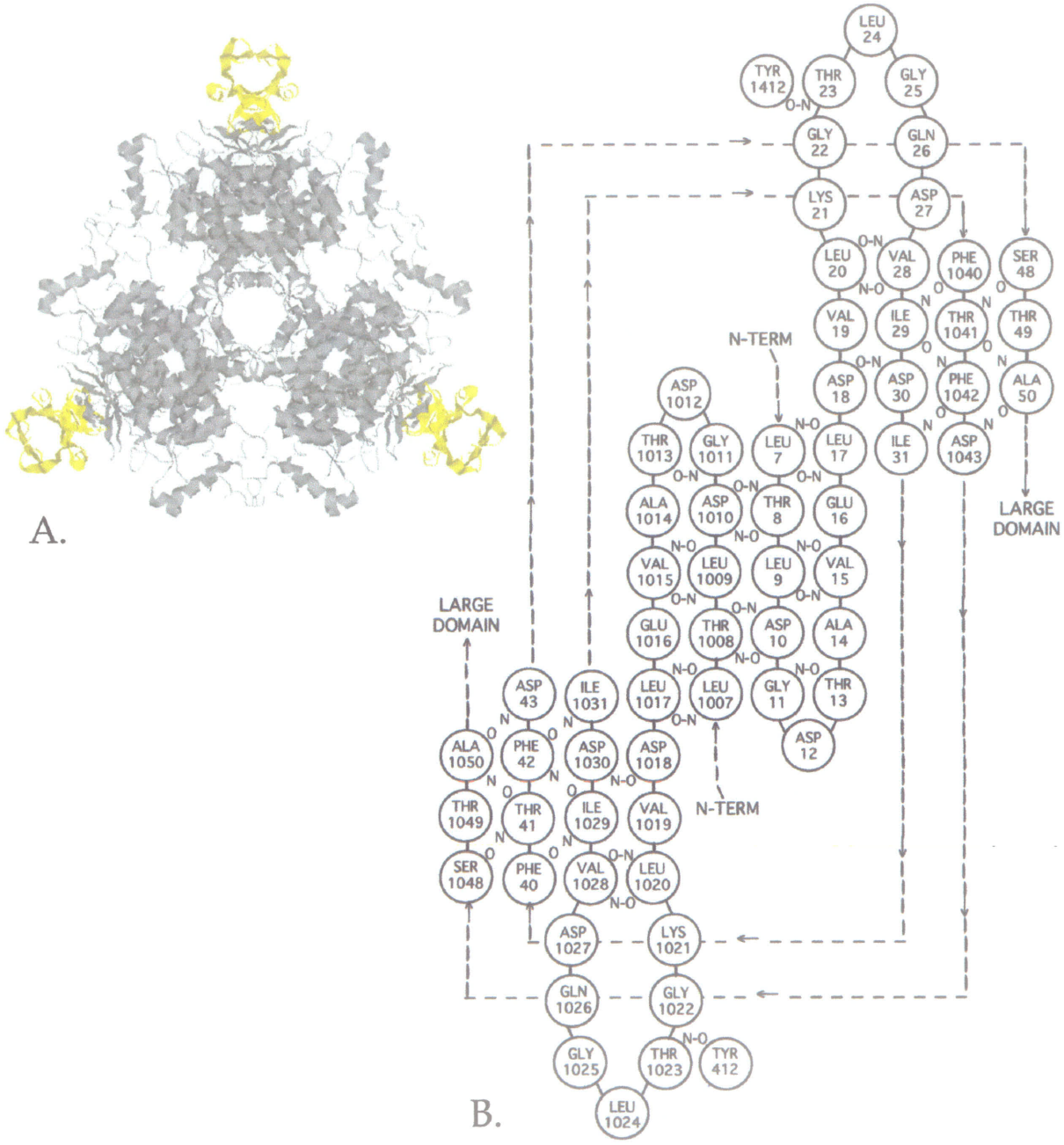

Figure 11: A. shows in yellow the residues which comprise the N-terminal domain in *E. coli* citrate synthase that is unique to gram negative bacteria. B. depicts the orientation of the three anti-parallel β sheets, which make up the core of the N-terminal structure. Figure based on the crystal structure of Nguyen et al., 2001.

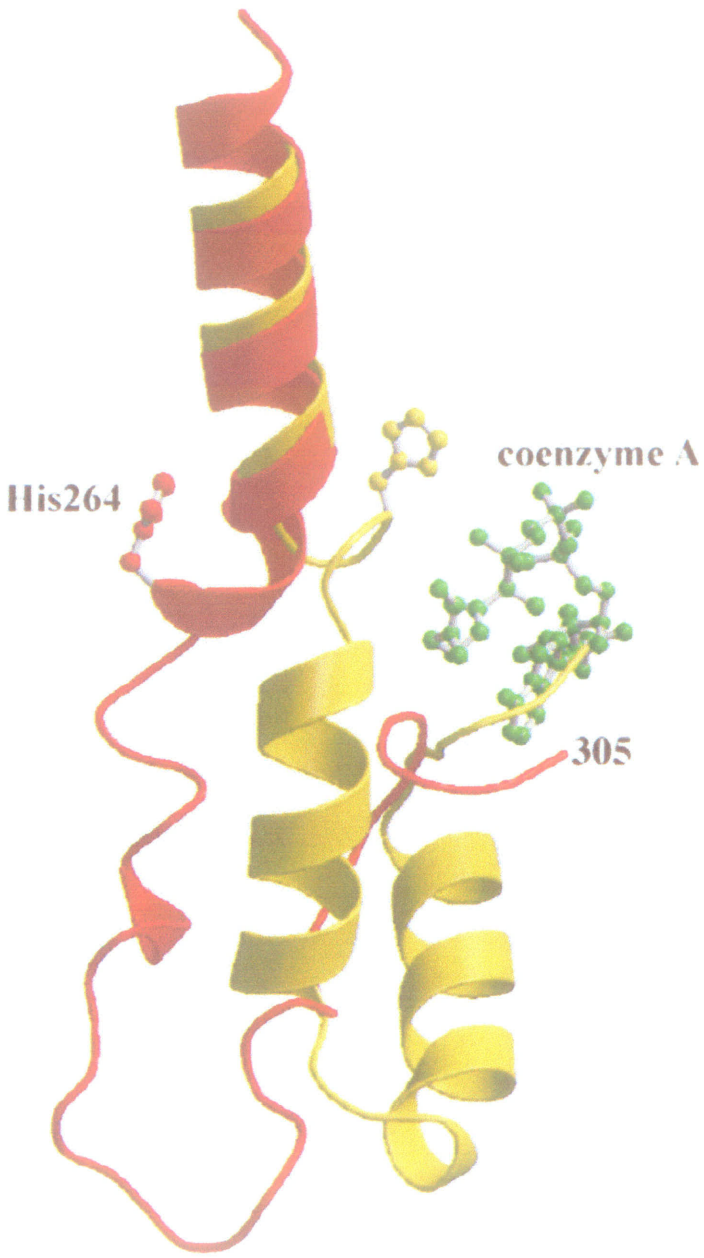

Figure 12: Comparison of the AcCoA binding loop, and the relative position of histidine 264, in the crystal structures of *Pyrococcus furiosus* CS (yellow) and *E. coli* CS (red). Figure based on the crystal structure of Nguyen et al., 2001.

adjacent polypeptide chain composed of residues 267-297 showed high mobility in their structure. Therefore, considerable structural rearrangement along with possible polypeptide chain refolding, prior to acetyl-CoA binding, may represent some aspects of the allosteric properties of the type II enzymes.

Although the first crystal structure of the *E. coli* enzyme complex gave a clear view into the orientation of the type II hexamer, it gave little information into the allosteric properties or the position of the NADH binding site. Utilizing a variant protein, F383A, whose kinetics suggest a stable T state, crystals of the *E. coli* CS-NADH complex have also been obtained (Figure 13). With the understanding that only hexameric citrate synthases show allosteric properties, it is not surprising that the NADH binding sites lie near the contact regions between dimers, with residues from adjacent dimers contributing to each site. Interestingly, the side chain and main chain residues, which make up the allosteric site, impose a "twisted horseshoe" conformation upon the bound NADH molecule. From the crystal structure, the residues, which appear to provide side chains within the typical hydrogen bonding distance of 3.2Å, include R109, H110, T111, Y145, R163, K167, Q182, and N189. However, it must be noted there are two different forms of the NADH binding site within the crystal structure, which show slight variations in the side chain positions. For example, the side chain of T204 sits within 3.38Å in one site compared with 4.36Å in the second site. Therefore this residue has been included as a possible hydrogen-bonding residue. Figure 14 shows the complete set of residues just mentioned and their relative positions with respect to bound NADH. One notable observation upon comparing the crystal structure of the unbound versus the bound protein is that there is little positional change seen in any of these

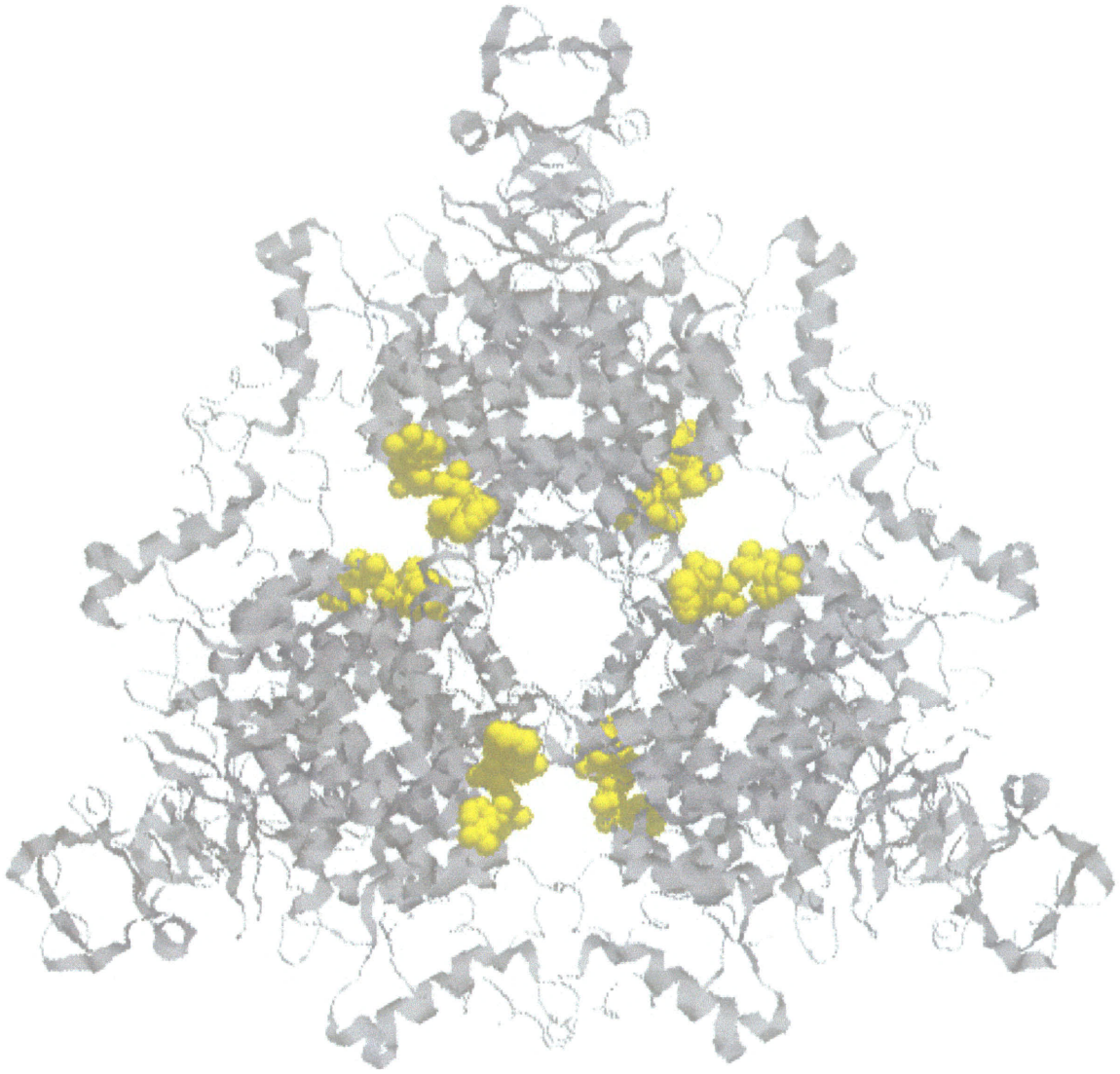

Figure 13: Crystal of the F383A variant with six NADH (yellow) molecules bound. Note the position of the allosteric site, which lies in close proximity to the contact region between dimers. Figure based on the crystal structure of Nguyen et al., 2001.

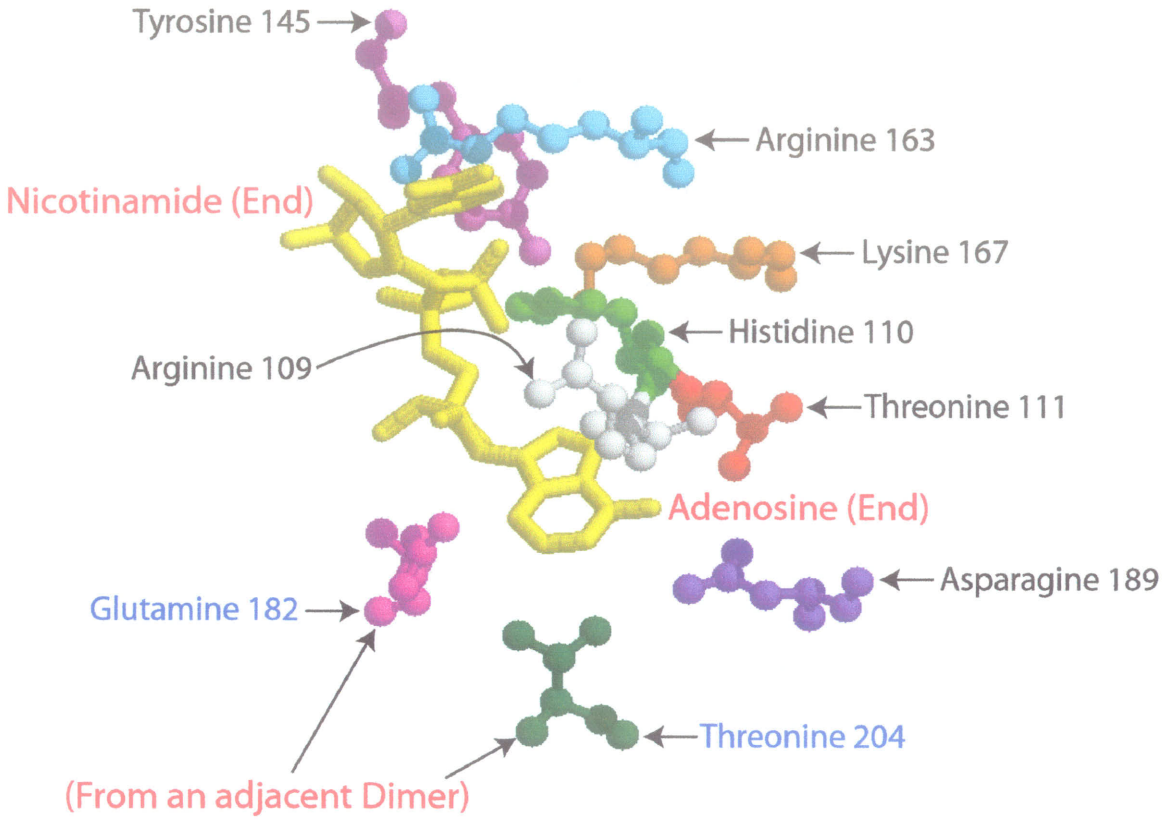

Figure 14: Arrangement of residues surrounding NADH within the allosteric site, according to the crystal structure of the F383A variant with bound NADH. Note that residues Q182 and T204 are provided by an adjacent dimer. Figure based on the crystal structure of Nguyen et al., 2001.

residues (unpublished). One might expect some structural change within the allosteric site upon ligand binding, unless both the bound and unbound structures represent an inactive T-state conformation.

One striking observation regarding the NADH site, is the high level of positive charge, which lines the surface of the pocket (Figure 15). Positive repulsive forces may explain why NAD^+ is unable to bind and inhibit *E. coli* citrate synthase. A second interesting aspect of the NADH site is the presence of a sulfur patch, composed of the side chains of Met112 and Cys206, which lies along the adenosine end of the site (Figure 15). Whether this doublet of sulfur groups plays any functional role within the NADH site is not yet known. However, the positioning of the Cys206 side chain, does explain the negative effects on NADH binding, which accompanied early experimental modifications to this residue.

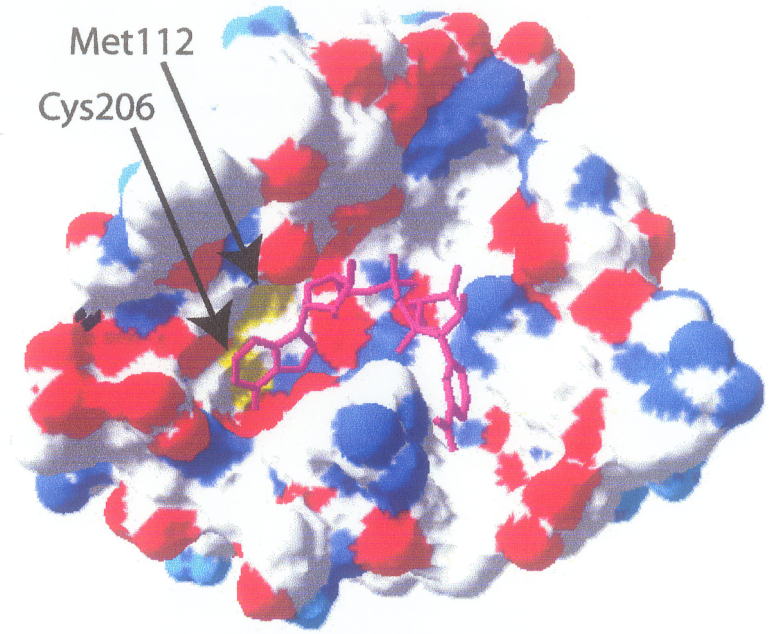

A.

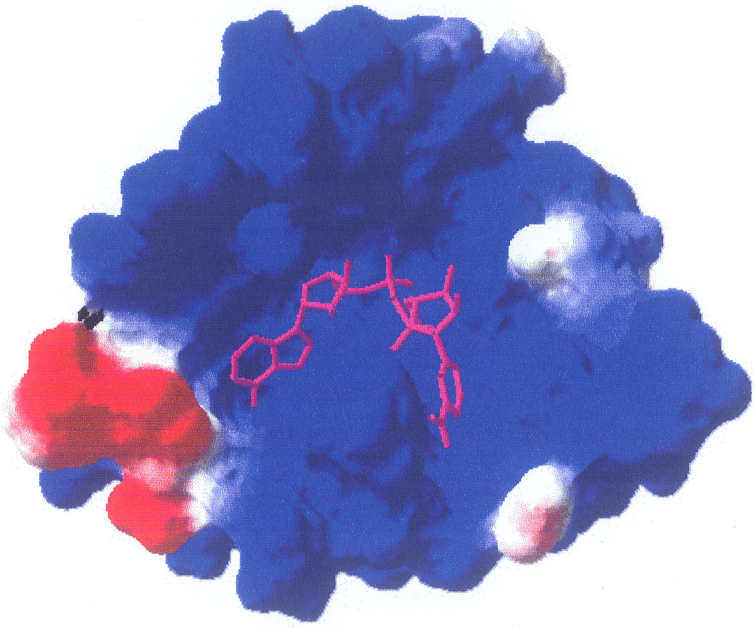

B.

Figure 15: Structure of the NADH pocket, created using the Swiss PDB viewer. Atoms within 8Å of the NADH molecule are shown. A. depicts the atoms which line the pocket and shows the presence of the sulfer patch composed of methionine 112 and cystine 206. B. demonstrates the highly positive (blue) electrostatic field, which lines the pocket. Figure based on the crystal structure of Nguyen et al., 2001.

Thesis objective

With the recent development of the *E. coli* citrate synthase crystal structure, a flood of new questions has arisen regarding functional properties as they relate to structure. The most obvious question which has been on the minds of anyone studying gram negative and other Type II citrate synthases is: Where is the location of the allosteric binding site for NADH? Using the crystal structure of the F383A variant, which co-crystallized with NADH, the general position of the allosteric site has been located. However, the specific residues involved in binding NADH cannot be determined, but only inferred using the crystal structure alone. The first section and bulk of this thesis focus on the determination of the specific residues involved in hydrogen bonding NADH, using site directed mutagenesis as the key tool.

Another question, which has arisen following the crystal structure of *E. coli* CS, is: What, if any, is the function of the central cationic pore composed of arginines 119, 125, and 126? The second section of this thesis focuses on the site directed mutagenesis of these three arginine residues and the effects on the protein's kinetics and ligand binding that results from the loss of these individual side chains.

When comparing the amino acid sequences of gram negative citrate synthases with those of the mammalian and gram positive sequences (see appendix 2), it is apparent that there is an N terminal sequence, coding for ~50 amino acid residues, which is unique to the Type II enzymes. Viewing the crystal structure of *E. coli* citrate synthase, it is seen that these 50 residues interact with their counterparts on an adjacent subunit to fold into a novel N-terminal domain, composed mainly of β-sheet structure. One distinct possibility

is that this domain, being unique to allosterically regulated citrate synthases, has some role in the allosteric properties of these enzymes. The third section of this thesis will focus on a deletion variant, lacking the first 39 N-terminal amino acids, used to give some insight into the function of this novel domain.

Materials and Methods

Media

LB liquid medium was used in the growing of host MOB154 cells (10g Bactotryptone, 5g yeast extract, and 10g NaCl per liter, pH adjusted to 7.2 with NaOH). Combining 100ml LB liquid medium and 100ml melted 3% agar produced LB plates used to maintain the MOB154 culture.

LB-Ampicillin liquid medium was used for the amplification of MOB154 cells harboring a mutant gltA gene (LB liquid media containing 100mg/L ampicillin), while LBA plates were used in screening of NADH variants (100mL LBA combined with 100mL 3%agar).

LB-Chloramphenicol liquid medium was used for amplification of the BL21DE3pLysS host strain used for the production of the truncated variant. (LB liquid media containing 34mg/L chloramphenicol). LB-C plates were used to maintain a pure BL21DE3pLysS stock culture.

LB-Chloramphenicol-Kanamycin medium was used in the amplification of the BL21DE3pLysS cells harboring the pET-24b(+) vector containing the truncated gltA gene (LB liquid medium containing 34mg/L chloramphenicol and 25mg/L kanamycin).

LB-Rifampicin medium was used to decrease the levels of host background proteins during the induction stages of the truncated variant preparation (LB liquid media containing 200mg/L rifampicin).

NZY^+ broth was used in the transformation of Epicurian Coli XL1-Blue cells (1-liter = 10g casein hydrolysate, 5g yeast extract, 5g NaCl, pH adjusted to 7.5 using NaOH). The following supplements were added prior to use: 12.5ml 1M $MgCl_2$, 12.5ml 1M $MgSO_4$, 20ml 20% sterile glucose. For convenience a small 5ml sample was prepared for each experiment, as the protocol calls only for 0.5mL per transformation.

Expression and Purification of CS

NADH Variants

Expression of NADH binding variant *E. coli* citrate synthase proteins was carried out using the high-copy number plasmid pCCgltA containing the appropriate mutation in the gltA gene. A bacterial strain termed MOB154 was the required host, as it lacks a functional gltA gene within its genome (Wood et al., 1987). The MOB154 strain made it possible to produce NADH variants in the absence of contaminant wild type protein. Purification of CS was carried out using a protocol adapted from the procedure devised by Duckworth and Bell (1982). A 2L culture of MOB154 cells harboring the pCCgltA plasmid were grown overnight at 37°C in a shaking incubator. Cells were harvested by centrifugation and resuspended in a minimal volume of standard citrate synthase buffer (CS buffer: 20 mM Tris-Cl, 1 mM EDTA, 50 mM KCl, pH 7.8). Following passage through an Aminco French Press, cell debris was removed via centrifugation, and the protein rich supernatant was loaded onto a 10 x 5cm DE52 (diethylaminoethyl cellulose) anion exchange column equilibrated with CS buffer. Unbound proteins were removed by washing the column with several liters of CS buffer. Citrate synthase and other bound proteins were then eluted using a linear 50 to 300 mM KCl gradient. Fractions of ~12mL were collected and tested for protein by measuring A_{278}. A typical elution profile (Figure 16) is characterized by a sharp CS peak, which centers around fraction 38. The standard CS assay (described later in this chapter) was then used to determine the edges of the CS peak, hence the appropriate fractions to pool.

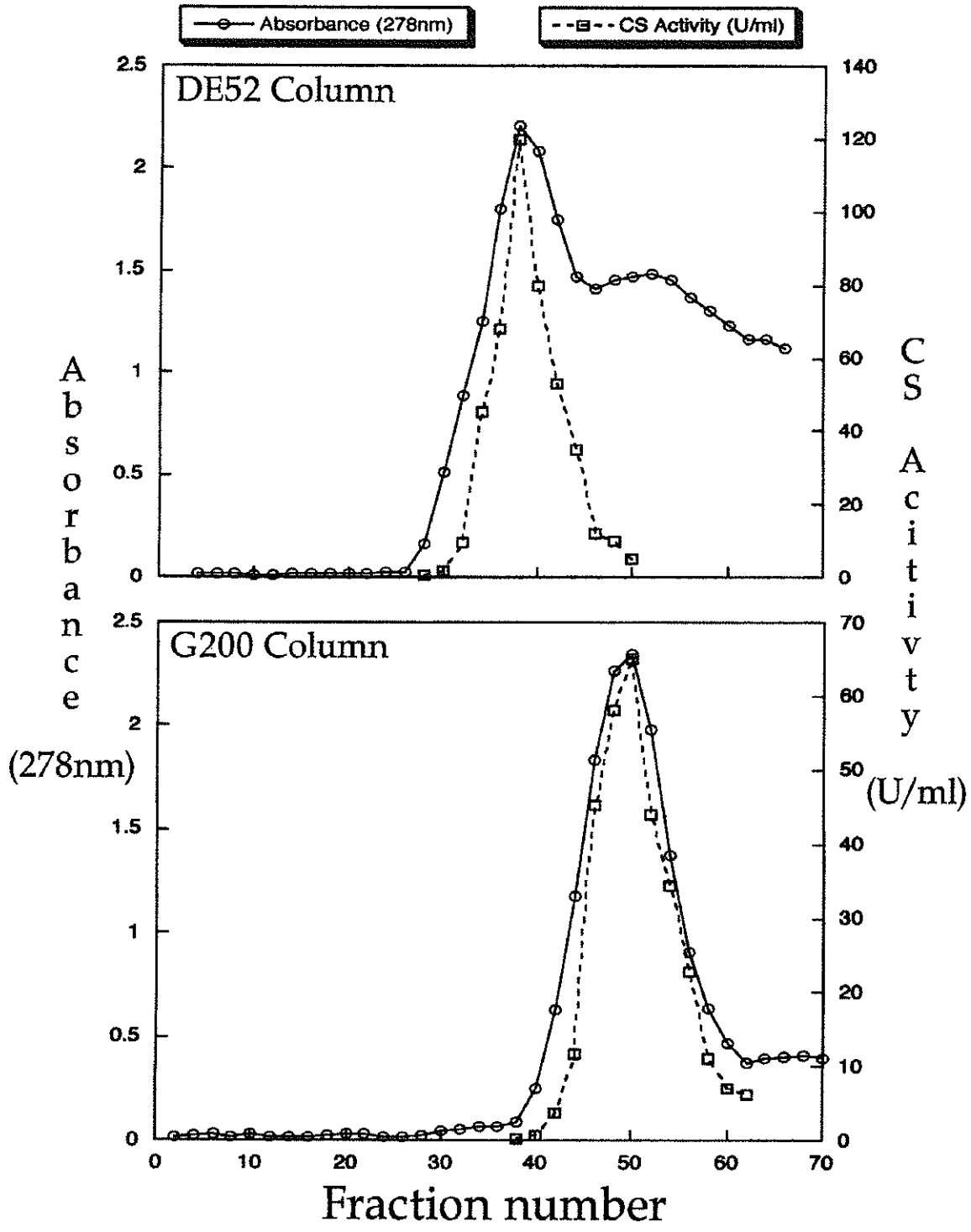

Figure 16: Typical elution and activity profiles for wild type citrate synthase off DE52 anion exchange and G200 size exclusion columns. (200 drop fractions = ~12mL)

Fractions were then pooled and concentrated to a final volume of ~10ml using an Amicon cell with a YM 30 (30 000 MWCO) membrane. The concentrate was then loaded onto a Sephadex G-200 size exclusion column and eluted with CS buffer, collecting 12mL fractions. Appropriate fractions were again pooled and concentrated to a volume of 10mL as above. The final volume was then brought down to ~1mL by vacuum dialysis using 50 000 MWCO Spectra/Por dialysis tubing.

Truncated Variant

The truncated variant was expressed using the pET-Vector system. Using several molecular biology techniques (described later), a modified gltA gene, lacking the first 39 amino acids, was inserted into the expression vector pET-24b(+). The vector was then transformed into the required strain BL21DE3pLysS (screened via a chloramphenicol resistance gene). The DE3 designation indicates the presence of a chromosomal copy of the T7 RNA polymerase gene, which is required, as the pET vector system utilizes a T7 promoter for gene expression. The pLysS designates low level host expression of T7 lysozyme responsible for the suppression of basal expression of T7 RNA polymerase prior to induction. The suppression of T7 RNA polymerase allows for cells to be grown to mid log phase without possible interference from pET vector encoded proteins. Transformed cells from a single colony were initially grown in 2mL LB-Kanamycin/Chloramphenicol at 37°C throughout the day, followed by a scale up to 100mL at the end of the day. The 100 mL culture was then used the following day to inoculate 2L LB-K-C (40 mL cell culture/1L). Cells were grown to mid log phase (A_{600} =

0.6) followed by induction of T7 RNA polymerase via the addition of 10mL 100 mM isopropyl-β-D-thiogalactosidase (IPTG) (final concentration of 1mM). A growth period of 1 hour was used to increase cellular levels of T7 RNA polymerase. To each liter, rifampicin dissolved in DMSO was then added (200mg/L) to shut down the host cell RNA polymerase, hence decreasing the levels of background host proteins. Cells were grown for an additional 2 hours at 37°C prior to harvesting. The typical citrate synthase protein preparation was then followed for purification.

Molecular Biology and Mutagenesis

Site Directed Mutagenesis (NADH variants)

The generation of NADH variants was done using a QuikChange™ Site-Directed Mutagenesis Kit obtained from Stratagene. The Stratagene kit allows for site-specific mutation within double stranded DNA, allowing for the use of plasmid DNA in the PCR reaction. The template used was the pCCgltA plasmid (pUC18 plasmid containing the gltA insert via Sal1 and EcoR1 restriction sites) created by Charlton Cooper of the Duckworth lab. The original template stock was purified using the Qiagen Plasmid Midi Kit. Pairs of complementary oligonucleotides with melting temperatures of ~72-78°C , based on the equation provided in the Stratagene Kit (Tm = 81.5 + 0.41(%GC) – 675/number of bases - % mismatches) were obtained from Genosys (Sigma). Two design parameters to note with respect to proper annealing of oligo are: 1) the mutations should be located in the center of the oligo to provide stable binding on both sides ; and

2) guanine or cytosine bases should be found on the ends, especially the 3' end where extension will occur. A list of the oligos used and their corresponding variants can be seen in Table 2. The PCR conditions used for mutagenesis were as follows:

Table 1: PCR conditions used for site-directed mutagenesis.

Step	Temperature	Time(min)
1	95	0.5
2	95	0.5
3	55	1
4	68	9
5	Cycle 16 times to step 2	
6	68	11
7	4	infinity

The steps involved in mutagenesis using the Stratagene kit are depicted in Figure 17. The reactions were carried out using 5µl Pfu buffer (supplied with the kit), 1µl dNTPs (stock of 20mM each), 125ng of sense and antisense primers (stocks of ~25ng/µl), 50ng template (stock of 7-10ng/µl), and ddH_20 to a total volume of 50µl. The PCR reaction produced a small quantity of homogeneous mutant plasmid DNA containing staggered nicks. The DNA was then digested for 1 hour at 37°C with the addition of 1µl of Dpn1 restriction endonuclease (digests only methylated template DNA). The undigested mutant DNA was then transformed into supercompetent Epicurian Coli XL1-Blue cells (1µl DNA/50µl cells), which take up the DNA and repair the staggered nicks. Cells were initially incubated on ice for 30 minutes following DNA addition. Cells were then heat-shocked for 2 minutes (modified from 45 second heat shock suggested by the QuikChange™ kit) in a 42°C water bath, followed by a two minute incubation on ice. NZY^+ broth equilibrated to 42°C was added (0.5mL), followed by a 1 hour incubation at

Variant	Oligonucleotide
R109L(sense)	CTACGGTGACCC**T**TCATACCATGATCCACG
R109L(antisense)	GATGCCACTGGG**A**AGTATAGGTACTAGGTGC
H110A(sense)	CGGTGACCCGT**GC**TACCATGATCCACG
H110A(antisense)	GCCACTGGGCA**CG**ATGGTACTAGGTGC
T111A(sense)	CGGTGACCCGTCAT**G**CCATGATCCACGAGC
T111A(antisense)	GCCACTGGGCAGTA**C**GGTACTAGGTGCTCG
Y145F(sense)	GGCGGCGTTCT**T**TCACGACTCGCTGG
Y145F(antisense)	CCGCCGCAAGA**A**AGTGCTGAGCGACC
R163L(sense)	GCCGCGTTCC**T**CCTGCTGTCG
R163L(antisense)	CGGCGCAAGG**A**GGACGACAGC
K167A(sense)	CCTGCTGTCG**GC**AATGCCGACCATGGCC
K167A(antisense)	GGACGACAGC**CG**TTACGGCTGGTACCGG
Q182A(sense)	GTATTCCATTGGT**GC**GCCATTTGTTTACCCGC
Q182A(antisense)	CATAAGGTAACCA**CG**CGGTAAACAAATGGGCG
N189A(sense)	GTTTACCCGCGC**GC**CGATCTCTCCTACG
N189A(antisense)	CAAATGGGCGCG**CG**GCTAGAGAGGATGC
T204A(sense)	CCTGAATATGATGTTCTCC**G**CGCCGTGCGAACCG
T204A(antisense)	GGACTTATACTACAAGAGG**C**GCGGCACGCTTGGC
Trunc(sense)	CGGTTCAAAA**CA**TATGTTCACCTTTGACCCAGG
Trunc(antisense)	CTATAGTTCGCAATT**TC**GAACTAACGATTCAAC

***Note: Sense strands go 5'-3', while antisense strands go 3'-5.' Bases in bold represent mutation sites.**

Table 2: Mutagenic oligonucleotide pairs used in creating variant citrate synthases

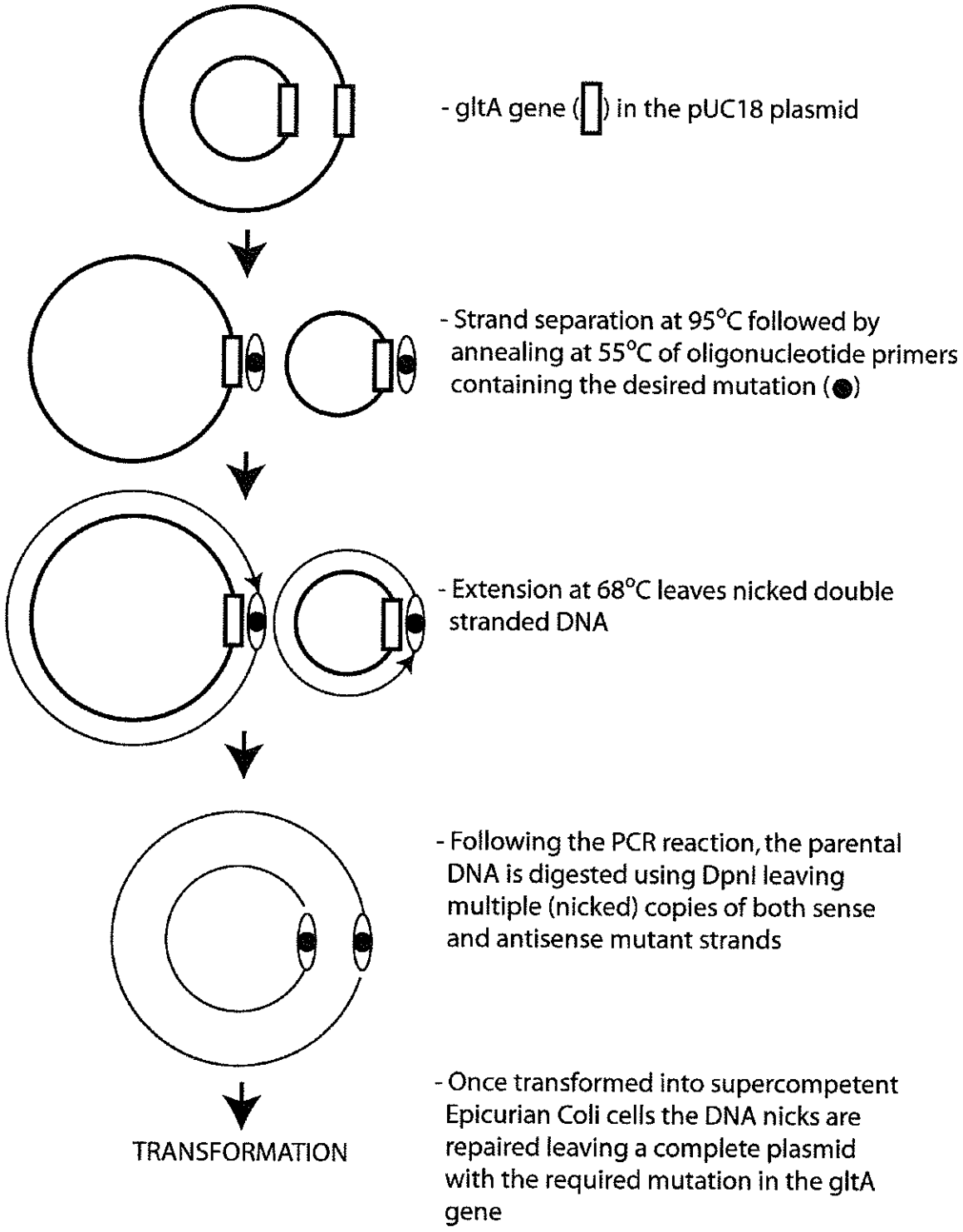

Figure 17: Site directed mutagenesis method for the production of NADH variant citrate synthase.

37°C. The entire culture was then spread on several LBA plates and incubated overnight. The Stratagene kit relies on four key factors for high mutant efficiency: 1) high fidelity of PfuTurbo DNA polymerase; 2) small amount of wild type DNA template in the PCR reaction; 3) low numbers of PCR cycles, which decrease the possibility of random mutations; and 4) removal of methylated wild type DNA through digestion with DpnI restriction endonuclease prior to transformation.

Truncated Mutant Insert Design

Generating the truncated insert required several key factors: 1) the insertion of a start codon (ATG) in place of the GTG codon of amino acid 39 (valine); 2) the creation of an NdeI restriction site at amino acid 39, which would allow for removal of the N-terminal amino acids and the introduction of a new start codon; and 3) introduction of a HindIII restriction site adjacent the stop codon. A sense primer (Table 2) was designed with a central NdeI restriction site (contains a start codon within recognition sequence), which would replace the guanine at position one of codon 39 with adenine, hence creating a new start (ATG) codon at amino acid 39. The antisense primer (Table 2) maintained the natural stop codon, while introducing a new HindIII restriction site just downstream of termination. The PCR reaction was carried out using 250ng of each primer (stocks of ~10ng/μl), 100ng of the pCCgltA plasmid as the template (stock of 7ng/μl), 1μl dNTPs (20mM of each nucleotide), 10μl of Pfu buffer, and ddH_20 to a total volume of 100μl. The PCR conditions used were as follows:

Table 3: PCR condition for generating the Truncated mutant insert.

Step	Temperature	Time(min)
1	95	0.5
2	95	0.5
3	55	1.5
4	68	1.5
5	Cycle 18 times to step 2	
6	68	4
7	4	infinity

Following the PCR reaction, the template DNA was digested via a one hour incubation period at 37°C in the presence of 1µl of DpnI restriction endonuclease. Once digestion was complete the insert DNA was purified using a Qiagen nucleotide removal kit. Gel electrophoreses (1% agarose gel) was used to verify the size of the insert DNA (~1200bp).

Preparation of Insert and Template DNA for the Ligation Reaction

The pET-24b(+) plasmid (vector) and the insert DNA were digested simultaneously with HindIII and NdeI restriction enzymes (~1.5µg DNA for each digestion). Three 1µl additions of each enzyme every half-hour for 1.5 hours was used to ensure complete digestion. One hour into the digestion, 1µl of Calf Intestinal Alkaline Phosphatase (CIAP) was added to the vector digest in order to dephosphorylate the 5'-termini and prevent self-ligation. Following digestion, vector and insert DNA were purified using a Qiagen kit (PCR clean up procedure), and resuspended in 30µl of double distilled water.

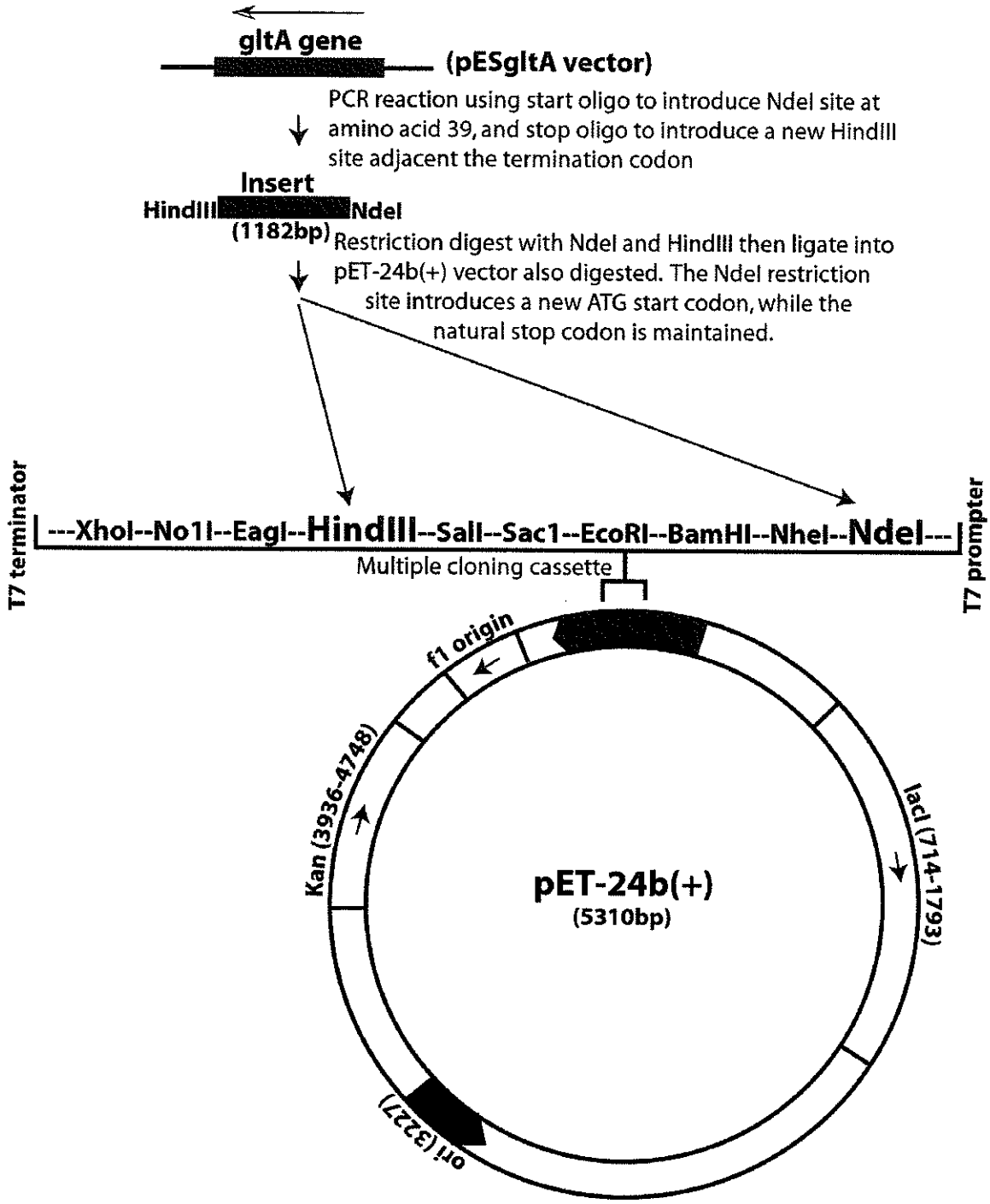

Figure 18: Molecular biology behind the introduction of the truncated citrate synthase gene into the pET-24b(+) vector.

Ligation and Transformation

Several different concentrations of insert and vector DNA were tried for the ligation reaction. The best result was obtained using 5µl vector (~30ng/µl = 30fmols in the reaction based on MW of 3731676g/mol), 5µl insert (~3ng/µl = 90fmols in the reaction based on MW of 157435g/mol), 4µl (5X) T_4 ligase buffer, 6µl ddH_20, and 1µl T_4 DNA ligase. The reaction was incubated overnight at 16°C. The following day 10µl of the ligation reaction was used to transform competent BL21DE3pLysS cells using the transformation procedure described in the "Routine Procedures" section.

Citrate Synthase Enzyme Assay

As already mentioned, citrate synthase catalyses the condensation of AcCoA and OAA to create citrate and free CoASH. The standard method for determining CS activity is to measure the levels of free CoASH via the use of 5,5'-dithiobis-2-nitrobenzoate (DTNB) (Srere et al., 1963). DTNB reacts rapidly with the sulfhydryl group of free CoASH generating 2-nitro-5-thio-benzoic acid, a yellow thionitrophenolate which absorbs at 412nm with an extinction coefficient of 13 600 $M^{-1}cm^{-1}$ (Figure 19). The production of the thionitrophenolate was measured using a Milton Roy Spectrophotometer, and activity was defined as the amount of enzyme required to produce 1µmol CoA per minute (1µmol CoA = 1µmol thionitrophenolate). Citrate synthase reactions were carried out in a total volume of 1ml consisting of 100µM

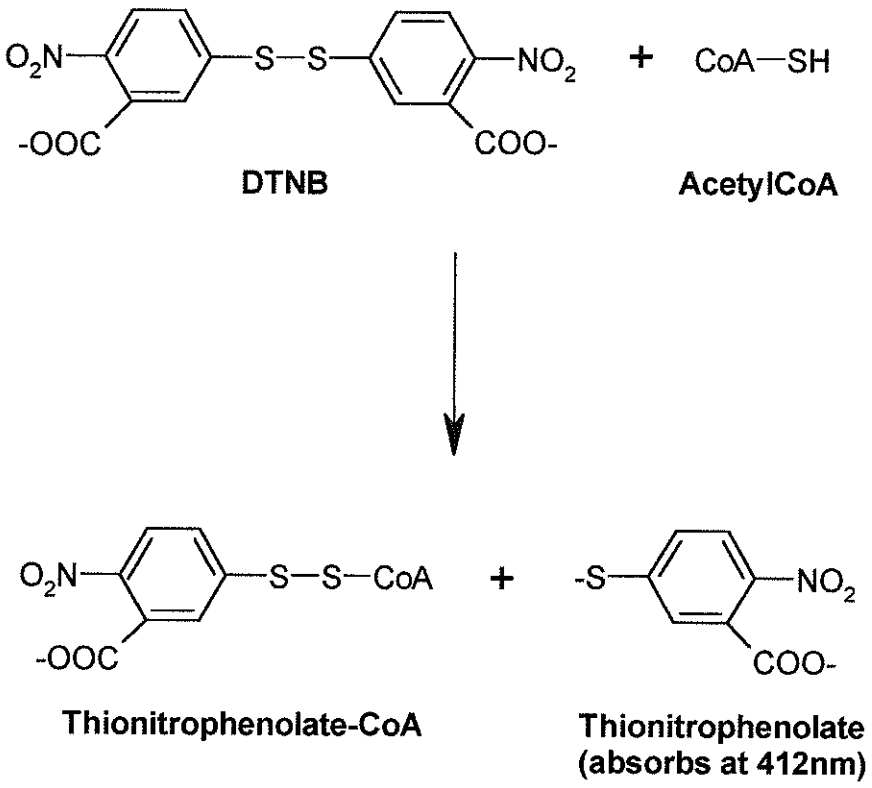

Figure 19: Free coenzyme A generated from the citrate synthase condensation reaction reacting with DTNB to form a yellow thionitrophenolate.

AcCoA, 100μM OAA, 50μM DTNB, 100mM KCL and standard Tris buffer (20mM Tris, 1mM EDTA, pH 7.8). A variety of kinetic experiments were carried out on each variant in order to determine the effects the mutation had on activity, substrate binding, and allosteric inhibition/activation. Saturation curves were determined for both OAA and AcCoA in order to determine the relative binding efficiency (Km) of substrates to the enzyme. For oxaloacetate, a range of 0-240μM OAA was used for saturation, while in the case of acetyl-CoA, a range of 0-2000μM AcCoA was used. A saturation curve for KCl was developed using a range of 0-180μM KCl. NADH inhibition curves were determined in the absence of KCl, using a 0-1000μM range. NADH inhibition, along with NADH binding (discussed in the next section), gave direct evidence of amino acid involvement in the NADH binding site. An array experiment was used in which the concentrations of each substrate were varied in respect to one another in order to study possible cooperativity within the active site. The array consisted of an AcCoA range of 25-500μM and an OAA range of 5μM-1mM. The array assays were carried out in total volumes of 600μl using the typical CS reaction mixture. A single CS stock was used when possible in order to decrease the error resulting from multiple dilutions. There are two things to note regarding the citrate synthase assay used for the kinetic studies: 1) the reaction of DTNB with free CoASH is much faster than the CS condensation reaction, therefore it was not essential to maintain a constant DTNB concentration providing that DTNB was in excess of the substrates; and 2) the enzyme concentration in all assays was low enough to prevent any false activity from the sulfhydryl groups on the protein reacting with the DTNB.

NADH Binding via Fluorescence Enhancement

NADH binding was studied using the fluorescence enhancement procedure from Duckworth and Tong (1976). The fluorescence studies were carried out on an Aminco-Bowman Spectrophotofluorometer using an excitation wavelength of 340nm and an emission wavelength of 430nm. Fluorescence cuvettes with a pathlength of 1.0cm were used for the analysis. NADH and citrate synthase stocks of 200μM and 150μM respectively, were made up fresh prior to each study. The NADH stock concentration was determined spectrophotometrically by way of the nicotinamide ring, which absorbs at a wavelength of 340nm with an extinction coefficient of 6220 $M^{-1}cm^{-1}$. Protein concentrations were determined using the absorbance at 280nm and the corresponding variant extinction coefficient (determined by Edelhoch method).

In order to determine the levels of NADH binding, three values must first be determined: 1) the fluorescence enhancement factor for bound NADH (E); 2) the specific fluorescence of free NADH (F_f); and 3) the specific fluorescence of bound NADH (F_b). The Enhancement factor is a measure of the increase in fluorescence, which arises when free NADH becomes associated with protein. A simple titration of a set amount of NADH with CS allows for the determination of (E). The F_f value is the slope of a plot of fluorescence vs free [NADH], and represents the fluorescence equivalent of 1μM free NADH. The F_b or specific fluorescence of 1μM bound NADH is the product of E and F_f. Following the equations below, a simple titration of a set amount of CS with increasing NADH levels yields the amounts of bound and free NADH present, and in turn leads to

the determination of the dissociation constant and number of available binding sites per subunit.

1) $F = [NADH]_{free} * F_f + [NADH]_{bound} * F_b$
2) $[NADH]_{total} = [NADH]_{free} + [NADH]_{bound}$

Combining equations 1 and 2 and solving for $[NADH]_{free}$ yields:

3) $$[NADH]_{free} = \left(\frac{[NADH]_{total} * F_b - F_f}{F_b - F_f} \right)$$

Knowing the levels of free and bound NADH allowed for the determination of Y ($[NADH]_{bound}/[CS]$) or the number of NADH per CS molecule. Using KaleidaGraph curve fitting, a plot of Y vs. $[NADH]_{free}$ gave a Michaelis-Menten plot with an asymptote equivalent to the number of NADH sites per subunit. A Scatchard plot of Y/ $[NADH]_{free}$ vs. Y gave a straight line with slope equal to $-1/K_D$.

Non-Denaturing Gels

The use of non-denaturing polyacrylamide gel electrophoresis (PAGE) gave insight into the shift from dimer/hexamer to dimer/tetramer equilibrium, found with both the R163L and K167A variants. The procedure described by Molgat et al., (1992) was used. A stacking gel of 5% acrylamide was used to focus the protein bands, while a running gel of 8% acrylamide was used for the separation of different CS multimers. A mini gel apparatus was used with a gel thickness of 0.1cm and dimensions of 15.7 X 18cm. A buffer of 33mM Tris-glycine, pH 7.5 was used to run the gel while a 10% acetic acid and 25% 2-propanol solution containing Coomassie Blue was used to stain the

protein bands. A single gel typically required a running time of ~1.5 hours at 25 milliamperes for gentle and distinct separation of bands.

Routine Procedures

DNA Isolation and Purification

Mutant DNA was routinely prepared in large scale for long term storage using a modified form of the alkaline-SDS method of Birnboim and Doly (1979). Following the phenol/chloroform extraction, the DNA was precipitated using 0.6 volumes isopropanol and incubated overnight at 4°C. Precipitated DNA was spun out and resuspended in 500µl dd$H_2$0. Once resuspended, an equal volume of 10M LiCl was added to the sample, which at a concentration of 5M selectively precipitates RNA. The precipitated RNA was spun down and the supernatant was combined with 0.6 volumes of isopropanol to precipitate the DNA. Following a half-hour precipitation period, the DNA was spun down and allowed to partially dry before resuspension in 100µl TE buffer (20mM Tris-Cl, 1mM EDTA, pH 8.0). The DNA was then placed in a –20°C freezer for long term storage.

Transformation

Preparation of competent cells for transformation of mutagenic DNA was carried out using the calcium chloride chemical method of Mandel and Higa (1970). A 2ml

overnight culture of the desired host was used to inoculate 100ml LB, which was then grown at 37°C for ~1.5 hours (mid log phase) followed by a 5 minute incubation on ice. Sterile culture tubes were filled and used for concentrating cells by centrifugation (5 minutes at 3 000g). The supernatant was replaced with 6ml of sterile, ice cold, 100mM $CaCl_2$ and left on ice for 20 minutes. The cells were again concentrated by centrifugation and resuspended in 150µl of 100mM $CaCl_2$. After 10 minutes on ice, a small volume of DNA solution was added (5-10µl depending on stock concentration) and the cells were again chilled on ice for ~20 minutes to allow for efficient DNA uptake. The culture was then heat shocked at 37°C for 15 minutes followed by the addition of 150µl of LB and a 45 minute incubation at 37°C. To finish the transformation and select for cells containing the desired plasmid, the complete culture was plated on LB plates containing the appropriate antibiotic.

Mutant Screening

Individual colonies from mutagenesis were selected, and used to inoculate 4mL LBA from which DNA was purified using the QIAprep Spin Miniprep Kit obtained from Qiagen (note: 2 washes of ethanol were used instead of the single wash suggested, followed by a 5 minute drying period on the bench). Concentration of purified DNA was determined (A_{260}) (OD of 1 = ~50ng/µl) and a volume equaling 1500ng was dried using a Speed-Vac system and sent to the Plant Biotechnology Institute in Saskatoon for sequencing. The antisense 210 oligo was used for all the NADH variants except T204A,

which was sequenced using the 163 sense oligo (Table 2.0). Mass spectrometry was used following protein purification to confirm that each variant protein had the expected mass.

Mass Spectrometry

The Mass spectrometry presented in this thesis, was done by Dr. Lynda Donald of the Duckworth lab. The time-of-flight instrument, TOF3 (Verentchikov et al., 1994 & Krutchinsky et al., 1998) used for the analysis is maintained by the lab of K. G. Standing and W. Ens from the University of Manitoba Physics Department. Sample preparations included the use of both Centricon 50 (Amicon) (Krutchinsky et al., 2000) and waterbugs (Orr et al., 1995) for buffer exchange. Buffer concentrations typically varied from 5mM NH_4HCO_3 to 100mM NH_4HCO_3 for nanospray experiments, following the procedure of Krutchinsky et al., (2000) (Donald, unpublished). Electrospray experiments were carried out in 5mM NH_4HCO_3 using the procedure of Ayed et al., (1998). Protein concentrations typically ranged from ~10μM for electrospray to 1-10μM for nanospray experiments. Denatured spectra were acquired using samples prepared in 2-10% acetic acid and 50% methanol, and run at a declustering voltage of 150 volts using N_2 as the collision gas. For analysis of the dimer/hexamer equilibrium, SF_6 was used as the collision gas, while the declustering voltage varied from 200-350 volts, depending on the stability of the multimeric states of the individual variants. For all spectra, the TOFMA program (Department of Physics, University of Manitoba) was used to carry out a deconvolution on all prominent charge envelopes in order to determine the mass and in turn the multimeric-state of each species.

Data Analysis of Kinetic Results

The Kinetic data presented in this thesis were all interpreted based on the Ordered Bisubstrate mechanism and equations which it predicts (Cleland et al., 1963). The four kinetic constants solved using the array experiment coupled with the equation of Cleland, included: 1) K_{iOAA} (dissociation constant for OAA in the absence of AcCoA); 2) K_{OAA} (Michaelis-Menten constant for OAA in the presence of saturating AcCoA); 3) k_{cat} (enzyme turnover rate); and 4) Vmax (maximum velocity acquired in the presence of saturating OAA and AcCoA). The data from the array experiment were fit to the Ordered Bisubstrate equation using the SigmaPlot Regression Wizard, with initial guesses for each parameter defined according to the wild type values.

Ordered Bisubstrate equation of Cleland (1963):

$$\frac{1}{v} = \frac{1}{V\max}\left(1 + \frac{K_{OAA}}{[OAA]} + \frac{K_{AcCoA}}{[AcCoA]} + \frac{(K_{iOAA})(K_{AcCoA})}{[OAA][AcCoA]}\right)$$

-Note: v represents the velocity for any combination of OAA/AcCoA concentration

Inverted and simplified for use with SigmaPlot curve fitting:

$$v = \frac{V\max[OAA][AcCoA]}{[OAA][AcCoA] + K_{OAA}[AcCoA] + K_{AcCoA}[OAA] + (K_{iOAA})(K_{AcCoA})}$$

The preliminary kinetic studies were carried out in the presence of 100mM KCl, and included saturation curves for both OAA (presence of 200μM AcCoA), and AcCoA (presence of 200μM OAA) along with a tentative value for k_{cat} (determined in the presence of 100μM AcCoA and 100μM OAA). Michaelis constants for both K_{OAA} and K_{AcCoA} were determined by fitting the data to the Michaelis-Menten equation using the curve fitting function in KaleidaGraph.

Kaleidagraph was also used to fit activation curves for KCl to a modified version of the Michaelis-Menten equation, which took into account the initial velocity measured in the absence of KCl.

Modified Michaelis-Menten equation:

$$V - V_i = \frac{(V_\infty - V_i)[KCl]}{K_m + [KCl]}$$

V = Velocity at any point along the curve
V_i = Initial velocity
V_∞ = Infinite velocity
K_m = Michaelis constant for KCl

Simplified for Kaleidagraph curve fitting:

$$V = \frac{V_\infty[KCl] + (V_i)(Km)}{Km + [KCl]}$$

In order to test the amount of cooperativity associated with KCl activation, Hill plots were also done, which fit log(v/Vmax-v) against the log[KCl]. The Hill number was determined from the slope of a straight line through the data using least-mean-square fit. A Hill number equivalent to 1 represents no cooperativity, and would represent a hyperbolic curve with no sigmoidal tendencies, for a plot of velocity against KCl concentration. A value greater then 1 indicates cooperativity, with the higher the value, equivalent to a greater sigmoid characteristic, associated with the Michaelis-Menten plot.

Results

NADH Variants

The allosteric inhibition of *E. coli* and other hexameric citrate synthases has been well documented in the past 20 to 30 years. However, the allosteric mechanism and site of NADH binding have not been determined due to the lack of a crystal structure for the Type II citrate synthases. The recent crystal structure of the *E. coli* CS variant, F383A with bound NADH (Nguyen et al., in preparation), has made it possible to target those residues which make up the allosteric site. Using the structure of the co-crystallized F383A/NADH, residues targeted for mutagenesis were selected based on the criteria discussed in the Materials and Methods section. The 8 residues, whose side chains are within ~3.2Å of NADH in the crystal structure, include R109, H110, T111, Y145, R163, K167, Q182, and N189. A ninth residue, namely T204 was also selected for mutagenesis, as it sits within 3.38Å of the N1 nitrogen of the adenine ring. Two of these residues under investigation, namely Q182, and T204, are provided to the allosteric site from an adjacent dimer to that of the other residues. If these two residues are, in fact involved in NADH binding, they would represent an allosteric connection between one dimer and another. In other words, Q182 and T204 may represent the transfer points for the allosteric signal within the hexameric complex, as the individual subunits shift concertedly from R to T state in response to NADH. One aspect of the NADH site that should be noted is that these above-mentioned residues only represent a portion of the interactions that occur between citrate synthase and NADH. The crystal structure also shows main chain atoms, which are situated in positions where possible hydrogen bonds

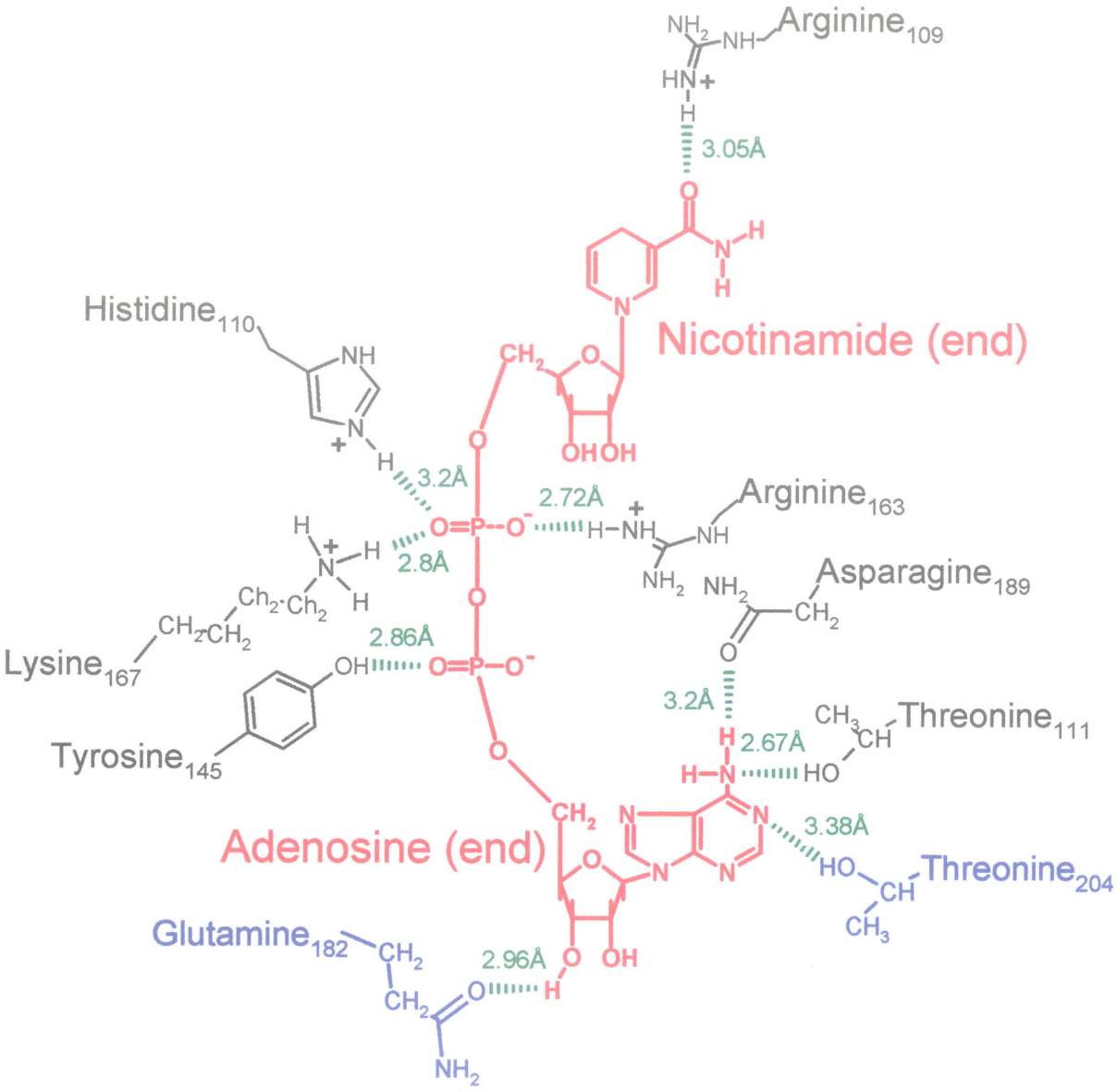

Figure 20: Two-dimensional arrangement of residues, within the allosteric site and their relative positions with respect to NADH. Possible hydrogen bonds are shown in green along with their corresponding distances. Glutamine182 and threonine204 are shown in blue, as these two residues are provided by an adjacent dimer. NADH is shown in red. This figure is based on the crystal structure of Nguyen et al., (in preparation).

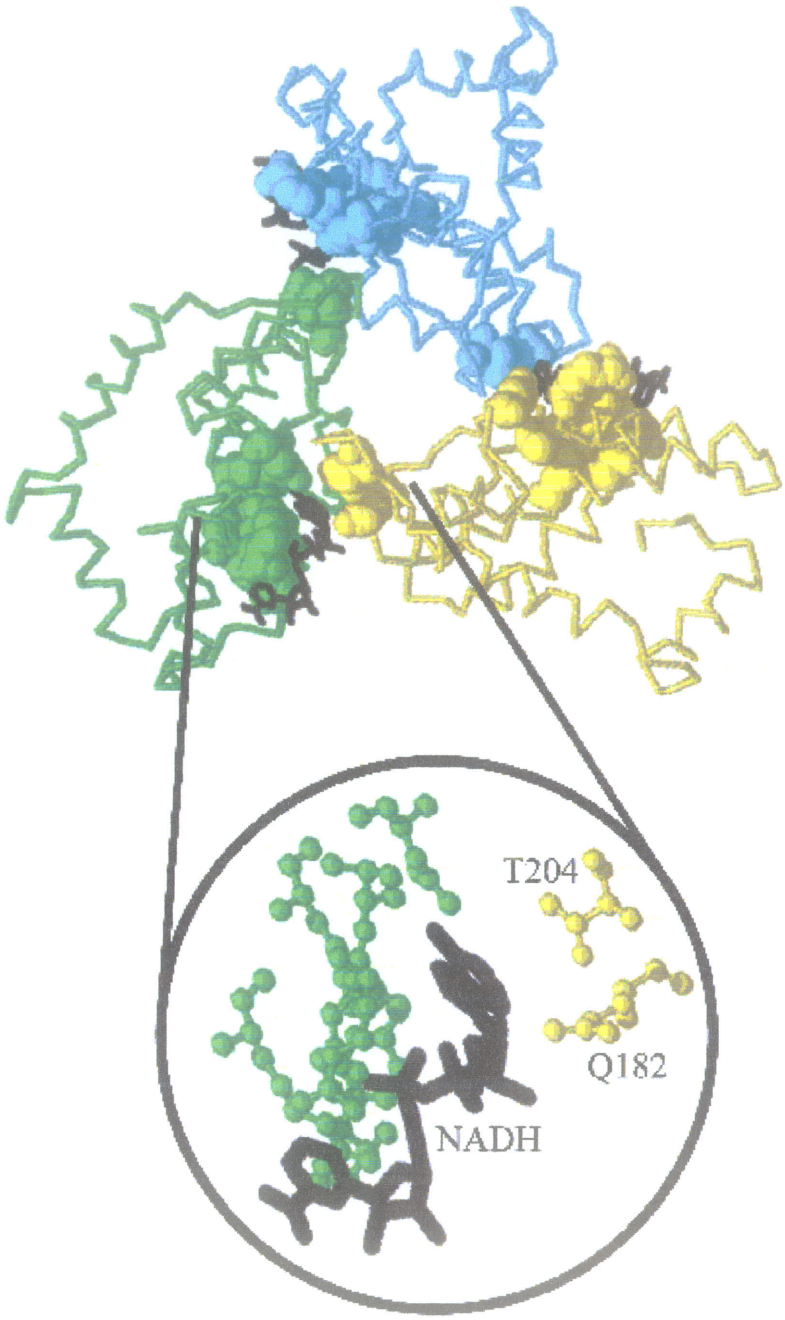

Figure 21: Crystal structure showing the relative positions of the residues which sit within 3.2Å of NADH. The top portion of the figure shows only residues 100-250 of each subunit (blue,green,red), with only one monomer from each dimer pair visible. The bottom portion of the figure shows contribution of T204 and Q182 to the allosteric site from an adjacent dimer (yellow), and the remaining residues shown in green. NADH is shown in black.

may occur. As well, a variety of van der Waals forces must also be involved in the binding mechanism.

With the exception of the Y145F protein, all of the NADH binding variants discussed in this chapter showed normal protein peaks from the DE52 and G200 columns, with slight variations in the levels of activity copmared to that of a wild type preparation. In contrast to the other variants, the Y145F showed decreased stability, apparent from small protein peaks off both columns, and low levels of activity. These two problems led to a final Y145F preparation, which contained higher levels of background proteins than normal, and this made it impossible to calculate a molar extinction coefficient for this protein. Therefore, it must be noted that the protein concentration for this variant was calculated using the average molar extinction coefficient of all the NADH variants.

NADH Binding and Inhibition

Before carrying out any kinetic studies, variants suspected of interacting with NADH were initially tested for NADH binding using the procedure of Duckworth and Tong (1976). Once it was verified that the mutation had some affect on the dissociation constant, a complete set of kinetic measurements was made. The NADH binding and inhibition results for the complete set of variants mentioned above are listed in Table 4. Of the variants studied, the R109L variant demonstrated tighter NADH binding with a dissociation constant (K_D, dissociation constant determined in the absence of substrates) of 1.16μM and an inhibition constant (K_i, inhibition constant determined in the presence

	NADH BINDING			NADH INHIBITION	
Parameter	**K_D, (μM)**	**# of Sites**	**ΔG, (KJ/mol)**	**K_i, (μM)**	**% Inhibition**
Wild Type	1.6±0.1	0.5	-	5.0±0.6	~99
R109L	1.16±0.04	0.9	0.79	1.6±0.3	94
H110A	5.2±0.2	0.2	-2.9	104±14	71
T111A	6.6±0.2	0.3	-3.5	34±8	50
Y145F	NPTD	NPTD	NPTD	NPTD	none
R163L	5.81±0.04	0.2	-3.2	NPTD	none
K167A	4.1±0.2	0.3	-2.3	NPTD	none
Q182A	6.1±0.5	0.9	-3.2	17±3	97
N189A	6.9±0.8	0.4	-3.6	127±25	50
T204A	10.2±0.4	0.2	-4.5	95±27	53

NPTD = Not Possible To Determine

Shaded rows are those residues from an adjacent dimer

Table 4: NADH binding and inhibition results for the nine residues under investigation compared with the wild type enzyme. Both experiments were carried out in the absence of KCl. The ΔG value represents the change in NADH binding free energy resulting from each mutation, calculated using the equation $\Delta G = -RT \ln K_D\text{variant}/K_D\text{wild type}$.

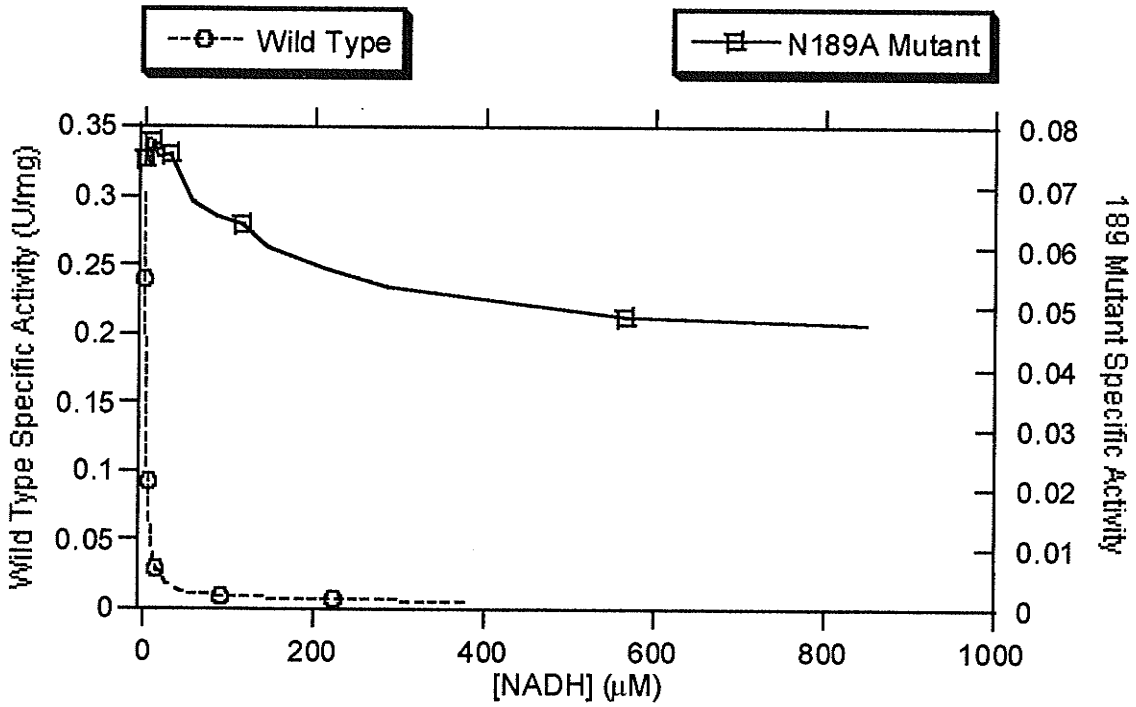

Figure 22: Sample plot showing the NADH inhibition of wild type citrate synthase compared with that of the N189A variant.

of substrates) of 1.6μM compared with 1.6μM and 5.0μM respectively for the wild type enzyme. Although to varying degrees, the eight remaining residues all showed decreased NADH binding and inhibition. One striking result was the complete lack of NADH inhibition with the Y145A, R163L, and K167A variants. In all three variants, attempting to saturate the enzyme with NADH led to a slight increase in activity. This is most likely due to contaminating salt, which would come from the NADH, originally stored as a disodium salt. As already mentioned the Y145A variant appeared to be unstable, which led to a purified stock with a low concentration and high levels of background contaminating proteins. Therefore, it was not possible to use the procedure of Duckworth and Tong (1976), to determine the dissociation constant for NADH, as the background contaminants appeared to cause fluctuations in the fluorescence values.

The K_D values for all the variants, with the exception of the R109L, showed an increase, which confirms that these residues are all involved in NADH binding. The loss in binding free energy as a result of each mutation, ranges from –2.3KJ/mol to –4.5KJ/mol, which matches well with the free energy change associated with the loss of a single hydrogen bond (2.0-6.0KJ/mol) as defined by Fersht, (1985). The K_i values for all the variants vary considerably, from high values of 127μM and 104μM, seen with the N189A and H110A variants respectively, to a low value of 17μM seen with the T182A variant. Of all the variants investigated, the T204A variant showed the greatest effect on NADH binding with a dissociation constant of 10μM. This result, coupled with the fact that this residue is provided by an adjacent dimer, along with the Q182A residue, gives direct evidence of a connection between the hexameric structure of *E. coli* CS and its allosteric properties. When looking at the R163L and K167A variants, it is interesting to

note that both these variants show K_D values similar to the other NADH variants, yet they demonstrate no inhibitory response in the presence of substrates. This result suggests that these two residues may be responsible for the "crosstalk" between the allosteric site and active site. However, upon further investigation, using mass spectrometry, Dr. Lynda Donald was able to determine that NADH binding to the R163 and K167A variants is non-specific. The mass spectrum of the wild type enzyme shows increased hexamer, at the expense of dimer, upon NADH addition. Further, the ions of the hexamer change to higher m/z in response to increased concentrations of NADH. In contrast, the R163L and K167A variants showed binding of NADH to both the dimer and hexamer, in a concentration dependent manner (Dr. Lynda Donald personal communication). Therefore, it would appear that with these two variants, and possibly the Y145A variant, which also shows no inhibition, the allosteric site has been blocked, such that NADH can no longer bind specifically.

One result to note, which matches that of Duckworth and Tong (1976), is that the number of occupied sites per subunit is in most cases much less than the expected value of one. With the knowledge that there is in fact one binding site per subunit (Ayed et al., 1998), this result implies that not all the possible binding sites within the hexamer are occupied during the time interval that the experiment is carried out. One possible explanation for this is that the conversion of dimers to hexamers in response to NADH is very slow. If the allosteric site is composed of residues from adjacent dimers, then it would follow that in order to get all six sites, hexamerization must occur. Therefore, not all the sites are available during the time allotted for the assay, which would explain the low number of sites observed.

A final comment, which should be made regarding the data in Table 4, is on the K_i/K_D ratio, which is a direct representation of the ability of substrate to affect NADH binding. Changes in the K_i/K_D ratio are reflected by changes in the allosteric constant L, which was defined by Monod, Wyman and Changeux (1965) as the ratio of the concentration of protein in the T state to that of the R state in the absence of ligand. Therefore, when looking at the results shown in Table 4, it appears that the different mutations have different effects on the equilibrium between T-state and R-state.

Steady State Kinetics

Preliminary Kinetic Results

Prior to running a complete array experiment, which involves varying both substrates with respect to one another to determine precise steady state kinetics, preliminary experiments were done on each variant in order to detect any general variations in their kinetic properties. The preliminary values for the k_{cat} (enzyme turnover rate), K_{OAA} (Michaelis constant for OAA), and K_{AcCoA} (Michaelis constant for AcCoA) were all determined. However, as already mentioned above, these values are only preliminary results, as the experiments were carried out with one or both of the substrates at fixed concentrations. Table 5 shows the preliminary kinetic results for all of the NADH variants, while Figures 23 and 24 show sample AcCoA and OAA saturation curves respectively. From the preliminary kinetic data, it is obvious that mutations of residues within the NADH site, to varying degrees, have some effect on binding of

substrates to the active site. The R109L and R163L variants, both appear to have slightly increased binding affinity for both substrates, while the Y145A and K167A variants showed the greatest decrease in substrate binding affinity. This type of counter-effect upon the active site, as a result of mutations to the allosteric site, is to be expected, as the two sites must communicate with one another in an allosteric protein.

Parameter	k_{cat} (sec^{-1})	K_{OAA} (μM)	K_{AcCoA} (μM)
Wild Type	81	26±5	120±20
R109L	63	18±1	68±5
H110A	25	115±14	268±27
T111A	28	64±1	152±13
Y145F	20	136±10	320±14
R163L	49	11±1	71±6
K167A	20	188±13	397±18
Q182A	53	32±2	123±7
N189A	43	56±6	147±12
T204A	28	66±5	291±13

Shaded rows are those residues from an adjacent dimer

Table 5: Preliminary kinetic data for the NADH variants. k_{cat}/sec was determined under standard assay conditions, while K_{OAA} was determined with a fixed AcCoA concentration of 200μM AcCoA, and K_{AcCoA} was determined with a fixed OAA concentration of 200μM as well. (wild type values taken from Anderson, 1988)

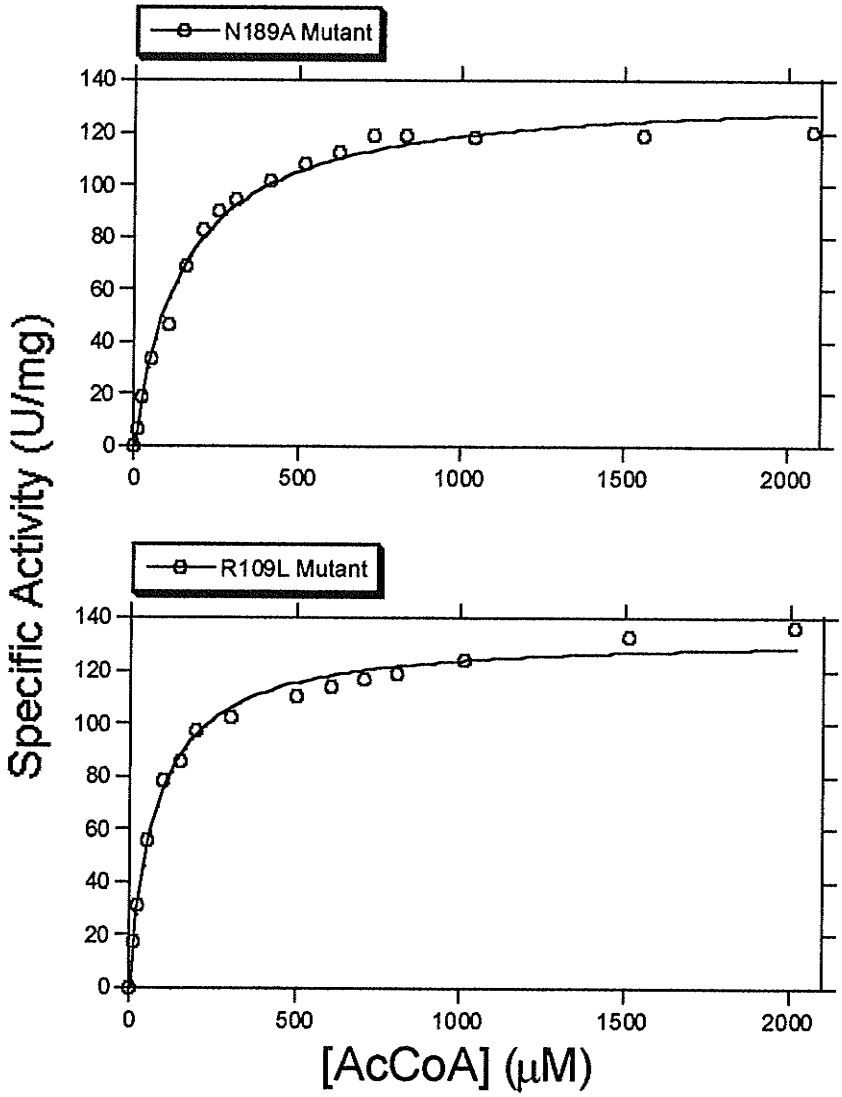

Figure 23: Sample AcCoA saturation curves, comparing the N189A variant, with the R109L variant, which shows similar values to that of the wild type. Data were fit to the Michaelis-Menten equation using Kaleidagraph. The OAA concentration used for the preliminary AcCoA saturation experiments was 200μM.

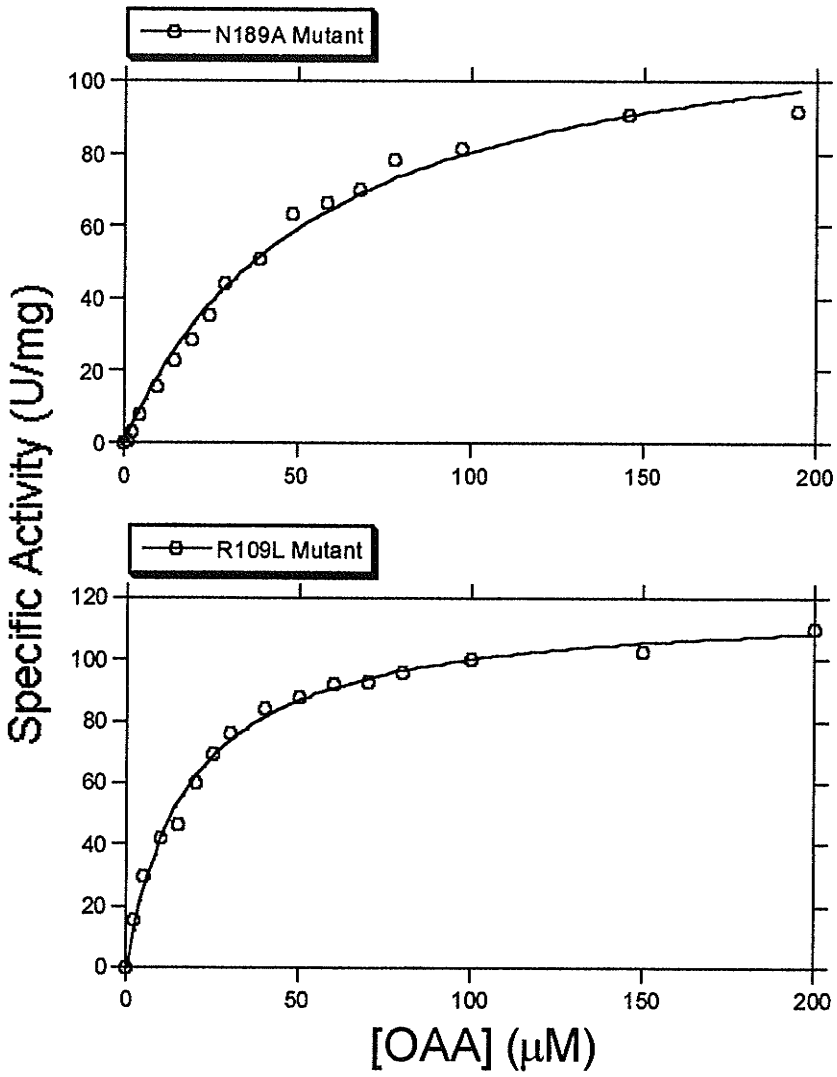

Figure 24: Sample OAA saturation curves, comparing the N189A variant, with the R109L variant, which shows similar values to that of the wild type. Data were fit to the Michaelis-Menten equation using Kaleidagraph. The AcCoA concentration used for the preliminary OAA saturation experiments was 200μM.

Kinetic Results based on the Array Experiment

Table 6 shows the complete set of steady state kinetic results, based on the substrate array experiment described in the Materials and Methods section. Figures 25 and 26 show graphical representations of the array data for one of the NADH variants. The array results appear, for the most part, to agree with the preliminary studies. One general observation that can be made is that the enzyme turnover rate for all the variants, with the exception of the Y145A, appears to be normal. The Y145A variant showed almost a 2 fold drop in specific activity. However, the fact that purifying this variant posed a problem, and that the extinction coefficient could not be determined accurately, may also contribute to the low k_{cat} value, as the enzyme concentration would not be accurately known. Excluding the Y145A and K167A variants, which both showed increases in K_{OAA}, the rest of the NADH variants appeared to show a general trend towards an increased binding affinity for OAA in the presence of AcCoA. Several variants, including H110A, R163L, Q182A, and T204A, all showed dramatic increases in OAA binding strength, with as much as an 8 fold decrease in K_{OAA} with the H110A variant. This result again strengthens the idea of "crosstalk" between the active site and allosteric site on the enzyme. The K_{iOAA}, in contrast to the wild type enzyme, appears to increase in all the variants to varying degrees. With the wild type enzyme, the values for K_{OAA} and K_{iOAA} are basically the same, which indicates that the presence of AcCoA has no influence on the binding of OAA. All the NADH variants, however, show a ten fold or greater K_{iOAA} compared with their K_{OAA} values, which would imply that in all the variants, AcCoA influences the binding of OAA. When looking at the K_{AcCoA} value for most of the NADH variants, it is apparent that mutations to the allosteric site result in an

Parameter	k_{cat} (sec^{-1})	K_{OAA} (μM)	K_{iOAA} (μM)	K_{AcCoA} (μM)	K_m, KCl (mM)	KCl Activation Ratio	Hill #
Wild Type	81±6	26±5	33±7	120±20	28±4	39±3	1.0
R109L	121±5	7±4	98±24	69±24	43±6	37±2	2.3
H110A	67±5	3±15	458±212	49±17	47±2	30±2	4.3
T111A	54±4	18±20	360±137	79±21	64±3	75±3	2.3
Y145F	36±2	51±17	108±26	229±31	45±3	18±4	2.6
R163L	108±4	5±4	55±13	80±8	15±2	46±1	1.0
K167A	84±6	37±19	134±34	223±35	36±1	22±1	3.0
Q182A	95±2	10±3	93±16	56±5	27±5	43±5	2.2
N189A	124±4	17±6	148±29	69±8	36±2	31±3	2.2
T204A	118±7	4±11	118±27	206±29	40±8	130±13	2.7

Shaded rows are those residues from an adjacent dimer

Table 6: Steady state kinetic results for the NADH variants, compared with the wild type enzyme. (wild type data from Anderson, 1988) The activity and substrate binding constants were determined in the presence of 100mM KCl.

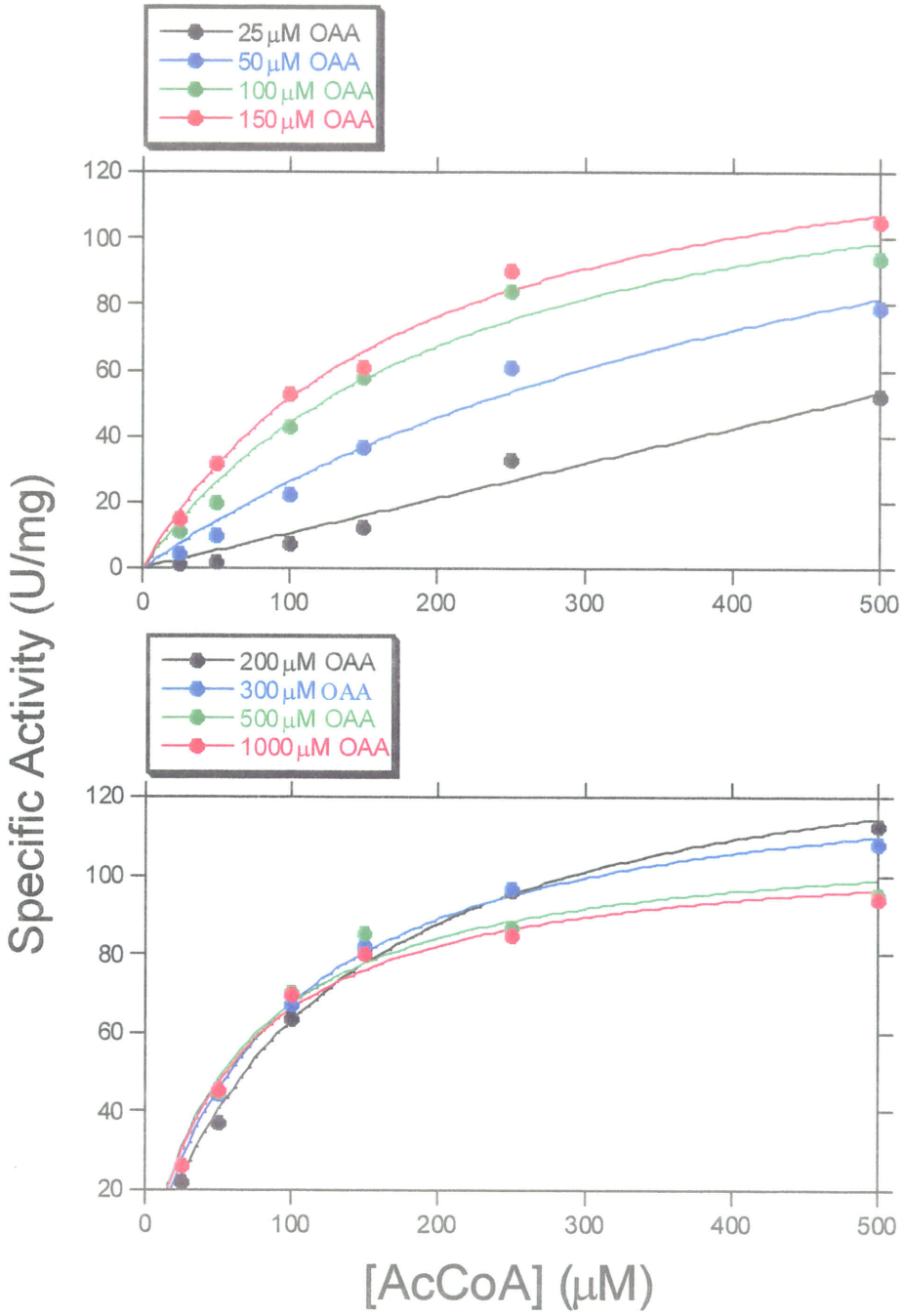

Figure 25: Graphical representation of a set of array data, showing the specific activity for the N189A variant, as a function of AcCoA concentration at various OAA concentrations. Note the small amount of substrate inhibition, which is clearly visible at ~500μM OAA.

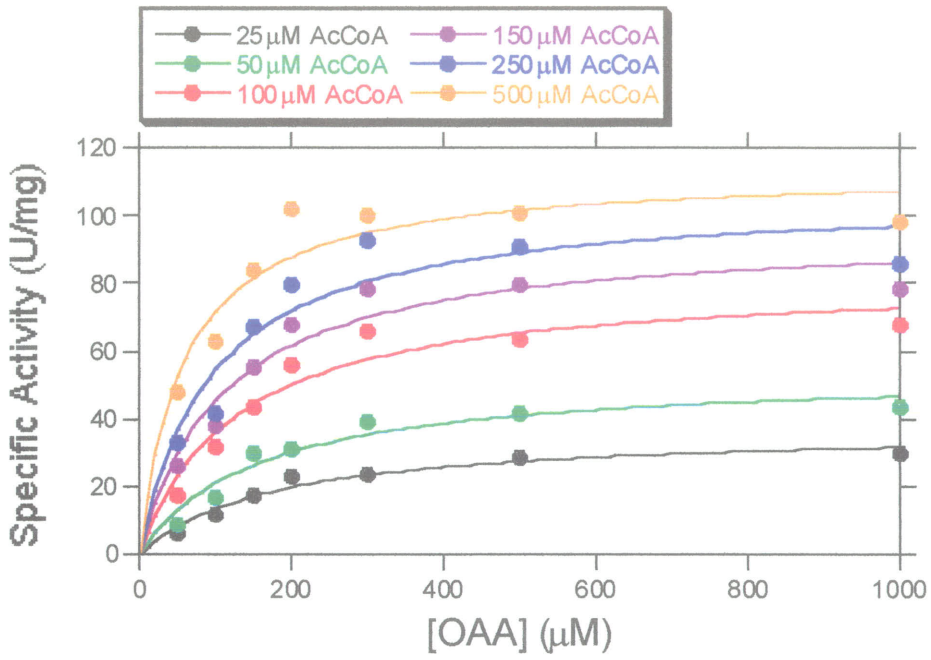

Figure 26: Graphical representation of a set of array data, showing the specific activity for the N189A variant, as a function of OAA concentration at various AcCoA concentrations.

increased binding affinity for AcCoA. The H110A and Q182A variants both showed 2 fold decreases in K_{AcCoA} with values of 49±17μM and 56±5μM respectively. The three variants which contrasted this trend included Y145F, K167A, and T204A, all of which showed almost 2 fold decreases in AcCoA binding. This would imply that these three residues are not only involved in NADH binding, but also through some indirect way (i.e. allostery), help to stabilize the AcCoA binding site.

KCl Activation

Table 6 shows the KCl activation results for the NADH variants, including the K_m, KCl (Michaelis constant for KCl), the "Activation ratio" (ratio of limiting catalytic rate at saturating KCl to the rate obtained without KCl), and Hill numbers (degree of cooperativity between subunits associated with KCl activation). From the results displayed in Table 6, it is apparent that the K_m, KCl value for most of the variants is slightly higher then that for the wild type enzyme. The T111A variant showed the greatest increase with a value of 64±3μM, a 2 fold increase from that of the wild type. Therefore, it follows that the ability for KCl to bind these variants has decreased to varying degrees, with the T111A having the weakest KCl binding. The Activation ratio for KCl represents the level to which saturating KCl activates the enzyme, or in terms of the allosteric equilibrium, the extent to which KCl shifts the enzyme from an inactive T-state, to an active R-state. With most of the NADH variants, the effect of KCl on the allosteric equilibrium is basically the same as the wild type enzyme. However, several variants, including Y145A and K167A, show 2 fold decreases in the activation ratio. These two variants respond to KCl only half as much as the wild type enzyme does. In

other words, these mutations have shifted the allosteric equilibrium in favor of an active R-state, such that in the absence of KCl, these variants show a larger portion of their overall activity than the wild type enzyme. In contrast to the Y145A and K167A variants, the T111A and T204A variants showed 2 and 3 fold increases in the KCl activation ratios respectively. Therefore, the allosteric equilibrium for both these variants is shifted towards the inactive T-state, as they respond to KCl more than the wild type enzyme.

One interesting result, which was found when studying the KCl activation of the NADH variants, was the apparent sigmoid saturation curve displayed in most of the variants. Of the NADH variants, only one displayed the characteristic hyperbolic KCl saturation of the wild type enzyme, R163L. Figure 27 shows the hyperbolic saturation curve of the R163L variant compared with the sigmoid result found with the N189A variant. This sigmoid KCl saturation curve, found with the majority of the NADH variants, indicates that there is cooperativity between subunits within the hexamers, as they convert from T-state to R-state in response to increasing levels of KCl. This result is shown by the Hill number, which is a direct representation of the degree of cooperativity. The greatest effect is shown with the H110A variant, which showed a Hill number of 4.3, which indicates that there is substantial cooperativity between subunits as the enzyme is activated by KCl. Figure 28 shows Hill plots for the R109L and H110A variants, compared with the R163L variant, which showed a Hill number equivalent to the wild type enzyme.

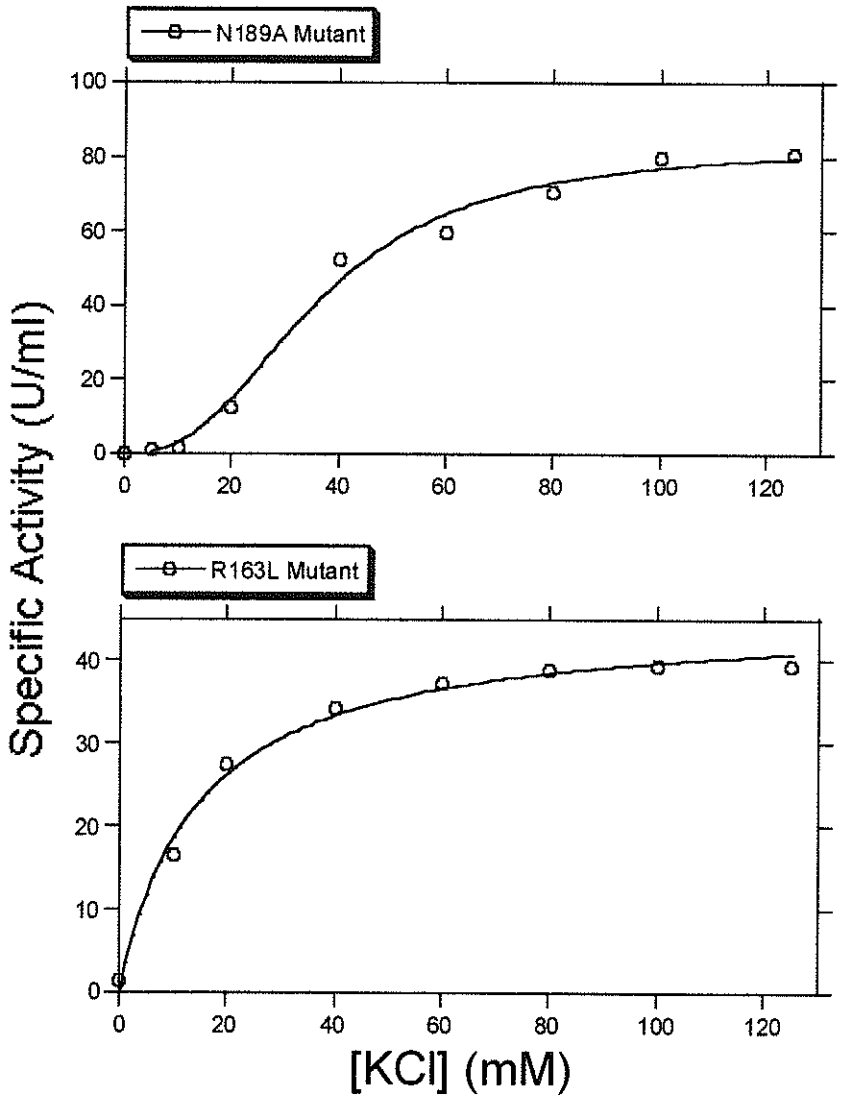

Figure 27: Sample KCl saturation curves comparing the sigmoid saturation seen with the N189A variant (characteristic of the majority of the NADH variants), and the hyperbolic saturation seen with the R163L variant.

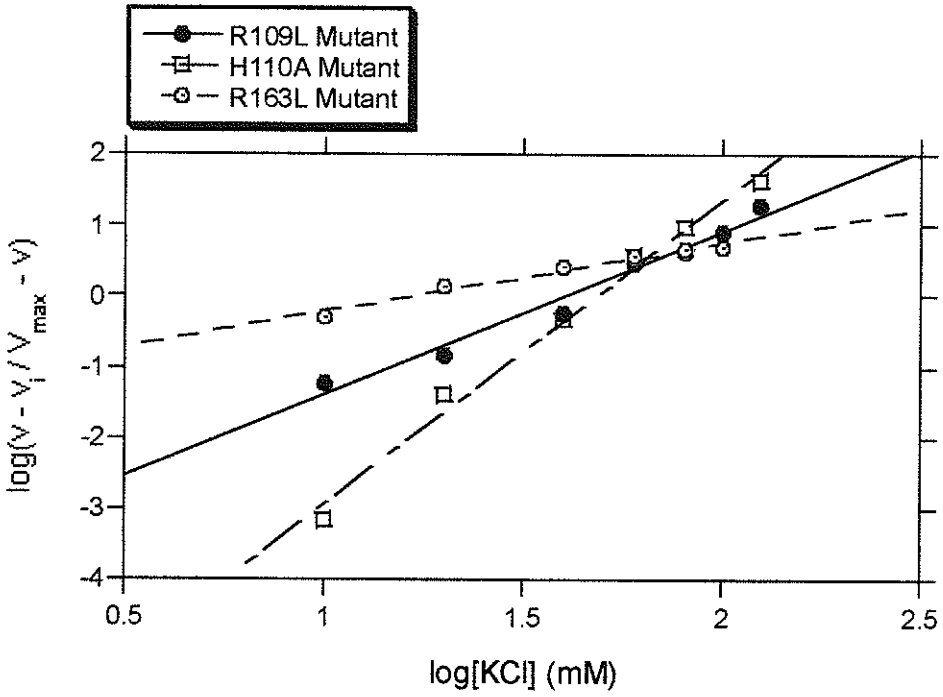

Figure 28: Hill Plots for KCl activation of the R109L (Hill # = 2.3), H110A (Hill # = 4.3), and R163L (Hill # = 1.0) variants. Determined under standard assay conditions.

Mass Spectrometry and Non-Denaturing Gel Electrophoresis

Electrospray and nanospray time-of-flight mass spectrometry served two key functions in the analysis of the CS variants described in this thesis. First, it allowed a check that the correct variant had been obtained by verifying the subunit mass. Second, it could be used to assess any effects of the mutation on the dimer/hexamer equilibrium. A typical denatured electrospray spectrum and the associated deconvolution, which generates a mass for the protein being studied, is shown in Figure 29. The subunit mass determined, 47860±27Da, agrees with that expected for the variant protein, 47856Da.

Non-denaturing gel electrophoresis was used as a crude method for looking at the dimer/hexamer equilibrium for the R163L and K167A variants. The advantage of the non-denaturing gels is that the proteins could be analyzed under native buffer conditions (presence of KCl), while only a limited number of buffer salts, which do not include KCl, can be used for mass spectrometry.

The dimer/hexamer equilibria for several of the NADH variants, including R109L, T182A, R163L, K167A, and T204A were studied using mass spectrometry. Of these selected variants, the R109L was the only one to show an equilibrium similar to that of the wild type enzyme, while the remaining variants showed variations in the stability of their hexamers. Sample spectra for the T182A, and R163L can be seen in Figures 30 and 31 respectively. From the spectra, it is apparent that these two NADH variants show higher levels of dimer compared with the wild type enzyme under similar conditions. Therefore, it follows that the stability of the hexamer in all these variants has decreased, resulting in greater dissociation of the multimeric-state to the dimeric-state.

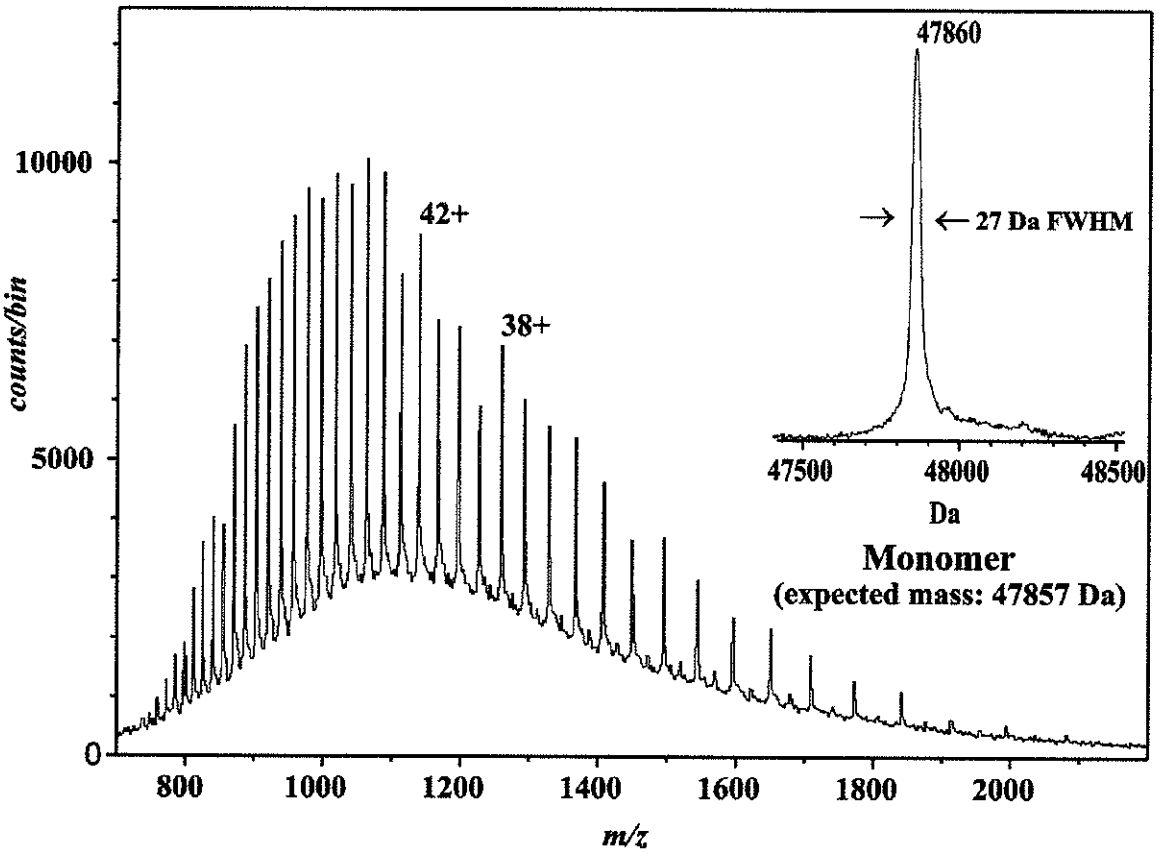

Figure 29: A typical ESI TOF mass spectrum, showing the denatured spectra of the T111A variant. The deconvolution of the denatured monomer gives a mass of 47860Da, with an error of ±27Da (width at half peak height). The sample was prepared using waterbug dialysis, with a final concentration of 6.3μM protein in 10% acetic acid and 50% methanol. The sample was run at 150V declustering voltage, using N_2 as the curtain gas.

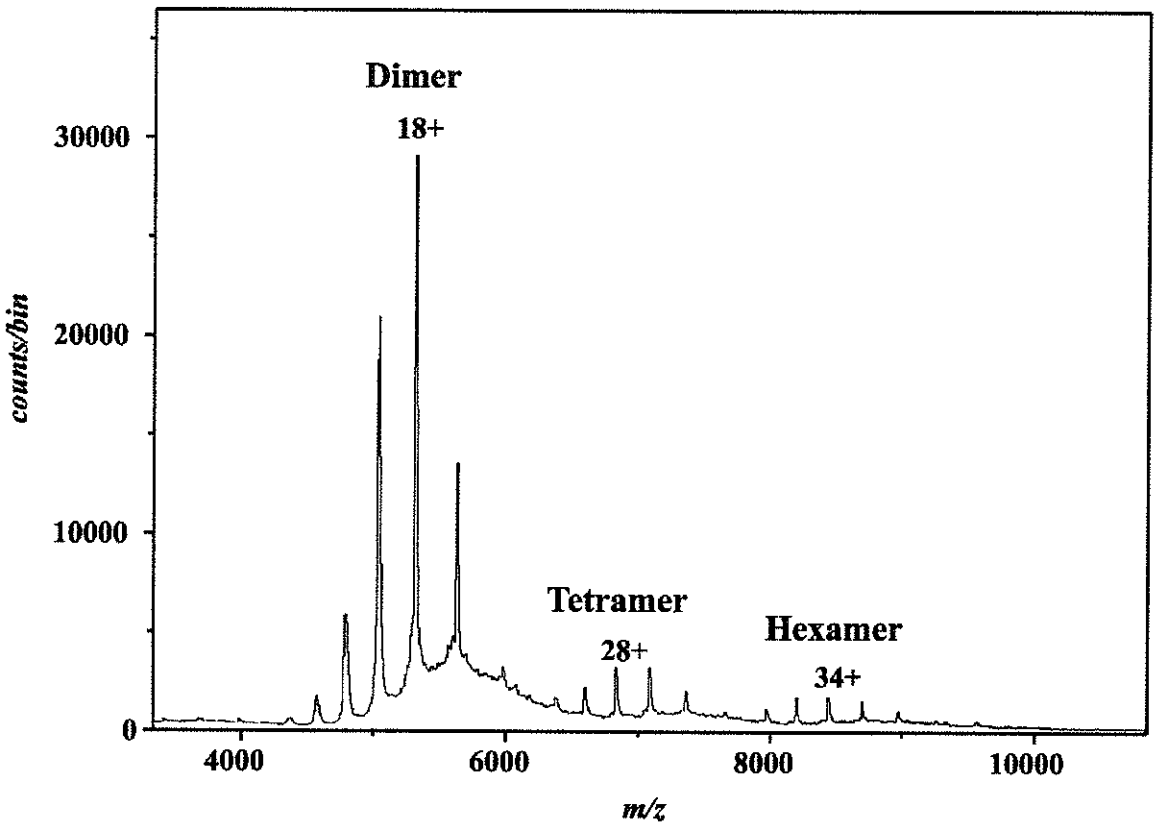

Figure 30: Nanospray ionization mass spectra of the Q182A variant, showing a predominant dimer conformation. The sample was prepared in a Centricon 50 in 100mM NH_4HCO_3. The protein concentration was 7.65μM monomer. Under these conditions the wild type protein would show all hexamer (Dr. Lynda Donald personal communication). The sample was run at 300V declustering voltage using SF_6 as the curtain gas.

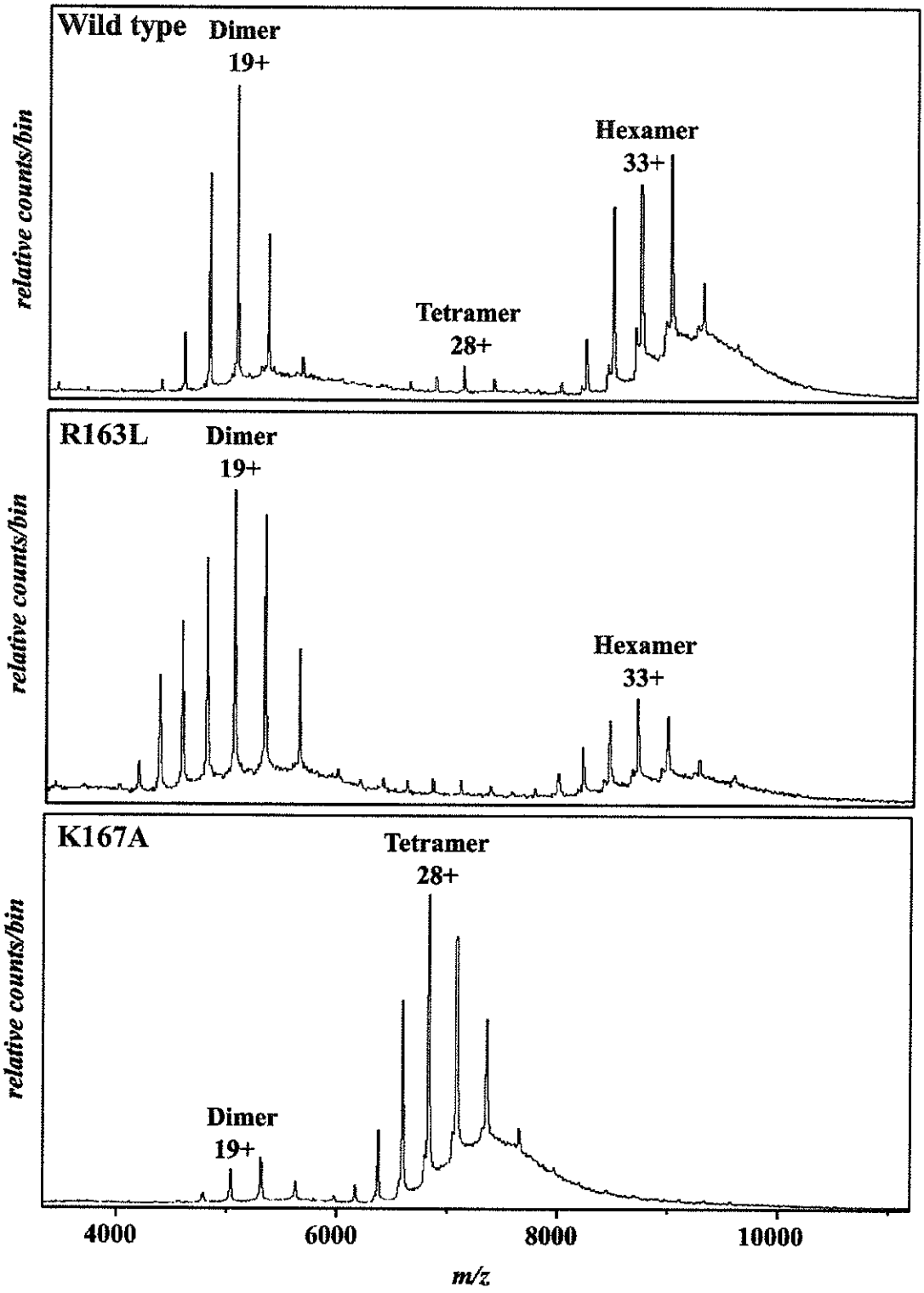

Figure 31: Nanospray ionization mass spectra of the R163L and K167A variants compared with the wild type. The samples were prepared in a Centricon 50 in 100mM NH_4HCO_3. The protein concentrations were all 10μM monomer. Note the decreased stability of the hexamer in the R163L variant, and the novel K167A tetramer. The samples were all run at 300V declustering voltage using SF_6 as the curtain gas.

The mass spectrometry results for the K167A and T204A variants are shown in Figure 31 and Figure 32 respectively. From the spectra of both variants, it is apparent that these changes have resulted in a tetrameric species, not typically found with the wild type protein. With the T204A variant, this result is not completely unexpected, as this residue sits within the contact regions between dimers. A second interesting aspect of the K167A variant is that the dimer is extremely stable. Under wild type denaturing condition, including 10% acetic acid and a declustering voltage of 400 volts the K167A variant shows a stable dimer, while the wild type protein is monomeric under these conditions (Dr. Lynda Donald personal communication). Further, SDS-PAGE of K167A showed two bands, the first running at the expected mass of ~47000Da and a second band at ~90000Da (data not shown).

To further verify the presence of this novel tetramer the K167A protein was run on a non-denaturing polyacrylamide gel. The R163L variant was also run, as it sits in close proximity to the K167 residue. From the non-denaturing gel shown in Figure 33, it appears that the K167A and R163L proteins both show a tetrameric association, under native buffer conditions. The result of the R163L variant was unexpected as it contradicts the dominant dimeric structure seen under mass spectrometry conditions.

One interesting question to ask regarding the K167A and T204A variants is: Which of the two conformations, namely tetramer or dimer, is the active form of the enzyme? To address this question, an experiment involving mass spectrometry and the DTNB enzyme assay were coupled. Several aliquots of the K167A variant were prepared in different buffer concentrations, with identical protein concentrations in each. The mass spectrometry results showed that as the buffer concentration was increased from

5mM NH_4HCO_3 to 100mM NH_4HCO_3, the K167A variant converts from all dimer to mainly tetramer (Dr. Lynda Donald personal communication). The samples which were used for the mass spectrometry were then tested for CS activity in the same buffer, and the result can be seen in Figure 34. As buffer concentration increased, so did the level of activity. From the results of the two experiments, it could be reasoned that the tetramer represents the active form of the this variant.

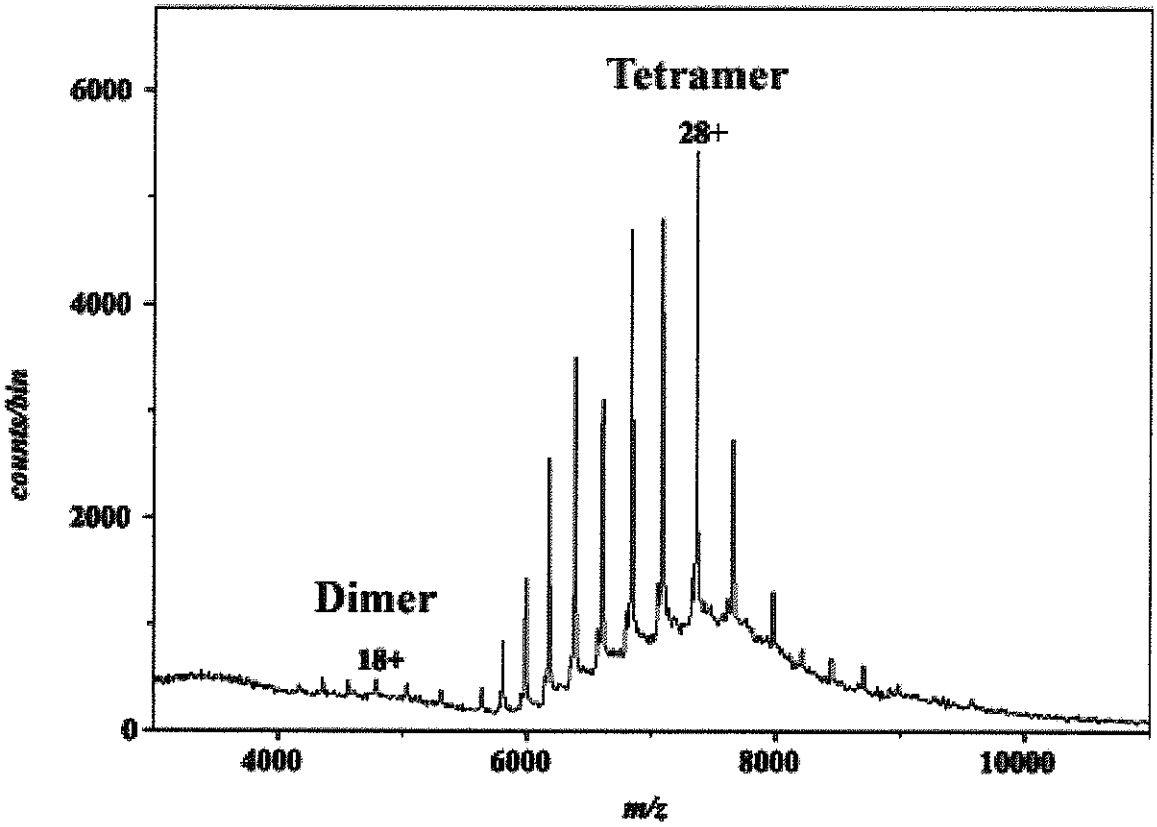

Figure 32: Nanospray ionization mass spectra of the T204A variant, showing a predominant tetramer conformation. The sample was prepared in a Centricon 50 in 100mM NH_4HCO_3, followed by dilution into 20mM NH_4HCO_3. The protein concentration was 2.0μM monomer. Under these conditions the wild type protein would show all dimer (Dr. Lynda Donald personal communication). The sample was run at 300V declustering voltage using SF_6 as the curtain gas.

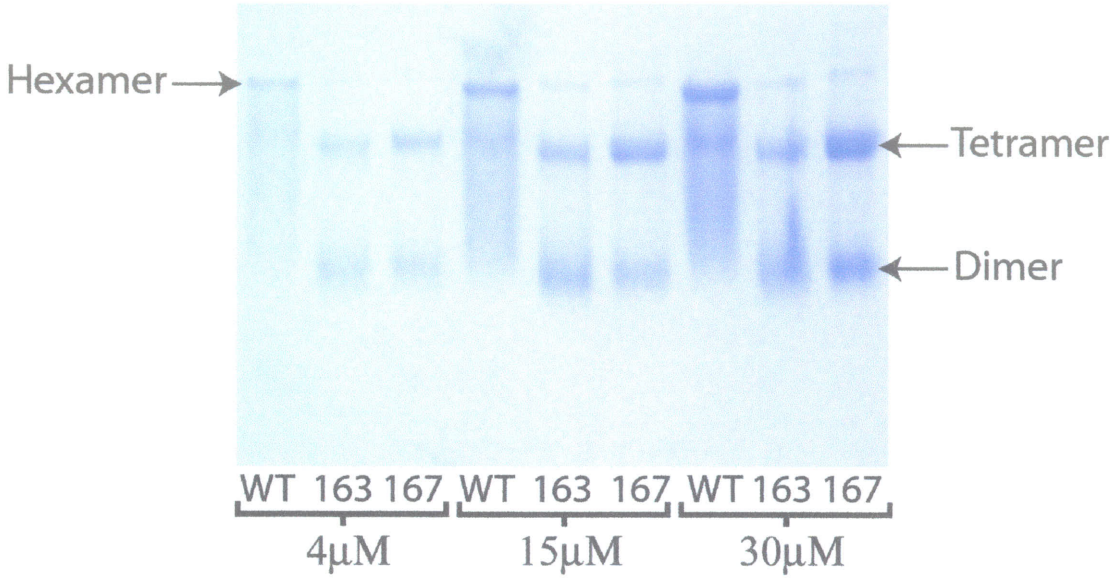

Figure 33: Non-denaturing gel showing the R163L and K167A variants compared with the wild type protein. The wild type sample used was several months old, which would account for the presence of the small amount of tetramer seen (old CS samples tend to show traces of the tetrameric species).

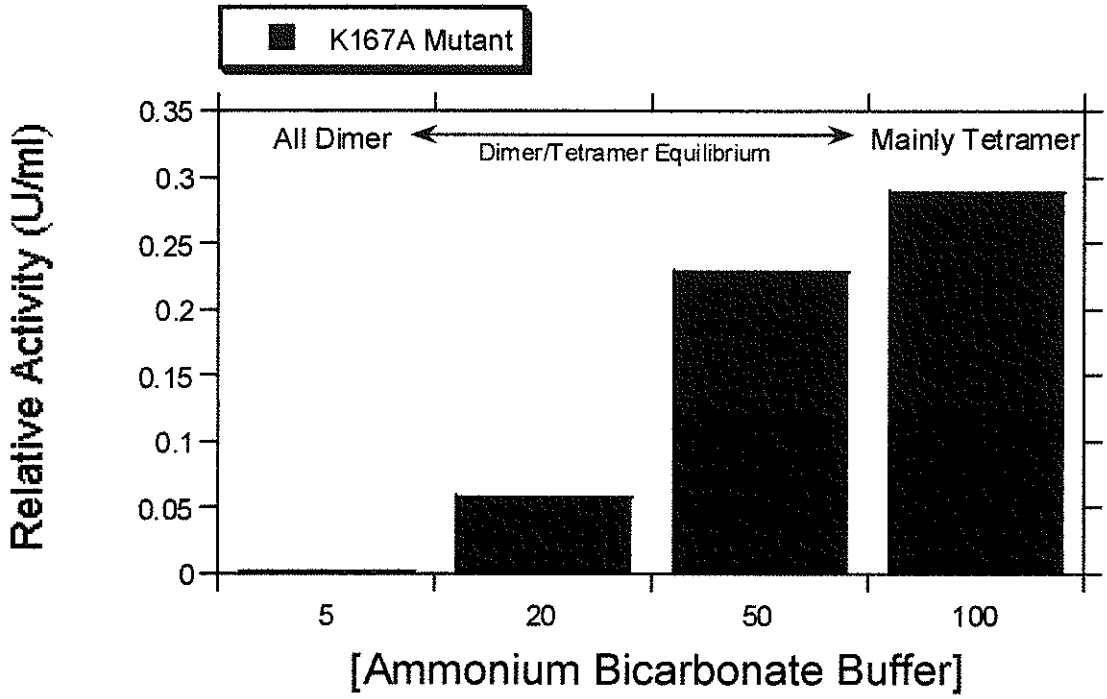

Figure 34: Activity of the K167A variant as a function of NH_4HCO_3 buffer concentration. The labels above the bar graph describe the dimer/tetramer equilibrium results, obtained by mass spectrometry.

Variants of Arginines in the Cationic Pore

One striking feature of *E. coli* citrate synthase seen in the crystal structure is the presence of a central cationic pore lined with six copies of a set of three key arginine residues, namely R119, R125, and R126. Upon closer inspection of this region, it has also been determined that these three key residues comprise an intricate hydrogen-bonding network. The presence of this centrally located H-bonding network raises several possibilities as to its functional role: 1) it may increase or decrease the structural stability of the hexamer, and 2) it may play a role in the allosteric properties, as it lies in close proximity to the NADH binding site. The residues of the central H-bonding network may also be involved in the allosteric activation via KCl. The cationic residues may represent points of electrostatic repulsion, which may function to destabilize the hexamer. Potassium chloride may decrease these repulsive forces through either: 1) a specific effect involving the chloride ion acting as a counter charge; or 2) a general effect, as increased ionic strength can mask electrostatic repulsive forces. If the hydrogen-bonding network is in fact involved in the allosteric activation of *E. coli* CS, one might expect that the K_M for KCl would be lower in these three variants.

To study possible functions of the cationic pore and the subsequent hydrogen-bonding network, each of the arginine residues was individually converted to leucine using site directed mutagenesis. Conversion to leucine, rather then alanine, made it possible to maintain most structural features of the original residues, while removing the positively charged guanidinium group.

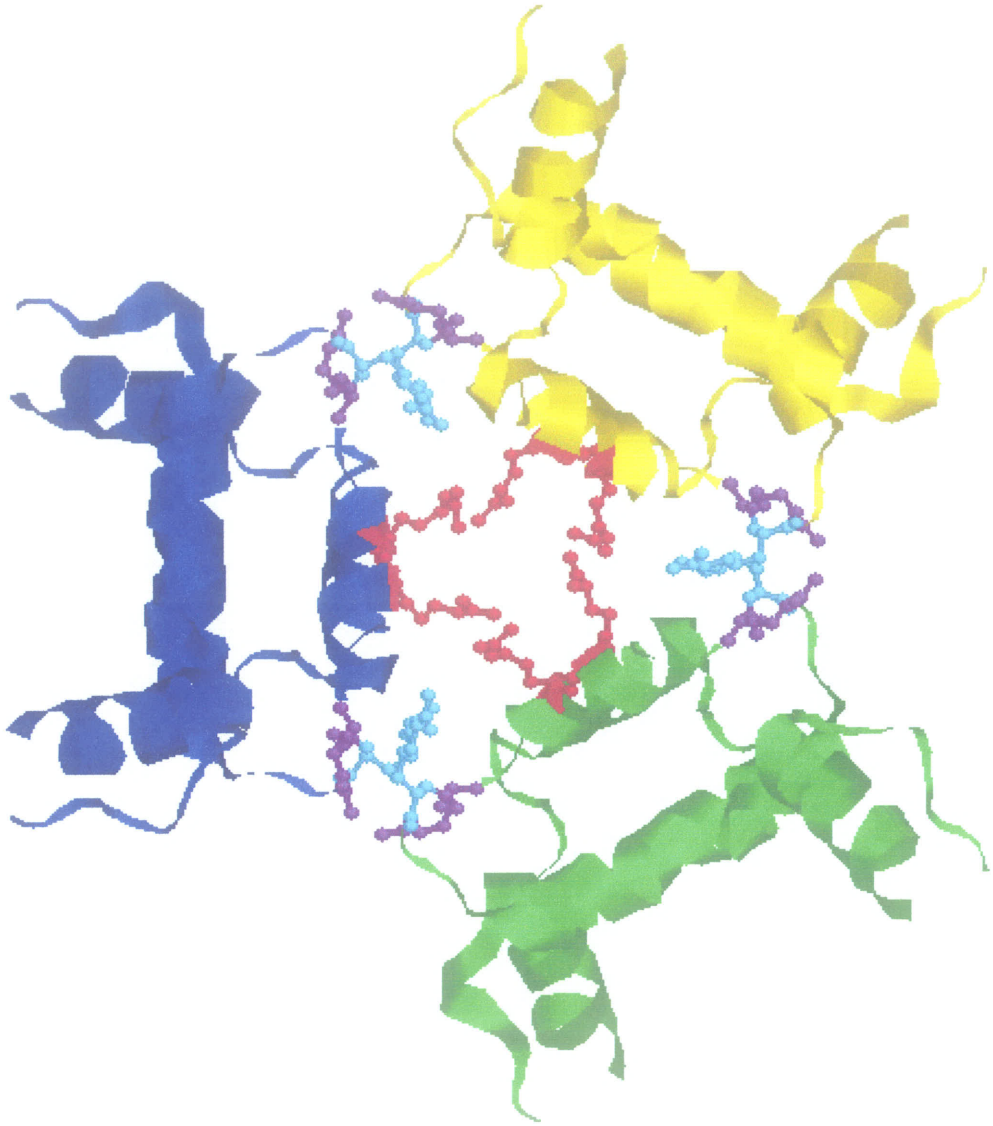

Figure 35: Central hydrogen bonding network composed of arginines 119 (red), 125 (purple), and 126 (cyan). Figure based on the crystal structure of Nguyen et al., 2001.

Steady State Kinetics

Preliminary kinetic results for the three arginine variants can be seen in Table 7. From the preliminary data, it is obvious that all three residues in the hydrogen-bonding network have some impact on the overall kinetic properties of the enzyme. All three variants demonstrated decreased activity throughout purification, with final specific activities off the G200 column of 53U/mg, 24U/mg and 28U/mg for the Arg119, Arg125, and Arg126 variants respectively. However, as already explained, these results rely on defined assay conditions, and do not take into account variations in substrate binding affinities.

The steady state kinetic parameters for the three arginine variants, based on the array experiment, are listed in Table 8. The k_{cat} for the R126L variant showed a 2 fold increase, while the R119L and R125L variants were comparable with that of the wild type enzyme. The K_{OAA} values for the R126L variant (-5±9μM) and R119L variant (-7±3), were both negative. The only plausible explanation for this result is that in the case of both of these variants, the binding of OAA in the presence of saturating AcCoA is very tight, with the value of K_{OAA} very close to zero. Therefore, the curve fitting function of SigmaPlot is forced to extrapolate into an area of the curve where no data can be obtained as it is impossible to determine accurate velocities at low OAA and high AcCoA, since OAA is used up too quickly. The K_{iOAA} values for the R125L and R126L variants show 4 fold and 7 fold increases respectively, while the R119L variant was similar to the wild type. When comparing the K_{OAA} and K_{iOAA} values for the three variants, it is clear that the presence of AcCoA increases the binding affinity for OAA.

Parameter	k_{cat} (sec^{-1})	K_{OAA} (μM)	K_{AcCoA} (μM)
Wild Type	81	26±5	120±20
R119L	53	13±1	76±6
R125L	24	49±2	511±24
R126L	28	157±14	243±23

Table 7: Preliminary kinetic data for the H-bonding variants. k_{cat}/sec was determined under standard assay conditions, while K_{OAA} was determined with a fixed AcCoA concentration of 200μM AcCoA, and K_{AcCoA} was determined with a fixed OAA concentration of 200μM as well. (Wild type values taken from Anderson, 1988)

Parameter	k_{cat} (sec^{-1})	K_{OAA} (μM)	K_{iOAA} (μM)	K_{AcCoA} (μM)	K_m, KCl (mM)	KCl Activation Ratio	Hill #
Wild Type	81±6	26±5	33±7	120±20	28±4	39±3	1.0
R119L	75	-7±3	28±11	72±9	25±6	33±2	1.0
R125L	97	14±5	128±26	112±15	45±4	66±8	1.9
R126L	124	-5±9	227±46	147±22	57±6	32±4	2.6

Table 8: Steady state kinetic results for the R119L, R125L, and R126L variants compared with the wild type enzyme. (wild type data from Anderson, 1988) The activity and substrate binding constants were determined in the presence of 100mM KCl.

The K_{AcCoA} value for all three variants were also comparable to the wild type value, with the R119L variant showing slightly stronger binding affinity.

KCl Activation

The values for the K_m, KCl, KCl activation ratio and Hill numbers for the three arginine variants are shown in Table 8. The K_m, KCl for the R119L variant was equivalent to the wild type enzyme, while the R125L and R126L variants both showed approximately 2 fold increases in K_m, KCl. Therefore, the R125L and R126L variants both have a 2 fold decrease in their affinity for KCl. The binding ratios for both the R119L and R126L variants were relatively the same as the wild type value. However, the R125L variant showed a slightly higher value, indicating that this change has increased the degree to which KCl allosterically activates the enzyme. Hence, this result, coupled with the increase in the K_m, KCl, would imply that the R125L mutation has shifted the R/T state equilibrium, in favor of the inactive T-state. From the Hill numbers, it is apparent that the level of cooperativity associated with KCl activation, has increased in both the R125L and R126L variants, while the R119L appears to show no cooperativity.

NADH Binding and Inhibition

The NADH binding and inhibition results for the three arginine variants are shown in Table 9. With all three variants, the dissociation constant for NADH increased,

	NADH BINDING			NADH INHIBITION	
Parameter	**K_D, (μM)**	**# of Sites**	**ΔG, (KJ/mol)**	**K_i, (μM)**	**% Inhibition**
Wild Type	1.6±0.1	0.5	-	5.0±0.6	~99
R119L	3.92±0.04	0.7	-2.2	29±13	23
R125L	7.4±0.2	0.7	-3.7	28±5	96
R126L	4.3±0.08	0.6	-2.4	171±49	75

Table 9: NADH binding and inhibition results for the 3 hydrogen bonding variants. The ΔG value represents the change in binding free energy associated with the each mutation, calculated using the equation $\Delta G = -RT \ln K_D\text{variant}/K_D\text{wild type}$.

with the R119L and R126L variants showing K_D values ~2.5 fold higher than wild type, while the R126L variant showed an increase of ~5 fold. The K_i values for the R119L and R125L variants showed a 6 fold increase from that of the wild type enzyme, while the R126L variant showed a surprising 35 fold increase. When looking at the K_i/K_D ratios for all three variants, it is obvious that the presence of substrates decreases the relative affinity for NADH, with the most striking result being the R126L variant, which demonstrated a K_i value 40 fold greater, than its K_D value.

Mass Spectrometry

The mass spectrometry results for the three arginine variants turned out to be the same for all three proteins. Figure 36 shows the spectra of R119L variant as an example. With all three variants, the hexamer represents the dominant conformation. The spectra of all three proteins showed only small amounts of dimer under conditions in which the wild type enzyme normally shows predominately dimer with little to no hexamer. Therefore, removing any of the three residues involved in the central hydrogen-bonding network results in a more stable hexamer. From this result, it could be reasoned that the concentration of positive charge in the central pore is a structural hindrance to hexamer formation, and that this accounts for the dimer/hexamer equilibrium seen with the wild type protein.

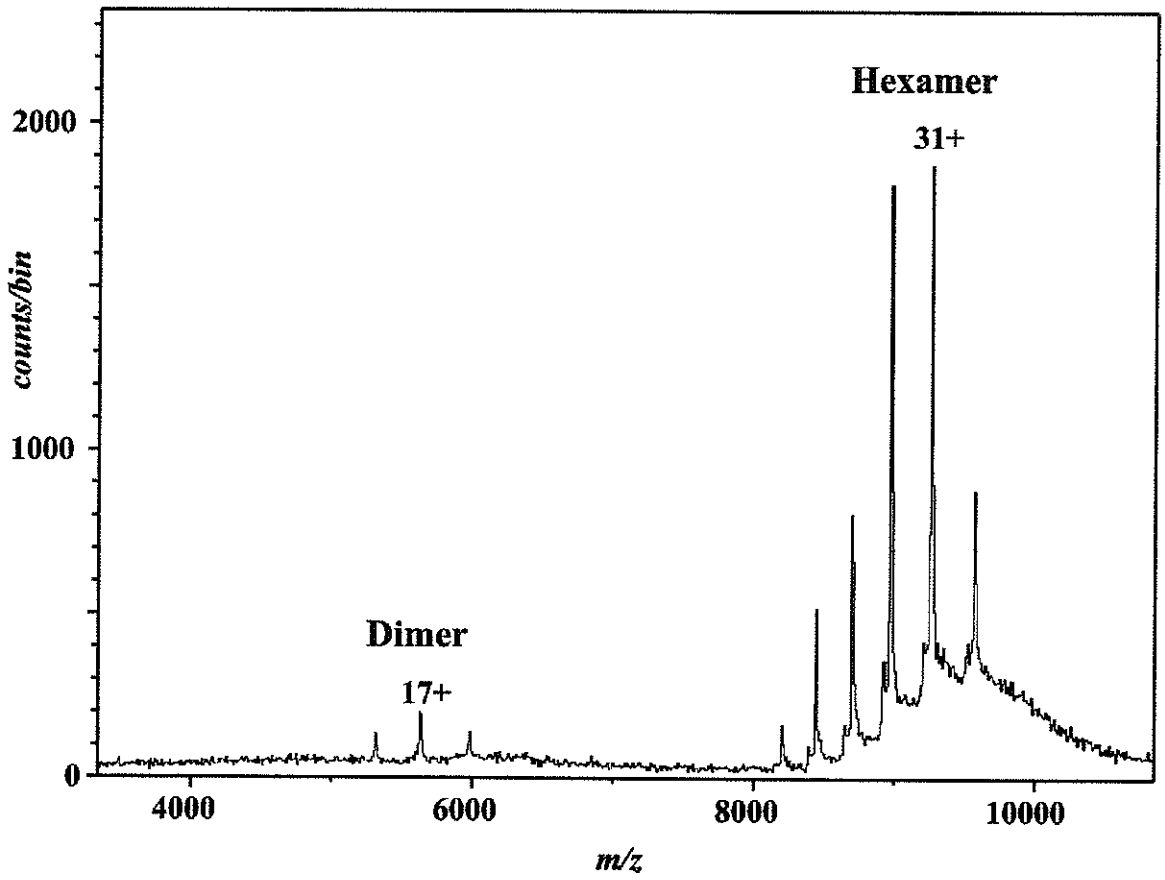

Figure 36: Nanospray ionization mass spectrum of the R119L variant, showing the highly stable hexamer, which is characteristic of the three arginine residues of the H-bonding network. The sample was prepared in a Centricon 50 in 100mM NH_4HCO_3, followed by dilution into 20mM NH_4HCO_3 prior to sample injection. The protein concentration was 1.51μM monomer. Under these conditions the wild type protein would show all dimer (Dr. Lynda Donald personal communication). The sample was run at 300V declustering voltage using SF_6 as the curtain gas.

The Truncated Variant

The crystal structure of *E. coli* citrate synthase gave a clear picture of the novel N-terminal domain found in the gram negative CS family. From the crystal structure, this novel domain is positioned on the outer edge of the protein, far from the central pore. The contact regions between dimers, and the NADH binding site, lie well toward the center of the protein, well clear of the N-terminal domain, which raises the question: What role, if any, does this domain play in the multimeric state or the allosteric properties of this enzyme? On the other hand, R407 of the active site lies in close proximity to several residues within the C-terminus of this domain, which raises a second question: Will removing this domain have any affect on the enzymes catalytic activity? One possible function for this domain, inferred from its peripheral location, may be to act as a binding/contact site for surrounding protein(s).

In order to determine any possible function for this novel domain, a variant protein, lacking most of the domain, was constructed. This involved introduction of a new start codon via an NdeI site spanning codons for residues 39 and 40, followed by digestion and introduction into the PET expression system. This produced a truncated CS gene lacking the first 39 codons. Following amplification via IPTG induction, the typical citrate synthase purification procedure was followed. The relative position of the protein peak off the DE52 anion exchange column appeared normal (see Figure 36) ranging from fraction 34-48, however one striking observation was the lack of any significant activity within these fractions. A typical wild type preparation shows a specific activity of ~25-30U/mg for the peak fractions eluting from the DE52 column, while the truncated

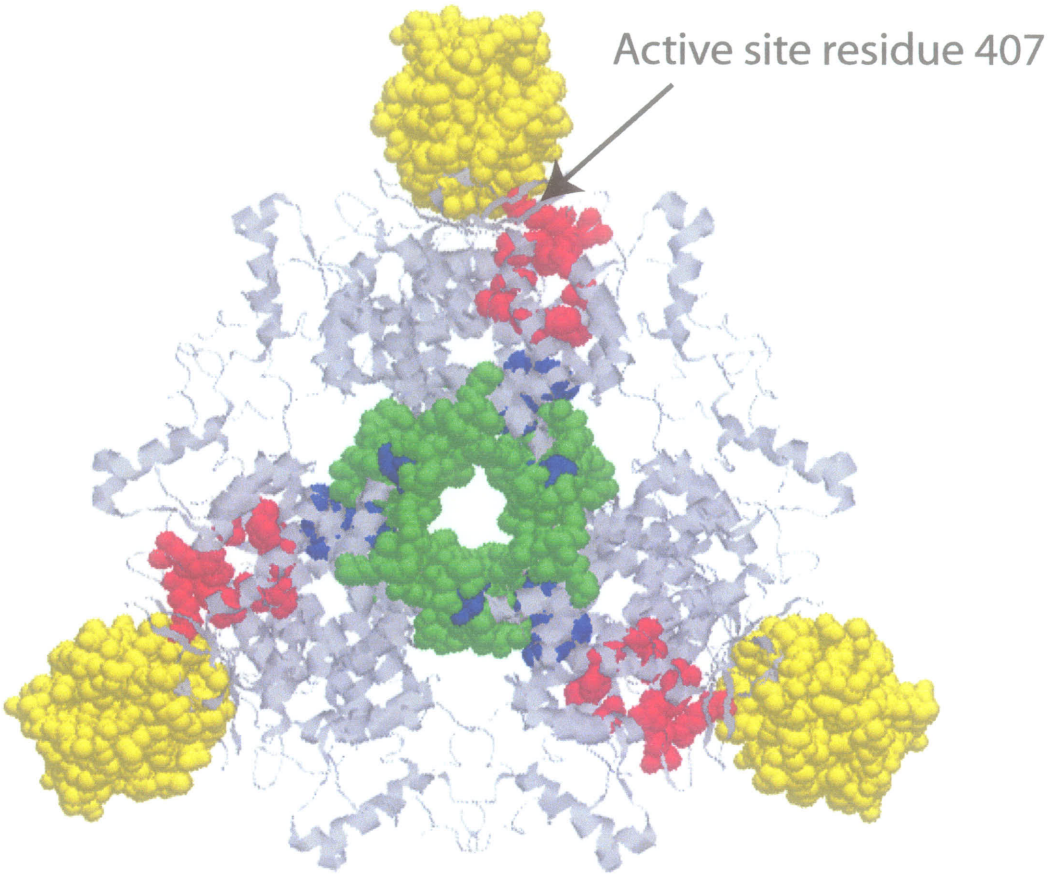

Figure 37: Position of the N-terminal domain (yellow), with respect to the active site (red), dimer/dimers contact regions (green) and the allosteric site (blue). Note that only one active site and NADH binding site are highlighted per dimer. Figure based on the crystal structure of Nguyen et al., 2001.

preparation showed on average ~0.065U/mg. Therefore, in order to determine the appropriate fractions to pool, SDS-PAGE analysis was implemented. The relative position of the protein peak off the G200 size exclusion column was shifted slightly to the right, as expected for a smaller protein (see Figure 38). This result gave the first indication that the mutation had not interfered with hexamerization, as a dimer would have run later in the profile. However, the activity levels for the peak fractions were again very low, with a specific activity of ~0.1U/mg compared with the typical wild type value of ~60U/mg at this stage in the purification. The final concentrated sample showed ~600 fold lower activity than a typical wild type preparation. As the truncated protein was produced using the PET expression system, the host strain used was the BL21DE3pLysS, which contains a normal citrate synthase gene. Therefore, there was a possibility that the small amount of enzyme activity was from background wild type protein, and that the truncated protein was completely inactive.

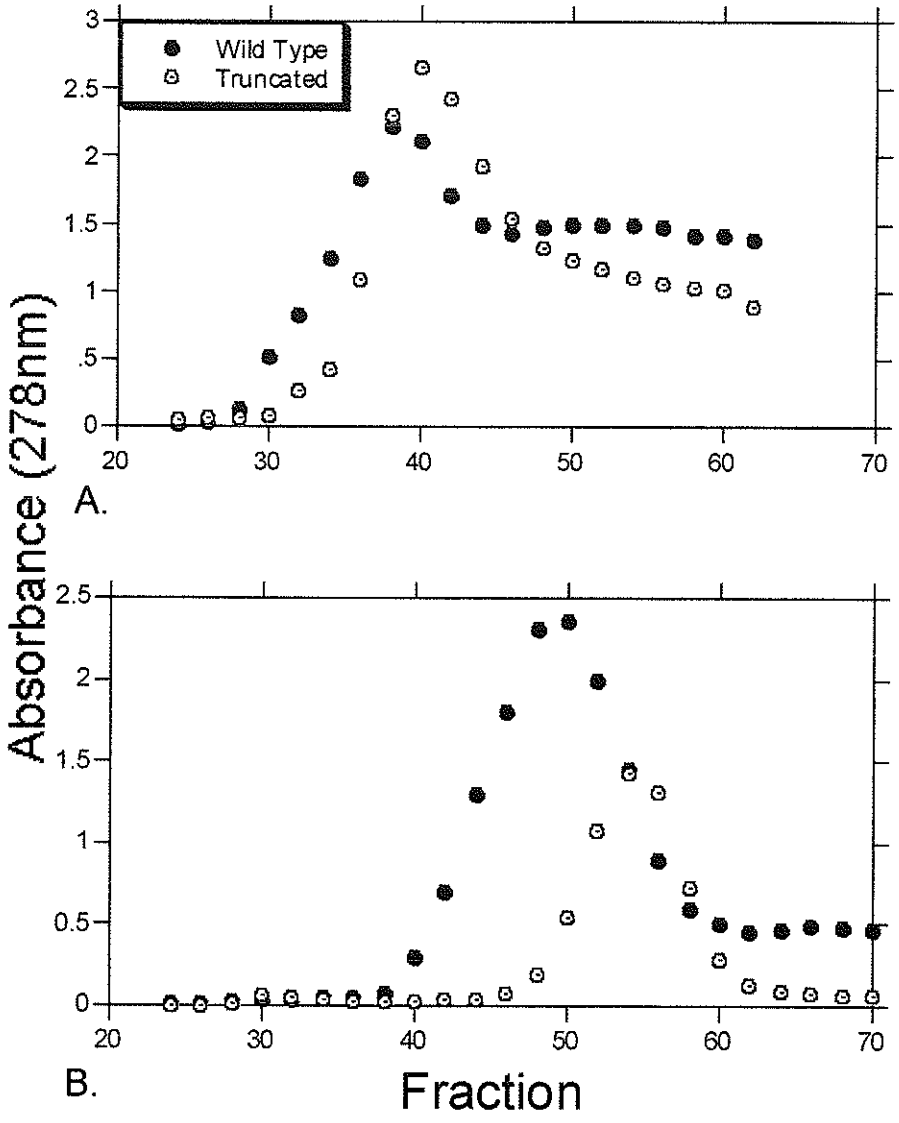

Figure 38: Comparison of the truncated and wild type elution profiles from the DE52 (A.) and G200 (B.) columns.

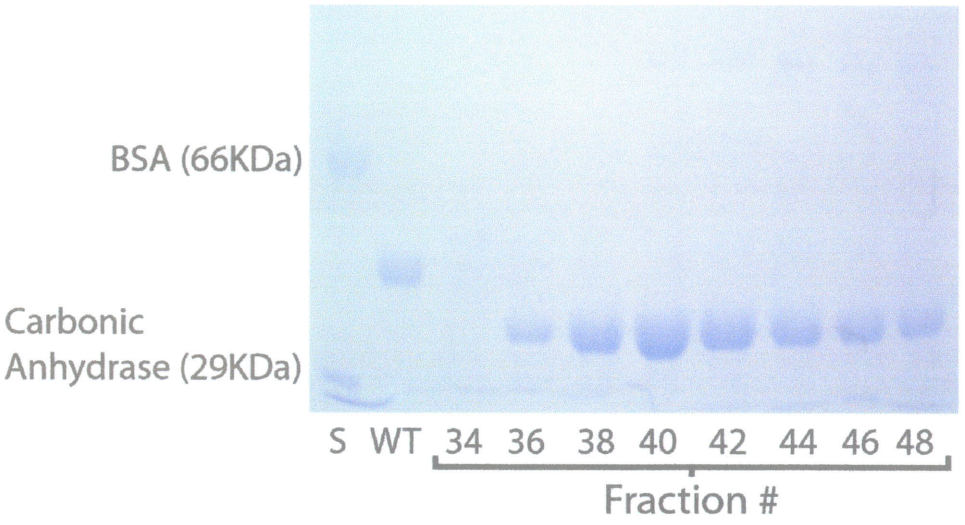

A.

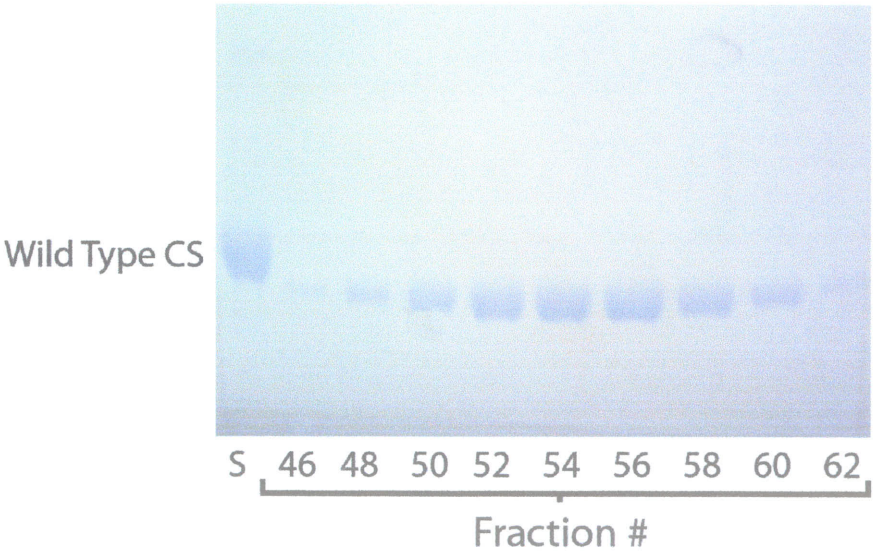

B.

Figure 39: SDS PAGE analysis of fractions off the DE52(A.) and the G200 (B.) columns, for targeting of fractions to pool which contain truncated CS protein.

Mass Spectrometry

Although SDS-PAGE gave clear evidence for the presence of a truncated CS protein, mass spectrometry was used to verify the correct mass. The expected mass for the truncated protein is 43877 Da. However, the deconvolution of the denatured spectrum gave a mass of 44004 Da, a difference of +127 Da (approximately the mass of a methionine (131Da) residue), from that of the expected mass. The most obvious explanation for the extra mass would be that the usual posttranslational modification, involving removal of the N-terminal methionine had not occurred with this truncated protein. This would seem a plausible explanation, as the host cell's machinery may not recognize the truncated protein as a self-product.

The dimer/hexamer equilibrium appeared to be normal, with a hexamer charge envelope centered around 8000m/z (Figure 40), which under high voltage conditions, could be broken down into monomers. The presence of the hexamer agreed with our early suspicions when looking at the typical protein peak from the size exclusion column. The presence of the normal multimeric-state was expected, given that this novel domain lies far from the points of contact between dimers as seen in the crystal structure.

One question which arose upon finding stable truncated hexamers, was: Would the truncated subunits associate with wild type subunits to create mixed species, and if so, would the truncated subunits act as inhibitors within the mixed species, as they appear to be inactive themselves? A preliminary experiment using a non-denaturing polyacrylamide gel, showed from a mixed sample of truncated and wild type protein, only two distinct bands equivalent to the truncated hexamer and the wild type hexamer, with no apparent mixed hexamers visible (gel not shown). Further, when wild type and

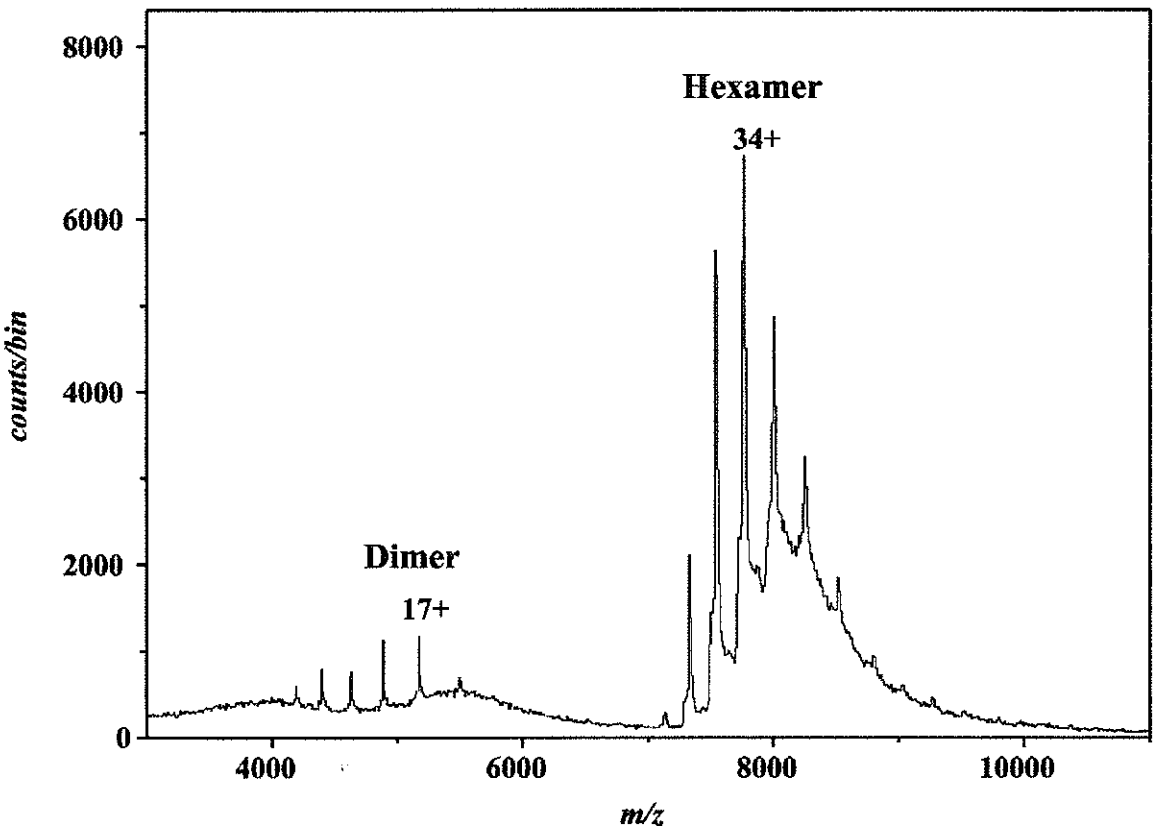

Figure 40: Nanospray ionization mass spectra of the truncated variant, showing dimer/hexamer equilibrium comparable to the wild type enzyme (Dr. Lynda Donald personal communication). The sample was prepared in a centricon 50 in 100mM NH_4HCO_3. The protein concentration was ~20μM monomer. The sample was run at 170V declustering voltage using SF_6 as the curtain gas.

truncated subunits were mixed together, the total activity did not change. This result suggests that no subunit exchange occurred within the course of the experiment (~1 hour incubation period prior to running on the gel).

Preliminary Kinetic Analysis

The preliminary kinetic results for the truncated variant are depicted in Table 10. As already mentioned, the specific activity for the truncated variant was determined to be ~0.11U/mg, which is ~600 fold lower then the wild type protein. Such a low specific activity made it difficult to obtain kinetic data, and a requirement to have high concentrations of protein in all assays. A typical concentration of ~6mg/ml was used as the main stock for all kinetic data, as opposed to ~0.2mg/ml used for most of the variants described in this thesis. The preliminary binding measurements for OAA and AcCoA in the presence of KCl gave values of 30±2μM and 100±7μM respectively. These values are very similar to those of the wild type, 26±5μM (OAA) and 120±20μM (AcCoA). The K_m for KCl turned out to be 43±8μM, while the KCl activation ratio was 35±6, which are also similar to the wild type values of 28±4μM and 39±3 respectively. Given that the truncated variant showed a very low specific activity, and had relatively stable binding to both substrates, I have concluded that the activity observed is not from the truncated protein, but from contaminating wild type protein. Therefore, further steady-state kinetic analysis has been omitted.

Parameter	k_{cat} (sec^{-1})	K_{OAA} (μM)	K_{AcCoA} (μM)	K_m, KCl (mM)	KCl Activation Ratio
Wild Type	81	26±5	120±20	28±4	39±3
Truncated	0.11	30±2	100±7	43±8	35±6

Table 10: Comparison of truncated (preliminary) and wild type kinetics. (Wild type value taken from Anderson, 1988)

NADH Binding and Inhibition

Given that the truncated variant lacked activity, it was not possible to carry out an NADH inhibition study. However, it was possible to determine the dissociation constant for NADH using the fluorescence method of Duckworth and Tong (1976). With a dissociation constant of 0.59±0.02μM, as opposed to the wild type value of 1.6±0.1μM, the truncated variant showed 3 fold tighter binding to NADH (see Table 11). This tighter binding to the allosteric inhibitor, coupled with the lack of activity, would imply that the truncated variant has most likely taken on a stable T-state conformation. Further, the fact that the number of binding sites measured is close to 1 per subunit also suggests that the truncated variant is completely in the NADH-binding state.

	NADH BINDING		
Parameter	**K_D, (μM)**	**# of Sites**	**ΔG, (KJ/mol)**
Wild Type	1.6±0.1	0.5	-
Truncated	0.59±0.02	1.1	2.4

Table 11: NADH binding results for the truncated variant compared with the wild type enzyme. The ΔG value represents the change in binding free energy associated with the each mutation, calculated using the equation $\Delta G = -RT \ln K_D variant/K_D wild\ type$.

Discussion

The research presented in this thesis focused on three structural features of *E. coli* citrate synthase, including the allosteric site, the residues of the central cationic pore, and the unique N-terminal domain. The recent crystal structures of the wild type enzyme and the F383A with bound NADH, solved by Nguyen et al., (manuscript in preparation) made this research possible, by giving a clear picture of these three distinct features.

NADH Variants

The NADH binding site of *E. coli* citrate synthase is an allosteric site, which by definition implies that it is structurally different when the enzyme is in the R-state as opposed to the T-state. Since the R-state is the active form of the enzyme, it is reasonable to assume that mutations to the allosteric site may effect the T/R ratio, or the ease with which the enzyme can convert to the R-state. The purpose of this study was to define the residues which make up the allosteric site, and see what effect mutating these residues has on the allosteric equilibrium.

From the results of the NADH binding experiment, it is clear that all the residues under investigation with the exception of the R109, are involved in the binding of NADH to the allosteric site. This conclusion is clear when looking at the loss in NADH binding energy (see Table 4), which in all variants (except R109L), is in the expected range for the loss of a single H-bond. The R109L variant showed increased binding energy, which would imply that this residue's side chain impedes NADH binding. From the results in Table 4, it is interesting to note that the K_i values for NADH inhibition do not change in proportion to the K_D. However, this result will be discussed further below.

With most of the NADH binding variants the enzyme turnover rates appeared to be normal with several variants, showing slight increases in activity. The only exception to this general trend was the Y145A variant, which showed almost a 2 fold drop in k_{cat}. This lower value was probably the result of lower purity, since the Y145A protein could not be purified free of all contaminating proteins. Although the various NADH variants showed changes in their affinities for the substrates, this normal catalytic activity was expected, since the allosteric model states that once substrates are bound the enzyme is in a fully active R-state. An interesting trend, seen with almost all the NADH variants, was the increase in K_{iOAA} and decrease in K_{OAA}. The changes in these two values must reflect changes in substrate cooperativity within the active site. With the wild type enzyme, which follows the Ordered Bisubstrate kinetic mechanism, all evidence suggests that OAA enters the active site prior to AcCoA, and induces a conformational shift, which ultimately leads to the correct conformation for AcCoA binding. For the wild type enzyme, $K_{iOAA}/K_{OAA} \cong 1$, implying that OAA binding is not actually improved by binding of AcCoA. However, with most of the NADH variants, the K_{iOAA}/K_{OAA} ratio is higher than the wild type enzyme, which implies that the OAA binding site is not fully formed until AcCoA binds. This result is most striking with H110A and T111A, where K_{iOAA} is more then 10X the wild type value. This result suggests that there is a connection between the OAA site and the allosteric site.

The most interesting kinetic result found with the majority of the NADH variants, was the drop, although small, in K_{AcCoA}. This result was not entirely unexpected, as it is known that the allosteric mechanism of *E. coli* CS is directly related to the binding of AcCoA. Therefore, the mutations to the allosteric site have allowed the proteins to take

on a conformation, which favors AcCoA binding, or in other words a shift towards an R-state conformation has occurred. Exceptions to this finding were seen with the Y145A, K167A, and T204A variants. With the K167A and T204A variants, which also showed increases in K_{OAA}, there is evidence that the proteins are tetramers rather than the usual hexamers, and this might also affect the active site such that substrate binding is impeded. In the case of the Y145A variant, it is difficult to determine why this enzyme has lowered affinity for both substrates. However, the loss in structural stability seen with this variant may signify structural variations, which could include the active site.

The K_m, KCl values for the majority of the NADH variants appear to be normal, with possibly a small decrease in KCl binding affinity. The R163L variant was the only variant to show an increased binding affinity for KCl. This result coupled with the lower K_{AcCoA} and K_{OAA} would suggest that this variant has shifted to an R-state conformation. However, when looking at the mass spectrometry results, which show an increase in hexamer dissociation, this result becomes a bit confusing, if one is to assume that the active form of the enzyme is, in fact, the hexamer. In other words, these two results may suggest that the dimer has activity as well as the hexamer. However, one must not forget that the mass spectrometry is done in the absence of substrates, as well as KCl. The fact that both substrates and KCl are known to shift the equilibrium in favor of hexamer may be the reason that the R163L variant shows very little hexamer via mass spectrometry, while demonstrating kinetics which suggest an R-state conformation. The Hill values for KCl saturation, with all the NADH variants except R163L, increased from the wild type value of 1. This result suggests that the mutations have shifted the enzyme into a T-state conformation, as the binding of KCl to one subunit is not sufficient to shift the enzyme

into an active R-state. In other words a greater push via KCl is required in order to achieve an R-state conformation.

This conclusion, however, is not borne out by the results with NADH binding and inhibition. The K_i and K_D values for the majority of the NADH variants, which show an increase, most notably with the N189A variant, contradicts the results of the KCl saturation experiment. As already mentioned, the K_i/ K_D ratio gives information about the R/T ratio. The MWC model states that the R-state has high affinity for substrates and low affinity for allosteric inhibitors. Therefore, as K_i is measured in the presence of substrates, and K_D is measured in the absence of substrates, the ratio of K_i/K_D reflects the effect of substrates on NADH binding. In this model, the higher the K_i/K_D ratio, the greater the enzyme is shifted towards an R-state, which favors substrate binding, rather than NADH binding. Hence, the majority of the NADH variants, according to the K_i/K_D ratio, have shifted towards an R-state conformation. In order to fully appreciate the connection between the K_i/K_D ratio and the R/T equilibrium, the allosteric constant (L = [T]/[R]) has been calculated (see Table 12), where possible, using the MWC equation shown below:

$$y = \frac{\alpha(1+\alpha)^{n-1}}{L(1+\beta)^n + (1+\alpha)^n}$$

y = fractional saturation of ligand sites on the protein (we will treat this as the fractional saturation of allosteric sites on the protein).
α = [NADH]/K_D
β = [AcCoA]/K_{AcCoA}
n = number of interacting subunits (can be 2, 3, or 6 for *E. coli* citrate synthase)
L = allosteric constant (ratio of concentration protein in R state to concentration of protein in T state).

These defined values are opposite to those of the original MWC equation, where the equation focused on the activator or substrate rather then the inhibitor. In the case of *E. coli* CS, the value of n, the number of interacting subunits, is not known, but, given the fact that the active form is a hexamer, the possible values are 2, 3 or 6. For NADH binding, K_D is the concentration of NADH where y is equal to 0.5 and [AcCoA] is 0, and for NADH inhibition, K_i is the concentration of NADH where y is equal to 0.5 while [AcCoA] is >0. The known variables include, [AcCoA] (100μM in the inhibition assay), K_D, K_i, K_{AcCoA} and y which mathematically is 0.5. Therefore, the allosteric constant can be calculated for the three possible n values.

Rearrangement of the previous equation to solve for the allosteric constant, using a y value of 0.5:

$$L = \frac{\left(1+\frac{K_i}{K_D}\right)^{n-1}\left(\frac{K_i}{K_D}-1\right)}{\left(1+\frac{AcCoA}{K_{AcCoA}}\right)^{n}}$$

The L values for the majority of the NADH variants, excluding R109L and Q182A, suggest that they have been shifted into an R state, which contradicts the finding that the KCl activation curves are sigmoid. The K_{AcCoA} values compared with the allosteric constants for several of the variants also show contradictions. The R109L and Q182A variants both show small increases in AcCoA binding, yet their L values indicate a shift towards the T state. The T204A variant shows the opposite contradiction. These contradictions suggest that the model used to explain the allosteric properties of *E. coli*

citrate synthase is too simple, and that more factors need to be considered to explain all the data.

Variant	K_{AcCoA} (μM)	K_i/K_D Ratio	L (n = 2) (μM)	L (n = 3) (μM)	L (n = 6) (μM)
R109L	69	1.4	0.2	0.07	0.01
H110A	49	20	43	271	76906
T111A	79	5.2	5.0	9.8	111
Q182A	56	2.3	0.9	0.7	0.6
N189A	69	18	56	403	170310
T204A	206	9.3	39	223	54237

In these calculations, L = R/T, so a large value of L should favor substrate binding.

Table 12: Allosteric constants for the NADH variants, where K_D and K_I for NADH are known. The allosteric constants (L values) were calculated for n values of 2, 3 and 6. The appropriate K_{AcCoA} values obtained from Table 6 are also shown.

Cationic Pore Variants

The 18 arginine residues (three per subunit), which comprise the central cationic pore, also make up a hydrogen bonding network, which could be involved in stabilizing the hexameric species. This hydrogen bonding network, along with possible electrostatic repulsive forces associated with the charges on these residues regulate the dimer/hexamer equilibrium that is seen in the absence of allosteric activators or inhibitors. The focus of study on these residues was to determine if they play any functional role in the allosteric or kinetic properties of this enzyme.

Each of the three variants made, R119L, R125L and R126L, removes six arginines from the cationic pore. The kinetics of the three arginine variants are, for the most part, similar to the NADH variants. As with the NADH variants, the K_{OAA} and K_{iOAA} values were the only variables which showed a consistent difference from the wild type enzyme, with all three variants showing decreases in K_{OAA} and increases in K_{iOAA}. Therefore, the arginine variants have also resulted in conformational alterations to the OAA binding portion of the active site in such a way that AcCoA is now needed for efficient OAA binding to occur. This result was not expected as all three residues lie >20Å away from any active site residue. In order for the active site to have been affected, the three mutations must have resulted in somewhat major structural changes.

If we consider the possibility, mentioned earlier, that each of these three residues is involved in electrostatic repulsive forces that destabilize the hexamer, then the loss of each arginine would result in a slightly collapsed hexamer as the repulsive forces would be lost. This collapsing of the hexamer could result in the structural changes to the active

site, which would result in the increased K_{iOAA} values observed. In contrast to the increase in K_{iOAA}, the R119L variant demonstrated almost a 2 fold increase in AcCoA binding affinity. This result suggests that the mutation, as with many of the NADH variants, has caused the two domains of each subunit to shift, such that AcCoA binding is favored, mimicking the effect found with high KCl concentrations, or bound OAA. That is, the R119L variant has taken on a conformation which is shifted towards the R-state, with some structural variations indicated by the high K_{iOAA}.

One final observation, which should be noted is the apparently high turnover rate associated with the R126L variant. This variant, although it shows the highest K_{iOAA} and K_{AcCoA} values, also demonstrates almost a 1.5 fold increase in catalytic rate. The mechanism of the CS reaction is believed to involve several conformational shifts including: 1) the conformational shift associated with OAA binding, which increases AcCoA binding affinity; 2) the conformational shift following AcCoA binding, which allows for the reaction to occur; and 3) the conformational change which allows for the release of the products. The kinetics of the R126L variant, including its high k_{cat}, K_{iOAA} and K_{AcCoA}, suggest that this protein has a conformation which is slightly different from the wild type enzyme. This small conformational difference may somehow mimic those involved in either the second or third shift mentioned above, which could allow for the reaction to go to completion faster upon binding of the two substrates.

With regard to the possible relationship between KCl activation and these three residues, it would seem from the K_m, KCl, and KCl activation ratio that the hydrogen-bonding network is not directly involved. It is, interesting to note from the mass spectrometry results that all three variants in the cationic pore region are predominately

hexamer, which mimics the effect of high salt concentrations. This result suggests that the dimer/hexamer equilibrium exists because of the charge repulsion in the pore, induced by hexamer formation, and that KCl may stabilize the hexamer by decreasing these electrostatic forces. However, one can only speculate as to whether the mechanism is specific, involving the chloride ion, or general, involving an overall increase in ionic strength surrounding these residues.

It is interesting to note that although the arginine variants all showed increased hexamerization, which mimics high salt concentrations, they also showed fairly normal values for their K_m, KCl and a KCl activation ratio. That is, reducing charge repulsion effects in the cationic pore is not enough to remove the need for KCl activation. This result would suggest that the mechanism of KCl activation must involve a second component at a different site on the protein. This second site must lie near the R319 residue, as mutations to this amino acid result in a variant with a very low K_m, KCl, and KCl activation ratio (Anderson et al., 1991), as well as a dimer hexamer equilibrium which is shifted towards hexamer (Lynda Donald personal communication). Therefore, one might expect that a double variant including the R319 residue and any of the 3 arginine residues discussed in this chapter would result in a CS variant with maximum activity in the absence of KCl.

The K_D values for NADH binding, for all three arginine variants were all greater than the wild type with the R125L variant, showing a K_D value four times that of the native enzyme (see Table 10). With the R125L and R126L proteins, it was not surprising that these variants showed decreased affinity for NADH, as they sit within close proximity to the allosteric site and the contact regions between dimers. The mass

spectrometry results indicated that all three arginine residues are involved in repulsive forces, which destabilize the hexameric species. Therefore, as previously mentioned, it would seem reasonable that in all three of these variants, a collapse of some sort has occurred within the central pore (in the case of the R119L variant), or around the central pore (in the case of the R125L and R126L variant). This collapse, especially in the R125L and R126L region would definitely affect the allosteric site, as it lies within the contact regions between dimers, near these two arginine residues. However, with the R119L variant, one might assume that the contact regions would be pushed closer together, if the central pore were to collapse inward. This tighter contact region would make the allosteric site less accessible to NADH.

One final note, which should be made regarding the NADH binding experiment, is that the number of sites per subunit is slightly higher for the cationic pore variants than for the wild type enzyme. As already mentioned, the conversion of dimers to hexamers in response to NADH must be very slow, such that the time allotted for the experiment will not provide all the available binding sites. If this assumption is correct, then the increased number of sites, seen with the three arginine variants, would be expected, as they are predominately hexamer to begin with.

The K_i values for all three variants were higher than the wild type enzyme, with the R126L variant showing a dramatic 34 fold increase. As with many of the NADH variants, the K_i/K_D ratio for the 3 arginine variants, was much higher than the wild type enzyme, which implies that all are shifted towards an R-state conformation. When looking at the K_i values for the R119L and R125L variants, which are basically the same, it is interesting to note that the R119L variant shows only 23% inhibition, while the

R125L variant shows 96% inhibition. This would imply that the NADH molecule, although able to bind the R119L variant, is not capable of shutting down the enzyme efficiently. As the kinetic data show normal activity for this variant, it would seem that the "crosstalk" between the active site and allosteric site, which is key to inhibition via NADH, has somehow been interrupted. However, a second possibility is that the low level of inhibition seen with this variant, is a reflection of a time dependency, such as with the number of binding sites in the binding experiment. In other words, NADH may be able to shift the enzyme completely into an inactive T-state, but it may take longer than the time allotted for the experiment.

The Truncated Variant

The *E. coli* CS crystal structure showed that the N-terminal domain is a unique feature of the Type II enzymes. The function of this N-terminal domain has become an interesting question, and the third area of study in this thesis, as it is unique to gram negative organisms.

The truncated variant lacking the N-terminal 39 amino acids exhibits a complete loss in enzyme activity. From the preliminary kinetic studies, the only plausible explanation for the fact that the enzyme shows a very low k_{cat} value, yet normal Michaelis constants for OAA, AcCoA and KCl, while showing increased affinity for NADH, is that the activity seen is from contaminating wild type protein. The complete loss of activity was not a total surprise, as the mutation was so severe. However, there are several possibilities, which could explain this catalytically ineffective variant: 1) the N-terminal domain may stabilize the structural integrity of dimeric interactions, which are required for the proper active site conformation; 2) the remaining residues (40-52) of the N-terminal domain, which contain several hydrophobic phenylalanine residues, and lie within 9Å of R407 and 12Å of H229, may dissociate and refold in such a way that they block entrance of substrates into the active site (see Figure 41); and 3) the N-terminal domain may be a key structural component involved in the allosteric properties of *E. coli* CS, which when removed results in the locking of subunits into a non-reversible T-state. The idea of a stable T-state is further strengthened by the increased binding affinity for NADH, however, without a crystal structure for the truncated variant it is hard to determine, which, if any, of the above statements are correct.

The mass spectrometry results verify that absence of the N-terminal domain does not effect the hexamerization of *E. coli* citrate synthase. As expected, the smaller dimer and hexamer show distinct charge envelopes at lower m/z values. The dimer/hexamer equilibrium appears to be normal, which would imply that the N-terminal domain plays little or no functional role in the multimeric conformation of the enzyme. This is consistent with the fact that the N-terminal domains are far from the dimer-dimer contact regions.

The preliminary studies focused on the possibility of mixed wild type/truncated hexamers suggest that the two proteins are not compatible with one another. One possibility, which could be concluded from this result, if it is in fact correct, is that the truncated variant must have undergone structural alterations, which prevent it from interacting with the wild type protein. The most obvious region to consider would be the contact regions composed of residues of the FG turn, IJ turn and the unique 7-residue loop. However, without a crystal structure for the truncated variant, it is impossible to be confident that conformational changes occur in this area, as these residues lie >40Å from residues of the N-terminal domain.

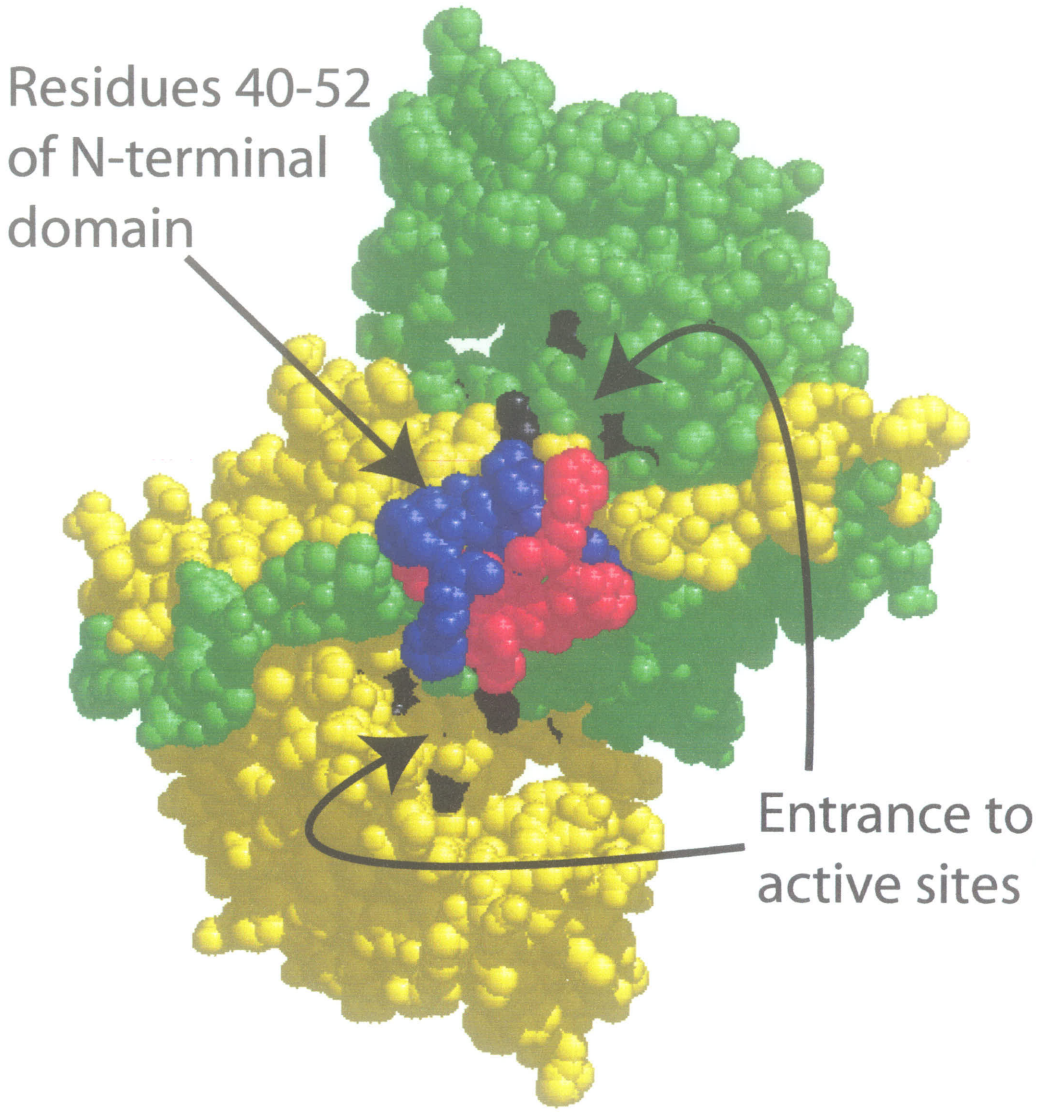

Figure 41: Top view of a single dimer, showing the residues of the N-terminal domain (red & blue), which are still present in the truncated variant. Active site residues are shown in black and give a clear picture of the possible entrance for substrates into the active site, which could be blocked upon dissociation and refolding of the remaining N-terminal residues in the truncated variant. Note: the crystal structure shown here is from wild type protein, with the N-terminal 39 amino acids absent.

Future Work

As several of the NADH variants have shown confusing results, it is obvious that more work must be done in order to understand the relationship between the kinetics and allosteric properties of this enzyme. One experiment, which may be useful, would be to test AcCoA saturation in the absence of KCl. The wild type enzyme shows a sigmoid AcCoA saturation curve in the absence of KCl, which implies that the enzyme in a resting state (absence of activators or inhibitors) is in a T-state conformation. This experiment would give a direct indication of the state of each variant, as the curve would show a sigmoid shape if the enzyme is in a T-state, as the wild type protein is, and a hyperbolic shape if the enzyme has shifted towards an R-state conformation. A second area of study, which could prove to be useful, would be to crystallize several of these variants in order to see what conformational changes have taken place. Crystallography of the K167A and T204A variants should prove to be very interesting, as both have demonstrated the novel tetrameric structure. It would also be interesting to see the position of NADH in the allosteric site of the R109L variant, as it shows stronger NADH binding. Although the crystal structure with the F383A variant has given the location of the NADH binding site, one question which has arisen, is: Why does the nicotinamide portion of NADH show no interactions with any specific residues, when it is believed to be the important component of the molecule? This seems a very important question, given the results of Talgoy and Duckworth (1979), who showed that a variety of adenylates could fit into the allosteric site, with no inhibitory effects. Therefore, it seems that further work must be done in order to define the allosteric site in its entirety.

The kinetic data on the three arginine variants located in the cationic pore, along with the results of the NADH binding and inhibition assays, suggest that these three proteins have taken on an R-state conformation. On the other hand, this conclusion is confusing when looking at the sigmoid curve associated with KCl saturation, which suggests a T-state conformation. As the mass spectrometry results on these variants show highly stable hexamers, it seems obvious that a crystal structure of these three variants would be beneficial to understanding their kinetic, allosteric and multimeric properties. It would be interesting to see if these mutations have resulted in the collapse of the central pore, and in turn tighter contacts between dimers. This type of result would help explain the higher K_D for NADH observed with these three variants. It would also be interesting to see the structural modifications that have occurred at the active sites of all three variants, which have resulted in the high K_{iOAA} values observed. The crystal structure, may also help clarify why the KCl saturation experiment suggests a T-state conformation, while the rest of the kinetic data, including NADH binding and inhibition, imply an R-state.

As already mentioned, it would be interesting to create a double variant of the R319L variant, and any of the three residues of the cationic pore, as this may result in a protein which does not require KCl for maximum activity. However, the R119L change might give the most interesting results, as this variant showed the highest affinity for both substrates, while also showing only 23% inhibition by NADH. Therefore, an R119L, R319L double variant may result in a highly stable R-state hexamer, which lacks any allosteric regulation.

Thus far, little information on the truncated variant has been obtained, as it appears to show no activity. Although we can conclude that the N-terminal domain has little functional relationship to the multimeric conformation of this protein, an explanation for the lack of activity remains elusive. Therefore, the only plausible course of action to understanding what has happened to this truncated enzyme would be to obtain its crystal structure. The crystal structure should prove invaluable, as it will show what structural changes have occurred, which have resulted in the inactive variant.

Appendices

Appendix I

Sequence alignment of *E. coli* citrate synthase compared with other hexameric gram negative organisms, dimeric eukaryotic organisms, and the shortened dimeric citrate synthases of gram positives and archaea bacteria.

1 *Escherichia coli* (gram negative, hexamer)
2 *Acinetobacter antitratum* (gram begative, hexamer)
3 *Pseudomonas aeruginosa* (gram negative, hexamer)
4 *Sus scrofa* (pig heart) (Eucaryotic, dimer)
5 *Saccharomyces cervisiae* (yeast) (Eucaryotic, dimer)
6 *Bacillus subtilis* (gram positive, dimer)
7 *Pyrococcus furiosus* (archaea bacteria)
8 *Escherichia coli* methyl CS (gram negative, dimer)

Alignment constructed by Dr. H. W. Duckworth (unpublished)

- underlined represent ever 10th residues
- dashes are included where residues are lacking in order to maintain the alignment
- the yellow highlighted residues are those removed in the *E. coli* truncated variant
- the residues studied for their involvement in the allosteric site are highlighted in red in the gram negative bacterial sequences
- the conserved active site residues are highlighted in green

```
1          ADTKAKLTLNGDTAVELDVLKGTLGQDVIDI-RTLGSKGVFTFDPGFTSTASCESKIT 57
2        SEATGKKAVLHLDGKEIELPIYSGTLGPDVIDV-KDVLASGHFTFDPGFMATASCESKIT 59
3          ADKKAQLIIEGSAPVELPVLSGTMGPDVVDV-RGLTATGHFTFDPGFMSTASCESKIT 57
4          ASSTNLKDILADLIPKEQARIKTFRQQHGNTVVGQITV-DMMYGGMRGMKGLV-YETS 56
5          ASEQTLKERFAEIIPAKAQEIKKFKKEHGKTVIGEVLLEEQAYGGMRGIKGLV-WEGS 96
6                                                MVNTNQFIPGLEGVIASETKIS 22
7                                              (M)NTEKYLAKGLEDVYIDQTNIC 21
8                                    MSDTTILQNSTHVIKPKKSVALSGVPAGNTALC 33

1  FIDGDEGILLHRGFPIDQLATDS----------NYLEVCYILLNGEKPTQEQYDEFKTTVTRHTMIHEQITRL- 120
2  FIDGDKGILLHRGYPIDQLATQA----------DYLEYCYLLLNGELPTAEQKVEFDAKVRAHTMVHDQVSRF- 122
3  FIDGDKGVLLHRGYPIEQLAEKS----------DYLETCYLLLNGELPTAAQKEQFVGTIKNHTMVHEQLKTF- 120
4  VLDP-DEGIRFRGYSIPECQKMLPKAKGGEEPLPEGLFWLLVTGQIPTEEQVSWLSKEWAKRAALPSHVVTM- 127
5  VLDP-DEGIRFRGRTIPEIQRELPKAEGSTEPLPEALFWLLLTGGIPTDAQVKALSADLAARSEIPGHVIQL- 167
6  FLDTVNSEIVIKGYDLLALSKTK----------GYLDIVHLLLEFTIPNEAEKQHLEETLKQEYDVPDEIIQV-  85
7  YIDGKEGKLYYRGYSVEELAELS----------TFEEVVYLLWWGKLPSLSELENFKKELAKSRGLPKEVIEI-  84
8  TVGKSGNDLHYRGYDILDLAKHC----------EFEEVAHLLIHGKLPTRDELAAYKTKLKALRGLPANVRTV-  96
```

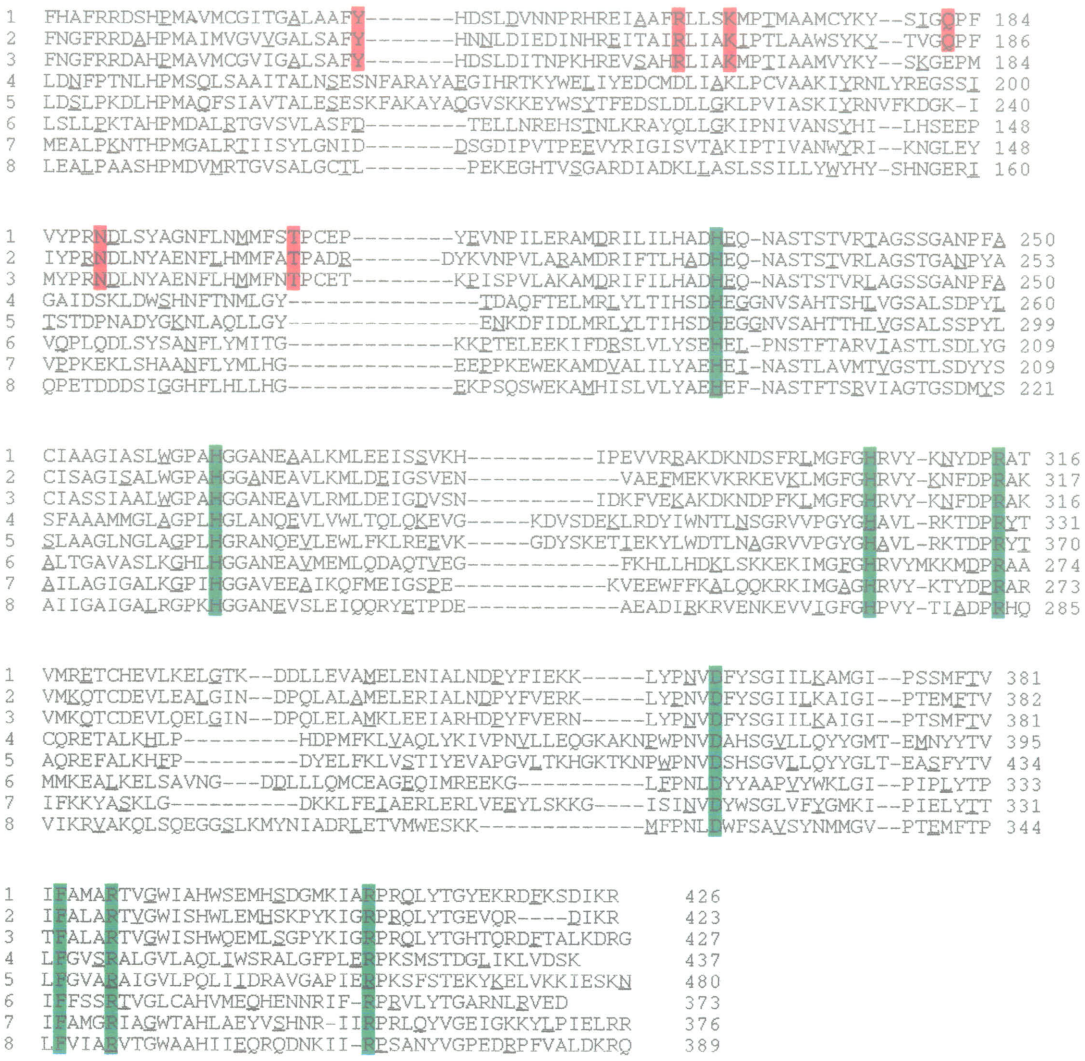

Appendix II

E. coli gltA sequence of Ner et al., (1983) and corresponding amino acid sequence of Bhayana & Duckworth, (1984).

(Sequence Range: 1 to 1284bp)

```
ATG GCT GAT ACA AAA GCA AAA CTC ACC CTC AAC GGG GAT ACA GCT GTT GAA CTG GAT GTG
TAC CGA CTA TGT TTT CGT TTT GAG TGG GAG TTG CCC CTA TGT CGA CAA CTT GAC CTA CAC
(M)  A   D   T   K   A   K   L   T   L   N   G   D   T   A   V   E   L   D   V>

                                                        100
CTG AAA GGC ACG CTG GGT CAA GAT GTT ATT GAT ATC CGT ACT CTC GGT TCA AAA GGT GTG
GAC TTT CCG TGC GAC CCA GTT CTA CAA TAA CTA TAG GCA TGA GAG CCA AGT TTT CCA CAC
 L   K   G   T   L   G   Q   D   V   I   D   I   R   T   L   G   S   K   G   V>

TTC ACC TTT GAC CCA GGC TTC ACT TCA ACC GCA TCC TGC GAA TCT AAA ATT ACT TTT ATT
AAG TGG AAA CTG GGT CCG AAG TGA AGT TGG CGT AGG ACG CTT AGA TTT TAA TGA AAA TAA
 F   T   F   D   P   G   F   T   S   T   A   S   C   E   S   K   I   T   F   I>

                        200
GAT GGT GAT GAA GGT ATT TTG CTG CAC CGC GGT TTC CCG ATC GAT CAG CTG GCG ACC GAT
CTA CCA CTA CTT CCA TAA AAC GAC GTG GCG CCA AAG GGC TAG CTA GTC GAC CGC TGG CTA
 D   G   D   E   G   I   L   L   H   R   G   F   P   I   D   Q   L   A   T   D>

                                                            300
TCT AAC TAC CTG GAA GTT TGT TAC ATC CTG CTG AAT GGT GAA AAA CCG ACT CAG GAA CAG
AGA TTG ATG GAC CTT CAA ACA ATG TAG GAC GAC TTA CCA CTT TTT GGC TGA GTC CTT GTC
 S   N   Y   L   E   V   C   Y   I   L   L   N   G   E   K   P   T   Q   E   Q>

TAT GAC GAA TTT AAA ACT ACG GTG ACC CGT CAT ACC ATG ATC CAC GAG CAG ATT ACC CGT
ATA CTG CTT AAA TTT TGA TGC CAC TGG GCA GTA TGG TAC TAG GTG CTC GTC TAA TGG GCA
 Y   D   E   F   K   T   T   V   T   R   H   T   M   I   H   E   Q   I   T   R>

                                                        400
CTG TTC CAT GCT TTC CGT CGC GAC TCG CAT CCA ATG GCA GTC ATG TGT GGT ATT ACC GGC
GAC AAG GTA CGA AAG GCA GCG CTG AGC GTA GGT TAC CGT CAG TAC ACA CCA TAA TGG CCG
 L   F   H   A   F   R   R   D   S   H   P   M   A   V   M   C   G   I   T   G>

GCG CTG GCG GCG TTC TAT CAC GAC TCG CTG GAT GTT AAC AAT CCT CGT CAC CGT GAA ATT
CGC GAC CGC CGC AAG ATA GTG CTG AGC GAC CTA CAA TTG TTA GGA GCA GTG GCA CTT TAA
 A   L   A   A   F   Y   H   D   S   L   D   V   N   N   P   R   H   R   E   I>

                        500
GCC GCG TTC CGC CTG CTG TCG AAA ATG CCG ACC ATG GCC GCG ATG TGT TAC AAG TAT TCC
CGG CGC AAG GCG GAC GAC AGC TTT TAC GGC TGG TAC CGG CGC TAC ACA ATG TTC ATA AGG
 A   A   F   R   L   L   S   K   M   P   T   M   A   A   M   C   Y   K   Y   S>

                                                            600
ATT GGT CAG CCA TTT GTT TAC CCG CGC AAC GAT CTC TCC TAC GCC GGT AAC TTC CTG AAT
TAA CCA GTC GGT AAA CAA ATG GGC GCG TTG CTA GAG AGG ATG CGG CCA TTG AAG GAC TTA
 I   G   Q   P   F   V   Y   P   R   N   D   L   S   Y   A   G   N   F   L   N>

ATG ATG TTC TCC ACG CCG TGC GAA CCG TAT GAA GTT AAT CCG ATT CTG GAA CGT GCT ATG
TAC TAC AAG AGG TGC GGC ACG CTT GGC ATA CTT CAA TTA GGC TAA GAC CTT GCA CGA TAC
 M   M   F   S   T   P   C   E   P   Y   E   V   N   P   I   L   E   R   A   M>
```

```
                                                                  700
GAC CGT ATT CTG ATC CTG CAC GCT GAC CAT GAA CAG AAC GCC TCT ACC TCC ACC GTG CGT
CTG GCA TAA GAC TAG GAC GTG CGA CTG GTA CTT GTC TTG CGG AGA TGG AGG TGG CAC GCA
 D   R   I   L   I   L   H   A   D   H   E   Q   N   A   S   T   S   T   V   R>

ACC GCT GGC TCT TCG GGT GCG AAC CCG TTT GCC TGT ATC GCA GCA GGT ATT GCT TCA CTG
TGG CGA CCG AGA AGC CCA CGC TTG GGC AAA CGG ACA TAG CGT CGT CCA TAA CGA AGT GAC
 T   A   G   S   S   G   A   N   P   F   A   C   I   A   A   G   I   A   S   L>

                          800
TGG GGA CCT GCG CAC GGC GGT GCT AAC GAA GCG GCG CTG AAA ATG CTG GAA GAA ATC AGC
ACC CCT GGA CGC GTG CCG CCA CGA TTG CTT CGC CGC GAC TTT TAC GAC CTT CTT TAG TCG
 W   G   P   A   H   G   G   A   N   E   A   A   L   K   M   L   E   E   I   S>

                                                                  900
TCC GTT AAA CAC ATT CCG GAA TTT GTT CGT CGT GCG AAA GAC AAA AAT GAT TCT TTC CGC
AGG CAA TTT GTG TAA GGC CTT AAA CAA GCA GCA CGC TTT CTG TTT TTA CTA AGA AAG GCG
 S   V   K   H   I   P   E   F   V   R   R   A   K   D   K   N   D   S   F   R>

CTG ATG GGC TTC GGT CAC CGC GTG TAC AAA AAT TAC GAC CCG CGC GCC ACC GTA ATG CGT
GAC TAC CCG AAG CCA GTG GCG CAC ATG TTT TTA ATG CTG GGC GCG CGG TGG CAT TAC GCA
 L   M   G   F   G   H   R   V   Y   K   N   Y   D   P   R   A   T   V   M   R>

                                                                  1000
GAA ACC TGC CAT GAA GTG CTG AAA GAG CTG GGC ACG AAG GAT GAC CTG CTG GAA GTG GCT
CTT TGG ACG GTA CTT CAC GAC TTT CTC GAC CCG TGC TTC CTA CTG GAC GAC CTT CAC CGA
 E   T   C   H   E   V   L   K   E   L   G   T   K   D   D   L   L   E   V   A>

ATG GAG CTG GAA AAC ATC GCG CTG AAC GAC CCG TAC TTT ATC GAG AAG AAA CTG TAC CCG
TAC CTC GAC CTT TTG TAG CGC GAC TTG CTG GGC ATG AAA TAG CTC TTC TTT GAC ATG GGC
 M   E   L   E   N   I   A   L   N   D   P   Y   F   I   E   K   K   L   Y   P>

                          1100
AAC GTC GAT TTC TAC TCT GGT ATC ATC CTG AAA GCG ATG GGT ATT CCG TCT TCC ATG TTC
TTG CAG CTA AAG ATG AGA CCA TAG TAG GAC TTT CGC TAC CCA TAA GGC AGA AGG TAC AAG
 N   V   D   F   Y   S   G   I   I   L   K   A   M   G   I   P   S   S   M   F>

                                                                  1200
ACC GTC ATT TTC GCA ATG GCA CGT ACC GTT GGC TGG ATC GCC CAC TGG AGC GAA ATG CAC
TGG CAG TAA AAG CGT TAC CGT GCA TGG CAA CCG ACC TAG CGG GTG ACC TCG CTT TAC GTG
 T   V   I   F   A   M   A   R   T   V   G   W   I   A   H   W   S   E   M   H>

AGT GAC GGT ATG AAG ATT GCC CGT CCG CGT CAG CTG TAT ACA GGA TAT GAA AAA CGC GAC
TCA CTG CCA TAC TTC TAA CGG GCA GGC GCA GTC GAC ATA TGT CCT ATA CTT TTT GCG CTG
 S   D   G   M   K   I   A   R   P   R   Q   L   Y   T   G   Y   E   K   R   D>

                              1284
TTT AAA AGC GAT ATC AAG CGT TAA
AAA TTT TCG CTA TAG TTC GCA ATT
 F   K   S   D   I   K   R   *>
```

Appendix III

Variant	Extinction Coefficient At 278 nm ($M^{-1}cm^{-1}$)	Tryptophan/Tyrosine Ratio
R109L	41585	0.179
H110A	40391	0.202
T111A	42780	0.195
R119L	39758	0.186
R125L	43719	0.142
R126L	39862	0.189
Y145A	NPTD	NPTD
R163L	39898	0.190
K167A	42034	0.202
Q182A	48791	0.171
N189A	52634	0.130
T204A	41098	0.217
TRUNC	55145	0.145

NPTD = Not Possible To Determine

References

Amarasingham, C. R., & Davis, B. D. (1965) J. Biol. Chem. 240, 3664-3668.

Anderson, D. H. (1988) Ph.D. Thesis, University of Manitoba.

Anderson D. H., & Duckworth, H. W. (1988) J. Biol. Chem. 263, 2163-2169.

Anderson, D. H., & Duckworth, H. W. (1989) Biochem. Cell. Biol. 67, 98-102.

Anderson, D. H., Donald, L. J., Jacob, M., & Duckworth, H. W. (1991) Biochem. Cell Biol. 69, 232-238.

Ayed, A. (1998) Ph. D. Thesis, University of Manitoba.

Ayed, A., Krutchinsky, A. N., Ens, W., Standing, K. G., & Duckworth, H. W. (1998) Rapid Commun. Mass. Spectrom. 12, 339-344.

Bayer, E., Bauer, B., & Eggerer, H. (1981) Eur. J. Biochem. 120, 155-160.

Birnboim, H. C. & Doly, J. (1979) Nucl. Acids Res. 7, 1513-1523.

Bhayana, V., & Duckworth, H. W. (1984) Biochemistry 23(13), 2900-2904.

Bloxham, D. P., Parmelee, D. C., Kumar, S., Wade, R. D., Ericsson, L. H., Neurath, H., Walsh, K. A., & Titani, K. (1981) Proc. Natl. Acad. Sci. 78, 5381-5385.

Bloxham, D. P., Permelee, D. C., Kumar, S., Walsh, K. A., & Titani, K. (1982) Biochemistry 21, 2028-2036.

Cleland, W. W. (1963) Biochim. Biophys. Acta. 67, 104-137.

Danson, M. W., & Weitzman, P. D. J. (1973) Biochem. J. 135, 513-524.

Donald, L. J., & Duckworth, H. W. (1987) Biochem. Biophys. Res. Commun. 141, 797-803.

Donald, L. J., & Duckworth, H. W. (1987) Biochem. Cell Biol. 65, 930-938.

Donald, L. J., Molgat, G. F., & Duckworth, H. W. (1989) J. Bacteriol. 171, 5542-5550.

Duckworth, H. W., & Tong, E. K. (1976) Biochemistry 15, 108-114.

Duckworth, H. W., & Bell, A. W. (1982) Can. J. Biochem. 60, 1143-1147.

Else, A. J., Danson, M. J., & Weitzman, P. D. J. (1988) Biochemistry 254, 437-442.

Evans, C. T., Owens, D., Casazza, J. P., & Srere, P. A. (1989) Biochem. Biophys. Res. Commun. 164, 1437-1445.

Evans, C., Kurz, L., Remington, S., & Srere, P. (1996) Biochemistry 35, 10661-10672.

Faloona G. R., & Srere P. A. (1969) Biochemistry 8(11), 4497-4503.

Fersht, A. (1985) Enzyme Structure and Mechanism, 2nd edition, W. H. Freeman & company, New York.

Gerike, U., Hough, D. W., Russell, N. J., Dyall-Smith, M. L., and Danson, M. J. (1998) Microbiology 144, 929-935.

Gray, C. T., Wimpenny, W. T., & Mossman, M. R. (1966) Biochim. Biophys. Acta. 117, 33-41.

Hammond, D. C. (1986) J. Biol. Chem. 261, 8424-8428.

Hanson, R. S., & Cox, D. P. (1967) J. Bacteriol. 93, 1777-1787.

Jin, S., & Sonenshein. A. L. (1996) J. Bacteriol. 178(12), 3658-3660.

Johansson, C. J. & Pettersson, G. (1974) Eur. J. Biochem. 42, 383-388.

Karpusas, M., Branchaud, B., & Remington, S. J. (1990) Biochemistry 29, 2213-2219.

Karpusas, M., Holland, D., & Remington, S. J. (1991) Biochemistry 30, 6024-6031.

Kornberg, H. L. (1963) Biochim. Biophys. Acta. 73, 517-521.

Kroeger, M., Wahl, R. (1997) Nucleic Acids Res. 25, 39-42.

Krutchinsky, A. N., Chemushevich, I. V., Spicer, V. L., Ens, W., & Standing, K. G. (1998) J. Am. Soc. Mass. Spectrom. 9, 469-579.

Krutchinsky, A. N., Ayed, A., Donald, L. J., Ens, W. Duckworth, H. W., Standing, K. G. (2000) Methods in Molecular Biology 146, 239-249.

Kurz, L. C., Ackerman, J. J. H., & Drysdale, G. R. (1985) Biochemistry 24, 452-457.

Kurz, L. C., & Drysdale, G. R. (1987) Biochemistry 26, 2623-2627.

Lehninger, A. L., Nelson, D. L., & Cox, M. M (1993) Principles of Biochemistry, 2nd Edition. Worth Publishers, Inc, NY.

Lesk, A. M. & Clothia, C. (1984) J. Mol. Biol. 174, 175-191.

Liao, D. I., Karpusas, M., & Remington, S. J. (1991) Biochemistry 30, 6031-6036.

Mahlen, A. (1975) FEBS Lett. 51, 294-296.

Mandel, M., & Higa, A. (1970) J. Mol. Biol. 53. 154-159.

Molgat, G. F., Donald, L. J., & Duckworth, H. W. (1992) Arch. Biochem. Biophys. 298, 238-246.

Monod, J., Wyman. J., & Changeux, J. P. (1965) J. Mol. Biol. 12, 88-118.

Nguyen, T. N., Maurus, R., Stokell, D. J., Ayed, A., Duckworth, H. W., Brayer, G. D. (2001) Biochemistry, in press.

Ner, S. S., Bhayana, V., Bell, A. W., Giles, I. G., Duckworth, H. W., & Bloxham, D. P. (1983) Biochemistry 22, 5243-5249.

Orr, A., Ivanova, V. S., &Bonner, W. M. (1995) Biotechniques 19, 204-206.

Patton A. J., Hough, D. W., & Danson, M. J. (1993) Eur. J. Biochem. 214, 75-81.

Pereira, D. S., Donald, L. J., Hosfield, D. J., & Duckworth, H. W. (1994) J. Biol. Chem. 269(1), 412-417.

Remington, S., Wiegand, G., & Huber, R. (1982) J. Mol. Biol. 158, 111-152.

Rosenkranz, M. T., Alal, T., Kim, S. S., Clark, B. J., Srere, P. A., & Guarente, L. P. (1986) Mol. Cell. Biol. 6(12), 4509-4515.

Schendel, F. J., August, P. R., Anderson, C. R., Hanson, R. S., & Flickinger, M. C. (1992) Appl. Environ. Microbiol. 58, 335-345.

Srere, P. A. (1972) Curr. Top. Cell. Regul. 5, 229-283.

Suissa, M., Suda, K., & Schatz, G. (1984) EMBO J. 3, 1773-1781.

Talgoy, M. M. & Duckworth, H. W. (1979) Can. J. Biochem. 57, 385-395.

Talgoy, M. M., Bell, A. W., & Duckworth, H. W. (1979) Can. J. Biochem. 57, 822-833.

Textor, S., Wendisch, V. F., De Graaf, A. A., Muller, U., Linder. M. I., Linder, D., & Buckel, W. (1997) Arch Microbiol. 168, 428-436.

Tong, E. K., & Duckworth, H. W. (1975) Biochemistry 14, 235-241.

Verentchikov, A. N., Ens, W., & Standing, K. G. (1994) Anal. Chem. 66, 126-133.

Weitzman, P. D. J. (1966a) Biochim. Biophys. Acta. 128, 213-215.

Weitzman, P. D. J. (1966b) Biochem. J. 101, 44c-46c.

Weitzman, P. D. J. (1967) Biochim. Biophys. Acta. 139, 526-528.

Weitzman, P. D. J., & Jones, D. (1968) Nature 219, 270-272.

Weitzman, P. D. J., Ward, B. A., & Rann, D. L. (1974) FEBS Lett. 43, 97-100.

Weitzman, P. D. J., & Danson, M. J. (1976) Curr. Top. Cell. Regul. 10, 161-204.

Wiegand, G., Remington, S. J., Deisenhofer, J., & Huber, R. (1984) J. Mol. Biol. 174, 205-211.

Wiegand, G., & Remington, S. J. (1986) Annu. Rev. Biophys. Chem. 15, 97-117.

Wood, D. O., Williamson, L. R., Winkler, H. H., & Krause, D. C. (1987) J. Bacteriol. 169, 3564-3572.

Wright, J. A., Maeba, P., & Sanwal, B. D. (1967) Biochem. Biophys. Res. Commun. 29, 34-38.

Wright, J. A., & Sanwal, B. D. (1971) J. Biol. Chem. 246, 1689-1699.

Wu, J. Y., & Yang, J. T. (1970) J. Biol. Chem. 245, 212-218.